SHEAR CAPABLE SOFT SENSOR TECHNOLOGY FOR THE APPLICATION OF PRESSURE ULCER DETECTION IN DIABETICS

by

Andres Velez Lopez

M.Sc., Boston University, 2015

A THESIS SUBMITTED IN PARTIAL FULFILLMENT OF

THE REQUIREMENTS FOR THE DEGREE OF

MASTER OF APPLIED SCIENCE

in

THE FACULTY OF GRADUATE AND POSTDOCTORAL STUDIES

(Biomedical Engineering)

THE UNIVERSITY OF BRITISH COLUMBIA

(Vancouver)

September 2021

© Andres Velez Lopez, 2021

The following individuals certify that they have read, and recommend to the Faculty of Graduate and Postdoctoral Studies for acceptance, a thesis entitled:

Shear capable soft sensor technology for the application of pressure ulcer detection in diabetics

submitted by Andres Velez Lopez in partial fulfillment of the requirements for

the degree of Master of Applied Science

in Biomedical Engineering

Examining Committee:

Dr. John D. W. Madden, Professor, Electrical and Computer Engineering, UBC
Supervisor

Dr. Lyndia Wu, Assistant Profesor, Mechanical Engineering, UBC
Supervisory Committee Member

Dr. Andrea Veljkovic, Associate Clinical Professor, Faculty of Medicine, UBC
Supervisory Committee Member

Abstract

Diabetic pressure ulcers (DFU) are one of the most common complications related to diabetes, a disease that has become a global epidemic affecting many countries, especially modern and rich ones. The financial cost of treating DFUs this disease is monumental, costing $550 million yearly in Canada alone to treat. the DFUs being one of the costliest outcomes of diabetes, can lead to a sedimentary lifestyle for individuals that could benefit from physical activity to combat their diabetes. There is a need to develop technology that can sense and monitor the condition of feet at this crucial crossroad. This thesis builds on a capacitive sensor developed in our lab that can measure normal and shear stress simultaneously, made from soft, comfortable, and affordable materials which could be implemented into an insole or modified shoe device. The sensor was characterized using modified protocols of existing methodology to establish sensitivity, repeatability, and proper calibration. Overall, the sensor can measure stresses in the prescribed ranges for normal (0-1000 kPa) and shear (0-200 kPa) and is responsive, in the lab as well as real-life testing, to the different time regimes it is being designed for (standing and walking). We show that the sensor is suited well for measuring displacement change in the foot to capture anatomy change in the foot and swelling. While the force characterization has been described, there is still a good amount of work to establish this sensing parameter to coupe with hysteresis and creep (in the worst case 24% of the full scale) present in the deformation of the materials being used. There is a tradeoff to contend with that combines the comfort and softness of the sensor to its ability to withstand high forces and how the modeling of these deformations is accurate and relevant to our clinical considerations. This technology could be a game-changer for the common diabetic and here we lay out the framework to make soft normal and shear stress in-shoe sensors a reality.

Lay Summary

Diabetic patients must deal with many medical issues that extend to many aspects of their lives. One common issue is the development of pressure ulcers on their feet which can be detrimental to your physical health and may lead to amputations. Currently, there is not enough technological advancement to help tackle this problem other than regular medical checkups. The work in this thesis presents the development of applicable pressure sensor systems that detect and monitors stresses in the shoes of diabetics. These sensors can be expanded into insole or shoe systems that could be worn by the participant to monitor excessive forces, capture gait changes, and log use on the plantar foot. Further work would miniaturize the system to be applicable for at-home systems and on-the-go applications.

Preface

The research work presented in this thesis was originally organized and written by the author with supervision from Dr. John D. W. Madden, along with guidance on clinical relevance from Dr. Andrea Veljkovic, who works at the Footbridge Clinic in Vancouver. Input was also provided by Dr. Lyndia Wu, who, along with Dr. Veljkovic, were members of the supervisory committee.

The work specifically is an application of previous work conducted in the Molecular Mechatronics laboratory at UBC primarily headed by Dr. Mirza Saquib us Sarwar and master's student Kieran Morton to study soft and stretchable stress sensors implemented as artificial skin. This thesis works to expand on the capabilities of this sensor by adapting its application to the higher forces needed in the foot by using different materials and structures. Manufacturing methods were modified from existing sensor methodology in the lab using molding, 3D printing, and similar elastomeric materials. Most of these methods are described in the thesis of Dr. Mirza Saquib us Sarwar and former master student Bertille Dupont. Electronics are also borrowed from previous work in the laboratory again previously described in these former theses. Undergraduate interns as a part of the ongoing project to develop these soft sensors in the lab have contributed greatly to that cause and the thesis described. These include but are not limited to Zi Chen, Austin Weir, Oliver Tong, and Konstantin Borissov. Their contributions include manufacturing methods, testing and calibration, and electronic development (PCB and software).

Table of Contents

List of Tables

List of Figures

List of Abbreviations

BC – British Columbia

CDC – Capacitance to Digital Converter

CRP- C-Reactive Protein

DFU – Diabetic Foot Ulcer

kPa – Kilopascals

ms - milliseconds

PAD- Perihelial Arterial Disease

PCB – Printed Circuit Board

PDMS - Polydimethylsiloxane

UBC – University of British Columbia

Acknowledgments

I would like to thank my supervisor, Dr. John Madden for the opportunity to work in his lab and the support and guidance to finish my project. I would also like to thank my committee, Dr. Lyndia Wu and Dr. Andrea Veljkovic, for supporting me in my efforts and giving guidance for a more impactful project. I would like to thank Master student Kieran Morton and his team for all the assistance and teaching they gave me to be able to apply the sensor in my application. I thank the School of Biomedical Engineering, particularly Dr. Karen Cheung for the opportunity to further my education and apply what I learned to further research in this ever-expanding field. Lastly, but certainly, not least I would like to thank my family who has supported me and given me everything to succeed in life and education, los amo gracias!

Dedication

I dedicate this work to my family first and foremost who has allowed me to advance myself in my career and to contribute to society with impactful and meaningful research. I hope this work is the foundation to further technology that could help the lives of many diabetics in the future.

Chapter 1: Introduction & Background

In this thesis, we will develop a soft and flexible sensor that can measure normal and shear stresses in the prescribed ranges experienced in the plantar foot. To introduce and formulate the motivation behind developing such a sensor, the first chapter lays out the physiology of diabetic foot ulcers and the need for technology to monitor this disease, this is leveraged by the cost and burden that diabetic foot ulcers and amputation have on the medical system. The second chapter will focus on the methodology used in the thesis, primarily focusing on the manufacturing of the sensors, and laying out experimental procedures for the results section. The third chapter reports and analyses the results of the experiments described in the previous chapter. Important to note that this thesis is not the development of an insole device that could be used but rather the steps that are needed to get to such a device. In the third chapter, we will outline a possible formulation for such a device and how it might be manufactured. The final and fourth chapter describes the challenges and limitations faced during the thesis, lays out future work to enhance and further the research done her, and finally wraps up the thesis as a stepping stone for more technology in this field.

This chapter will focus on the motivation for this thesis, defining foot ulcers in diabetics and the need to monitor them more closely using sensing technology. Firstly, we define the significance of diabetic foot ulcers in Canada and worldwide, their cost to the medical system, and individual lives. Next, we go into detail about the physiological changes a diabetic undergoes that result in a more prevalent and life-threatening situation with regards to the lower extremity. Lastly, we look at the current technology available for diabetics to mediate injury, monitor foot health, and describe the necessity for shear accessible, affordable, and user-friendly technology in this field.

1.1 Introduction

Diabetes has become a very common disease found in all regions of the world and it affects 8.8 % of Canadians [1]. It can be divided into two categories, type 1, and type 2. Type 1 is the rarer case and an autoimmune disease that is inherited, while type 2 occurs due to many different factors that can range from obesity, diet to socioeconomic status and even ethnicity [2]. Type 2 diabetes is by far the most common type and is associated with the global epidemic of diabetes. The disease can be broadly characterized by the inaction or decreased secretion of insulin. Insulin is an important hormone that regulates the amount of glucose in the bloodstream, mainly it works to store it in the liver for future use. The absence of this hormone results in hyperglycemia, or increased blood sugar in the blood, which can lead to long-term complications including cardiovascular disease, decreased life expectancy as well as neuropathy (loss of function of nerves including loss of sensation in the skin), and amputation [3]. Often these complications result from uncontrolled blood sugar. If unchecked, alongside cardiovascular disease, one of the most common complications is the neuropathy and physiological changes at the distal ends of the body, partially the lower extremity and feet.

The monitoring of the condition of the feet is paramount for diabetics to prevent the formation of pressure ulcers. Diabetic foot ulcers (DFU) are a common ailment that develops in the feet of diabetics and are caused by changes in physiology and prolonged stresses on vulnerable areas of the feet. These ulcers are often the sign that neuropathy has progressed to the point that individuals cannot properly feel pain, and so do not make proper adjustments to reduce stresses on the plantar feet. This often results in amputation of the foot if left unchecked diabetes is one of the leading causes of amputations in North America [4].

While pressure ulcers are well known in the diabetic community, there do not exist widely accepted diagnostic or monitoring tools for this vulnerable population. Often patients who are at higher risk need regular checkups and most patients are told to self-monitor and report if any ulcers are present. With the emergence of smart tech and its integration into the medical field, there is a growing community of researchers trying to make technology better the lives of diabetics. Often though, the technology can be very expensive and has only been made into research circles without any proper consumer or medical option.

This thesis works to develop stress sensors that can be implemented into easy-to-use and cost-friendly devices to monitor the environment of the foot. The material and capabilities of the sensor would allow them to capture both normal and shear stresses simultaneously and this information could be used to determine possibly dangerous situations, prolonged use, or even abnormalities in gait.

1.2 Motivation

1.2.1 Significance

Diabetic foot ulcers (DFU) are one of the most common complications of people living with diabetes. Patients with unchecked diabetes can develop neuropathy in the lower extremities which can lead to pressure ulcer formation without their knowledge. In Canada, people living with diabetes have a 15% higher probability of developing a DFU in their lifetime compared to non-diabetics [5]. Consequently, due to the danger of infection from DFU, Canadian diabetics have a 20-fold greater likelihood of having an amputation than adults without [4], [6]. An estimated 85% of amputations in people with diabetes result from non-healing DFU

[7]. The prevalence of DFU in Canada is about 75.1 per 100,000 people and there has been a 7.4% increase in the rate of prevalence over 5 years [8]. Often, diabetic foot ulcers and neuropathy are overlooked for other serious complications related to diabetes that include cardiovascular issues including myocardial infarction, stroke, or angina. DFU and amputation are some of the costliest conditions for diabetic patients and lower the quality of life dramatically [9].

In British Columbia, direct health care cost associated with DFU is estimated to be about $98-120 million annually and can be averaged for an individual to be anywhere between $14,580 to $21,820 yearly, depending on if they use an offloading device (a device to help heal and prevent further DFUs from developing) or not. The cost for treating a DFU includes physician visits, hospital days, long-term care, home care, disability, mortality, and offloading devices [10]. In Canada overall, DFU is associated with 16,883 hospital admissions, and 6,036 amputations, with an annual cost of $547 million, with an average of $21,371 annually per patient over their lifetime [8]. To expand the scope even further, the yearly cost in the United States can be USD 9,000 per patient which is comparable given the exchange rate, and the total medical cost for management of DFU can range from $9 to USD 13 billion [11]. In Figure 1, the cost of ulcers in the US can amount to $17,000 per ulcer and $40,000 for an amputation [12].

As described above, the impact of DFU can have health and financial implications on the individual but can also have mental and societal impacts as well. The biggest factor that contributes to a lower quality of life in these patients is the reduced mobility and adaptation of a lifestyle change, having to give up physical activities, and being confined to a wheelchair or using a cane. The decrease in mobility results in strained relations with loved ones, tension with caregivers, and an overall decrease in quality of life [13]. When talking about psychological impacts, many patients experience frustration, anger, and guilt based on restrictions that are imposed by the illness. These psychological effects can even lead to depression, especially in individuals that don't have close support groups [14]. Overall, it seems that, aside from what causes the problem or how much it cost to treat, there needs to be a big emphasis on how these induvial deal with their new reality, knowing that amputation is a very real concern. But if we can prevent the ulceration in the first place, or at least stop it from reaching a stage where amputation is required, this will have a major impact on maintenance of quality of life.

Figure 1: Significance of DFU in the USA. Information obtained from dreamit.com [12].

1.2.2 Need for technology

Often the treatment of DFU is limited only to the use of offloading devices, cleaning, and treating wounds directly with surgical methods. A methodology hasn't advanced to the point of monitoring or even diagnostic tools for DFU. Often the course of events is limited to the patient expressing discomfort from walking or standing and leading to a diagnosis of a developed pressure ulcer. There is a bulk of knowledge that has built up over the years about DFUs, as well as many campaigns trying to educate diabetic individuals about regular checkups and self-checks on the bottom of the feet, especially for elderly individuals. With that said, there don't exist any advanced technologies that are targeted toward the prevention of DFU, rather, many technologies do exist for the support of offloading or post DFU treatment. Only a handful of research-based systems exists that is used for academic investigation but not directly for consumers. The customer market is flooded with offloading devices and orthotics that are important for post-treatment but there are not many pre-treatment devices or insoles that monitor the health of the foot before diagnosis.

Often patients identify injury too late, to the point that an ulcer has developed, and it is only then that they seek out medical help. The timeline of a developing ulcer is dependent on the stresses being applied, but a pressure ulcer can develop in a matter of hours if a high enough pressure is introduced [15]. We hypothesize that a technology that can monitor the foot can act as a prevention device, alerting the user, their caregivers, and their doctor of a risk of ulceration. The user can check their footwear or, in serious situations, stop moving, to remove the risk. For example, they may need to remove a small rock from their shoe that they cannot feel or straighten their sock to remove a fold that is irritating.

A challenge with the prevention of DFU is that there are many risk factors associated with the disease, including weight, age, income level, and even race, and not one is enough to predict the onset of an ulcer. Nevertheless, there are indicative factors like elevated normal mechanical stresses, shear stresses, and temperature that can predict the formation of a DFU on the plantar foot [16], [17]. This previous work suggests that prevention through early detection is possible.

One major obstacle to the implementation of digital technology and smart systems that can warn of detrimental conditions is that older diabetics or caregivers of these patients can struggle with the transition or implementation [18]. Therefore, such technology must include easy-to-use and potentially app-based systems that can communicate the information in a very readable matter.

There needs to be a development of technology that bridges the gap between the beginning of ulceration and the realization of the problem. This is a crucial time where deep ulcers affecting underlying tissues and vessels could form as well as the introduction of infectious agents [19]. This thesis describes sensors that could be implemented in insoles or shoes that focus on measuring higher normal and shear stresses. The aim is to show that such measurement is possible, laying the groundwork for implementation. A device that can be used in the shoes of diabetics to monitor the presence of elevated stresses that could lead to pressure ulcers could inform individuals and caregivers before one develops or is developing. While a lot of amputations occur with people living with diabetic foot ulcers, most often is the mistreatment and prolonged time between the onset of one and what follows (infection, deeper more dangerous ulcer). Such a device can also add to the growing literature of diabetic foot ulcer clinical practices to better understand how fast and what time ranges are expected to result in a pressure ulcer.

1.3 Background

1.3.1 Pressure Ulcers in Diabetes

Ulcer formation in the feet of diabetics is a common and dangerous complication of progressing diabetes. Although the issue is the leading cause of hospital admissions for diabetes, it is often misunderstood and is caused by an amalgam of physiological risk factors. These factors include peripheral neuropathy, peripheral vascular disease, foot deformities, arterial insufficiency, trauma, and impaired resistance to infection [20]. All of these equate to an environment prone to wound formation, without individual knowledge, and can also affect gait. Each risk factor is now described.

Peripheral neuropathy affects the nerve endings at the extremities, particularly the feet and lower leg. If any risk factor for DFU is key to the formation of an ulcer, neuropathy is one of the most important. Up to 66% of patients with diabetes develop a form of peripheral neuropathy in the lower extremity [21]. Hyperglycemia, or high blood glucose, caused by diabetes results in some of the major pathways to neuropathy [22]. In simplest terms, most of the hyperglycemic effects deal with the upkeep of products in the cell and how they are dealt with. In the case of the polyol pathway, it is a problem of intracellular oxidative stress. When there is elevated glucose, enzymes in the polyol pathway are hyperactive, and the transformation of glucose to sorbitol increases, therefore increasing concentrations of byproducts that can damage nerve endings [23]. In the same way, glycated end products, formed from exposure to excess sugars, more specifically affect cells in two main ways, affecting proteins important in gene transcription and modifying extracellular communication between cells [24], [25]. These severed communications can affect synapses, which are the main communication to nerves in the body. Lastly, the final mechanism concerns the hexosamine pathway, which results in over modification by glucosamine as a part of the regular glycolysis pathway. This can affect gene expression, particularly of growth hormones which affect nerves and blood vessels. These mechanisms also contribute to other risk factors, primarily peripheral vascular disease, but as we will see this complication has its unique pathways as well.

As far as the nervous system is concerned, these mechanisms described affecting all its subdivisions that include motor, autonomic and sensory divisions [19]. In motor nerve degeneration we see a change in the anatomy of muscle groups which leads to altered gait and foot shape. Autonomic nervous damage affects the secretion of sweat and sebaceous glands in the foot which affects the moisture and upkeep of skin layers and leaves them more vulnerable to skin breaks and poor integrity. Sensory neuropathy resulting from damage to the nerve ends in the foot causes misinterpretation of sensation and recurrent injury without the knowledge of the patient, this may lead to infection and is a direct link to pressure ulcer formation.

Peripheral vascular disease is a manifestation of atherosclerosis in the lower extremities and is a major risk factor in the development of DFU and amputation [26]. Diabetes is one of the strongest risk factors for peripheral vascular disease due to the hyperglycemia that defines it. The metabolic state that diabetes puts the body into greatly affects the arterial structure and function, mainly through the pathway of atherogenesis. Atherogenesis is the disorder classified with endothelial cell migration, differentiation, and interaction of different cell types that create narrowing in blood vessels and restriction of flow [27]. Elevated levels of C-reactive protein or CRP are indicative of peripheral vascular disease and diabetes [28]. CRP is partially responsible for promoting apoptosis and stimulating the production of procoagulant tissue factors [26]. These cause clotting and cell death that affects blood vessels and nerves. Similarly, like in peripheral neuropathy, the endothelial cell dysfunction that comes from byproducts of hyperglycemia in the cells leads to irregular gene transcription, oxidate stress, and dangerous byproducts [29]. Vascular abnormalities continue and worsen throughout both diabetes and peripheral vascular disease. This causes vascular and nerve damage that leaves portions of the foot without oxygenation and sensation. These conditions are prime for wound damage and are where elevated pressures have their way in producing pressure-based ulcers.

Aside from neuropathy and vascular disease, there are other important risk factors for DFU that include a variety of classifications which include age, socioeconomic background health care, previous history of ulceration, and even education [30]. Additionally, being overweight, the presence and history of DFU as well as underlying disease including arterial or vascular disease can increase the likelihood of developing future DFUs. Often it is the lack of communication of symptoms and what to expect from living with diabetes that causes dangerous situations with worsening outcomes. The lack of available recommendations and healthcare, particularly in rural areas are some of the reasons ulceration is the number one cause of hospitalization in diabetics. Figure 2 outlines the major pathways to two important outcomes of diabetes including ulceration and gangrene. While not all diabetics suffer from either of these complications, the physiological changes and environment make the development of these complications much more common than in healthy individuals.

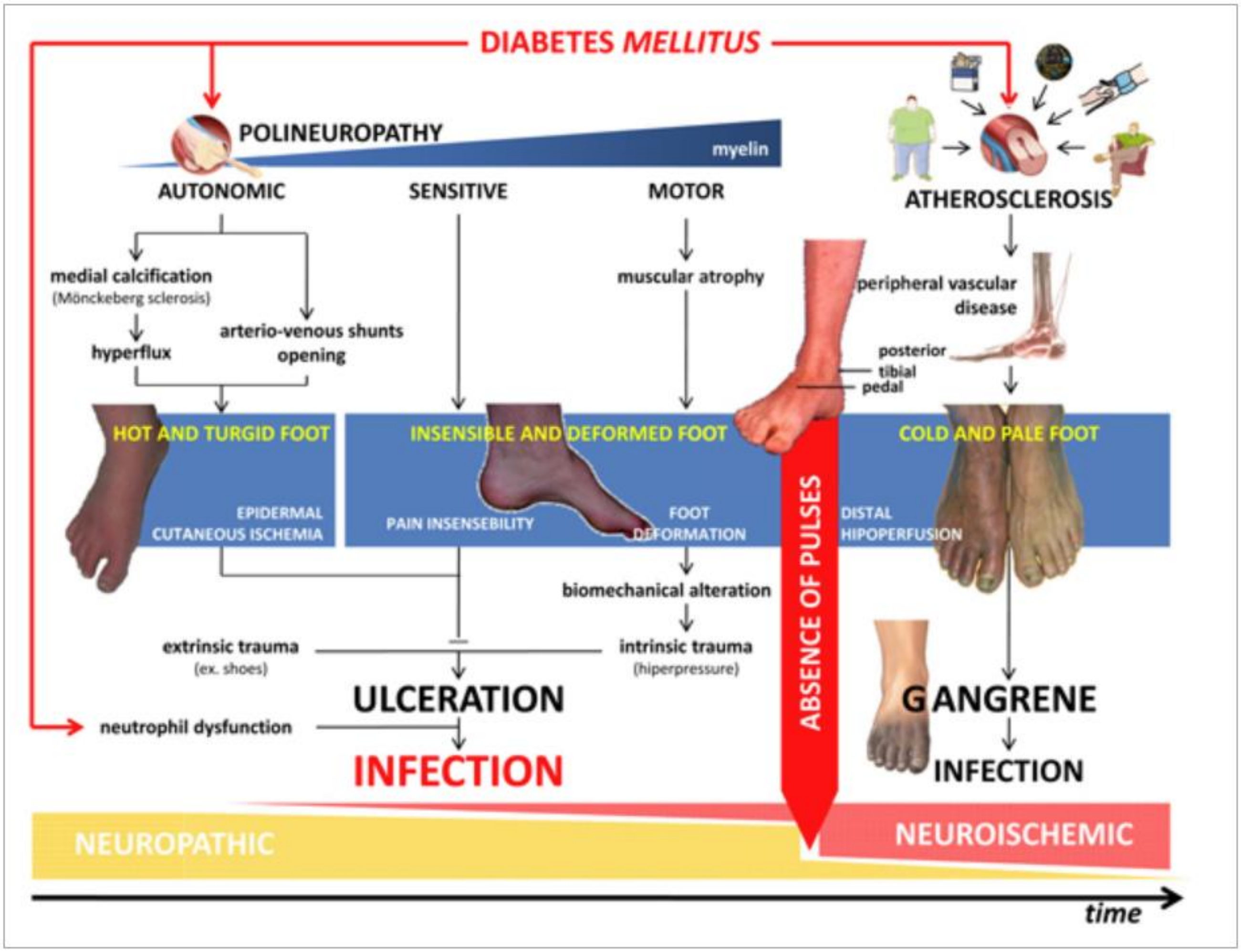

Figure 2: Pathological pathways to undesirable outcomes of ulceration and gangrene in diabetics and the diagnostic indications of each [31].

1.3.2 Normal Stress & Shear Stress Significance in DFU

Underlying risk factors lead to DFU formation in diabetics, and it helps form a basis for pathogenesis, but what kind of measurable variables are useful in developing a monitoring device? For a long time, it was accepted that the single most important factor for the pathomechanics of ulceration was normal stress (the pressure the foot feels perpendicular to the ground), but as recent research has shown this is not the entire picture [16]. The mechanisms are more complicated and while normal stress might be the key factor in spinal cord injury patients who are bed-ridden [32], it is not often the case, or at least it is only one of the causes with non-bedridden diabetics. The answer lies closer to a combination of normal stress, shear stress, and the environment of the foot including temperature and humidity [33]. All these measurable quantities help answer the question of when a DFU may be starting to form, how it progresses, and eventually when it can get to later stages and potentially harmful to the individual.

A study showed that it was peak shear stress and not peak normal stress that defined the presence of a pressure ulcer [34]. Similarly, a study that looked at how well temperature could predict the presence of a pressure ulcer was also effective [17]. With what has been discussed previously about the dysregulation of moisture and temperature as well as proprioception and sensation in diabetic feet it is evident that these variables change in DFU patients. While a combination of these factors might lead to smarter and better systems that could monitor the diabetic foot, currently the only research-based in-shoe systems only measure normal stress. A recent study looks at temperature and pressure regulating insoles as a prevention device [35]. The device used a cooling unit to regulate high temperatures during an exercise task while also measuring pressure in the process. While the experiment did not prove an improvement on behalf of the neuropathic patient group, it sets up the idea of using many different modalities to try to solve the complex issue of preventing DFU.

Measuring both shear and normal force adds complexity to the overall system. There is evidence that shear is important, but it is still unclear what the relative importance of shear, normal and other factors are. It wasn't until 2005 that shear was recognized as an underlying cause for pressure ulcers by the National Pressure Ulcer Advisory Panel [16]. Pressure mats and in-shoe research only measure normal stress as of writing, there needs to be more development in technology capable of combining many of these measurable variables in one package to monitor the condition more closely in diabetics feet. The possibility of added measurements like moisture and temperature are also important to consider as they would give a complete picture of the environment in the foot. This thesis works to establish a normal and shear stress sensor that can be the starting point to a brand-new device capable of mapping the environment in vulnerable diabetics' feet.

1.3.3 Pressure Ulcer Diagnosis, Monitoring & Prevention

The road to diagnosis for DFU is a combination of self-monitoring and regular checkups. As has been described before, often diagnosis happens late in the development of the disease. It is often prescribed that there be annual screening for DFU and the American Diabetes Association has developed a test that can be performed rapidly with minimal equipment called the Comprehensive Foot Examination and Risk Assessment [36]. According to the examination of the foot, there are weighted priorities based on the severity of the foot's condition, for example, "urgent" requiring an immediate consultation with a doctor, and "low" requiring a second look within a month of the consultation (Figure 3). The severity is graded based on the presence of some common symptoms including the loss of protection sensation (LOPS), Charcot arthropathy, open wounds, and vascular compromise based on PAD assessment of different pulses (These terms will be discussed in detail, in the coming parts). The general risk stratification pathway can be found in Figure 3. LOPS is a procedure for measuring the loss of sensation on the plantar surface of the foot, it is an indicator of early neuropathy. There are five simple clinical tests that a doctor can do to diagnose LOPS and these include using different tools and modalities to gather information about how deep and relevant the loss of sensation is

[37]. The tests use a variety of different tools which include a 10-g monofilament, 128Hz tuning forks, a disposable pin for pinprick sensation testing. Tests of ankle reflexes and vibration perception [30] are performed. These evaluations are to be done by medical professionals. They are based on accessing the responses of the patients - most of them have the patients answer simple yes or no questions as to whether they sense the object or vibration.

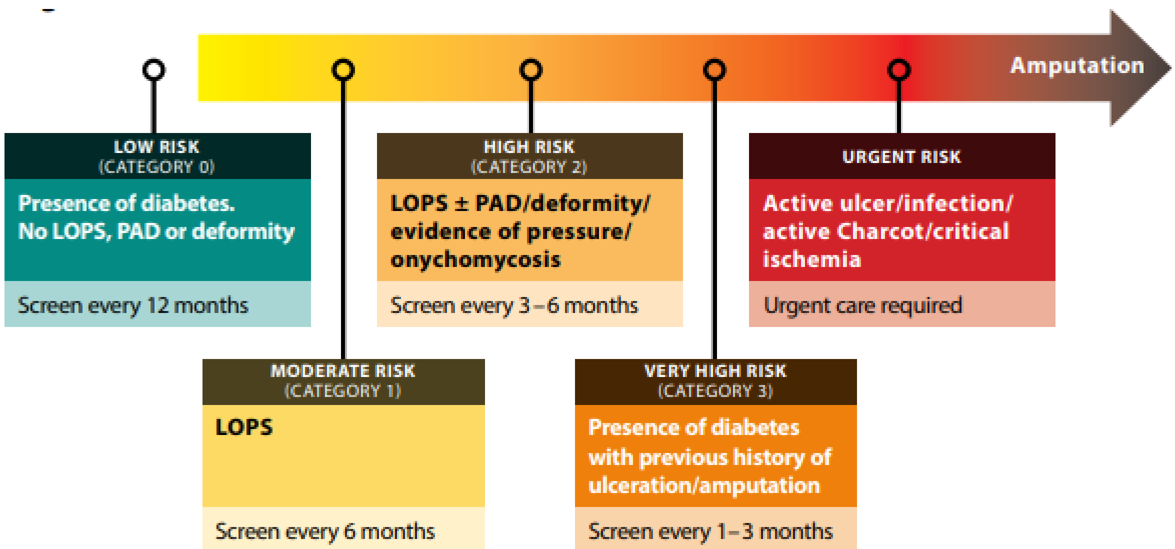

Figure 3: Risk Stratification of DFU with diagnostic assessment results as disease progresses [7].

Charcot arthropathy is diagnosed based on general observation of the muscular and bone condition of the foot. Generally, Charcot arthropathy is described as a unilateral red or swollen flat foot with profound deformity [38]. It elevates the urgency of the assessment because the deformities of the foot can put the patient in higher danger of developing DFU. The same goes with the presence of open wounds in the overall dermatological assessment, which checks also for nail dystrophy (distortion and discoloration), calluses, and abnormal erythema [39]. Lastly is the vascular assessment of the lower limbs, in particular the ankle and foot. Since PAD is relevant in DFU patients it is important to diagnose. This is done by palpating the posterior tibial and dorsal pedis pulses, and are characterized as either “present” or “absent” [40]. If there is an “absent” pulse, patients should go through an ankle-brachial pressure index test which is used to further access the foot’s health and needed to determine the next steps in the diagnosis and treatment.

Monitoring of DFU goes hand in hand with diagnosis, but also includes self-assessments of individuals, which is important to gain confidence or alert patients when they should seek further treatment. Self-assessment is not broadly defined as clinical assessments but includes similar questions that patients can answer from examining their own feet. Questions included in a self-assessment generally help determine if there are any deformities, wounds, calluses, or discolorations [41]. Given the answers to these questions, the patient can access their condition between checkups, which are still encouraged even if the patient is self-assessing. The checkups are also graded based on the risk factors that a patient has towards developing DFU’s. In short, these include age, history of ulceration, and other diagnoses relevant to DFU, like PAD and Charcot arthropathy. The monitoring of the feet has not advanced from these methods and warrants an approach by technology to be able to prevent and monitor the condition of the feet without relying on the individual's diligence to check and their knowledge base to spot a problem. These methods are not wholly ineffective, but early signs can be missed, and recommendations are often not followed properly (checking every week for example).

Prevention and treatment of DFU can be divided into various approaches including offloading devices, wound treatment, and surgical options. While the prevention of DFU is interlinked with the monitoring and assessment of the condition of the foot, various offloading devices can improve the condition. Often these devices work to remove or offload the stresses that are responsible or prevent the healing of pressure ulcers. Also, these devices improve the gait of DFU patients because they often change gait patterns based on wound location or deformities on the foot. Offloading devices can include insoles, shoes, and casts that all work to control the environment of the foot. Figure 4 gives a thorough overview of the options available to diabetics, and what complications they should be used for. Casts are removable molded boots or contact casts that are specific to the foot they were designed for. The issue with these is that they don't change with the foot as the disease progresses, so they are more expensive to replace than common insoles and therapeutic shoes that work to comfort the foot without precise manufacturing. The device that is being envisioned in this thesis tries to implement itself in these common offloading devices to give more information to the user and warn of potential ulcer formation. It might also be beneficial to prescribe these types of devices earlier to warn of some of the first ulcers that form faster than conventional checking or visits.

Wound treatment is specified on whether there is an infection, the localization of the ulcer, and the progression of the wound. Decisions at this stage are very important because of the implications of surgical options if not treated properly. Non-treated wounds can lead to enough damage or infection that they can affect deeper tissues. Infections that reach major vessels, start infecting bone, or are severe enough to alter the foot completely often are considered lost and require amputations. Before it gets to this stage though, there can be multiple surgical corrections that can be done to prevent further complications. These include surgical debridement that removes suspect tissue or artificially molds tissue to help shape the foot more naturally [42].

Offloading Device Choices

Offloading Device		Wound Location				Advantages	Disadvantages
		Toes	Forefoot	Midfoot	Heel (Rearfoot)		
Total contact cast (TCC)		✓✓	✓✓✓	✓✓✓	✓✓	•Gold standard •Reduces pressure under ulcer site between 84 and 92% •Custom moulded to shape of foot •Most studies indicate the shortest healing time as 8 to 12 weeks •Forced patient adherence to device	•Requires a trained professional to apply weekly •Can result in secondary ulceration with improper application •Contraindicated for infected or ischemic wounds; use with caution for heel ulcers •Difficult to sleep with •May prevent patient's ability to work •Patient may not tolerate device
Cast walker		✓✓✓	✓✓✓	✓✓	✗	•Effective at reducing plantar pressure at ulcer site with peak pressures similar to TCC •Can be used for infected wounds •All clinicians can be trained to apply •Same device can be used for the full the duration of treatment •Can be made irremovable with the application of a cohesive bandage to become an Instant Total Contact Cast (iTCC) (see below)	•Generic fit to the foot •Complicated by patients not wearing the device as prescribed because it is removable •Use of removable device results in longer healing times •Patient needs time to learn how to use device •May prevent patient's ability to work •Contraindicated for those with heel ulcers and poor balance
Instant total contact cast (iTCC)	 	✓✓✓	✓✓✓	✓✓	✗	•Cast walker made irremovable with the application of a cohesive bandage to become an iTCC •Same advantages as the Cast Walker •Same device can be used throughout the duration of treatment – and will require a change of the irremovable component	•Generic fit to the foot •May prevent patient's ability to work •Patient may not tolerate device
Half shoe (forefoot)		✓✓	✓✓	✗	✗	•Transfers pressure to mid-foot and rearfoot by eliminating propulsion •Low cost	•Very unstable •Contraindicated for patients with gait instability •High risk of falls
Half shoe (rearfoot)		✗	✗	✗	✓	•Low cost	•Difficule to ambulate

cont'd. . .

Offloading Device Choices

Offloading Device		Wound Location: Toes	Forefoot	Midfoot	Heel (Rearfoot)	Advantages	Disadvantages
Surgical shoe		❣	✓✓	❣	❣	•Low cost •Accommodates edema •Good for short-term management	•Offloading properties are limited •Use with orthotic or insert devices •Not ideal for activity
Over-the-counter walking footwear		✓	✓✓	✓	✓	•Affordable •Easy to access •For preventative care	•Offloading properties are limited •Use with orthotic or insert devices
Footwear modifications (rocker toe)		✓✓	✓✓	✓	✗	•Moves pressure from forefoot to rearfoot	•Requires trained professional to apply •Expensive
Custom-made footwear		✓✓	✓✓	✓✓	✓✓	•Distributes pressure under foot evenly •Ideal for foot deformity	•Requires trained professional to apply •Very expensive
Custom-made orthotics		✓	✓✓	✓✓	✓	•Distributes pressure under foot evenly •May be used with over-the-counter footwear	•Requires trained professional to apply •Expensive
Padding		✓	✓	✓	✓	•Low cost •Easily modified	•Offloading properties are limited •Can cause increased pressure at wound edge
Crutches/cane		✓	✓	✓	✓	•Low cost •Adjustable •Walking aid to support balance	•Offloading properties are limited •Can cause shoulder dislocation

✓ = indicated; ✗ = contraindicated; ❣ = can be used

Figure 4: Off-loading device choice based on ulcer location, advantages, and disadvantages [43]**.**

1.4 Current State of Technology

People with diabetes have the arduous task of self-assessing and making sure they visit their health professional regularly to avoid any complications, especially individuals with many risk factors that can contribute more to DFU development. Recent technology has leveraged the information that we know about the formation of pressure ulcers to develop devices and techniques that get closer to measuring the breakdown and progression of the disease. On one hand, technology that has been used for many years to diagnose and investigate gait issues like pressure pads and pressure gradients has been the basis for new emerging diagnostic and monitoring tools in DFU, these will be discussed in the following sections. Other technologies use the activity as a measurement of well-being and lessening risk factors for patients. The use of accelerometers and prescribed exercise go a long way in preventing some underlying conditions that worsen DFU outcomes. Lastly, is the on-the-go monitoring that can be achieved by incorporating the pressure mapping technology onto a shoe. This allows for the measurement of critical normal stresses during everyday activity and can also double as a gait analyzer while the disease progresses.

1.4.1 Pressure Pads/ Plates

Vertical (normal) plantar and shear stresses are some of the key measurable factors that actively progress the formation of pressure ulcers on the feet. The standard practice to measure these values is by using pressure plates that are placed flat on the ground [44]. By using this technology, we have been able to discern differences in the pressure profiles of a diabetic with pressure ulcers versus a healthy individual. The studies using flat and uniform sensor arrays work to define the basis of replicating this technology in shoes and gives us the parameters by which the ranges for normal and shear stresses were developed.

The forces measured at the plantar foot are dependent on the condition of the foot, history, and many physiological parameters, as has been described previously. Pressure mats and plates have been used to study the peak pressures found in patients with diabetes with ulcers and many studies indicate that peak pressure, pressure gradient, and particularly forefoot pressure are elevated in these individuals [45], [46]. The peak pressure is also elevated where ulceration is located [47]. While this might seem unintuitive since we usually think that patients with wounds will put less pressure on the injury, it is important to remember that these patients may have peripheral neuropathy and so will not feel superficial wounds. They may only be aware of them when they have progressed into more dangerous stages.

The role of shear stresses has not been studied extensively. It has not been until recently that shear pressures have been accepted as a major contributing factor to ulcer formation [16]. One study looks at shear forces on the heel based on heel height that is being worn, which could emulate the increased pressures that neuropathic patients experience. The study concludes that the increase in shear stress is present with increased normal stress on the heel and it affects all other measured stresses on the foot (hallux, metatarsal heads) [48]. In another study that looks at the shear stresses of neuropathic patients more closely, the authors had to invent their measuring array, since no mat or plate exists in the market that also measures shear. This study showed that in diabetics there is an increase in shear-time integrals and elevated shear for an extended amount of time relative to healthy subjects [49].

1.4.2 In- Shoe Technology

In-shoe systems, or systems that would be used in the shoes of patients whether is in the form of an insole or embedded into the shoe itself, can be an effective way to allow the use of sensor technology in vulnerable populations. There has been a good number of studies investigating the effect of physical activity regimens, offloading devices, and even the use of accelerometers to predict the formation and development of pressure ulcers. While these studies offer insight into changes in gait and behavior, some nuances might be missed without measuring the environment of the foot itself and could delay an observation of change that happens closer to the site of the ulcer.

While accelerometers and physical activity regimens go a long way in trying to prevent the development of ulcers, often these suffer from a drop in compliance and don't offer a complete solution for what is already a very sedentary group of patients. Monitoring of these stresses in the shoe could go a long way in providing warnings or even offering data to clinicians that can be faster and more informative than self-assessment, to give more impactful follow-ups. As it stands now, there are no commercially available in-shoe technologies that measure shear stresses for diabetics. Only a handful of in-shoe systems are available and are mainly used in the study of the disease in the academic setting. A brief market analysis of available in-shoe technology can be seen in Table 1. Most of the technology only focuses on normal pressure capture and none has shear pressure capability. Three specific systems in this list have been studied for validity and repeatability (Medilogic, Tekscan, and Novel, see Figure 5). The study reports that the Medilogic and Tekscan systems are more precise in the ranges of 200 to 300 kPa, while the Novel Pedar system is reliable along with all its ranges [50]. The technology is mostly consistent between many of the systems, utilizing miniature transducers or completely flat transducers that measure pressure based on piezoresistivity. Only one system uses capacitive sensing and that is of X sensor and their motion research insoles. Some systems also include step count and temperature, like the Sensory insoles from Orpyx. Temperature can also be an indicator of the present pressure ulcers as mentioned earlier [17]. The mark-up price for many of them makes these systems unreachable by the common individual without help from insurance-based assistance. A cheap but effective in-sole system is needed to reach many able diabetics willing to use technology in preventing pressure ulcers. This thesis looks to create sensors with inexpensive materials that measure both pressure and shear to be implemented in similar in-shoe systems that might reach these patients in need.

Figure 5: Three in-shoe measurement devices, Tekscan F-scan top left, Medilogic Insoles top right, Novel electronics Pedar on the bottom.

Table 1: Commercial analysis of in-shoe pressure measuring devices

System	UBC Sensors	Sensory Insoles	Pedar	F-Scan	Motion Research Insoles	StepLab	Medilogic Insoles
Company	UBC	Orpyx	Novel	Tekscan	XSensor	MoveSole	Noraxon
Use	Research	Health/Research	Health/Research	Health/Research	Research	Research	Research
Shear Capability	✓	x	x	x	x	x	x
Normal Stress Range (kPa)	0-1000	0-30	0-600	0-862	0-883	0-75	0-640
Resolution (kPa)	2	2.5	2.5	4	0.07	?	?
Price (CAD)	?	?	$21,000	$23,000	?	?	$17,500

1.5 Sensor Specifications

The specification for the sensor described in this thesis was researched based on the devices and abundance of literature related to DFU, pressure gradients on the plantar foot, and previous investigation of pressure mat specifications. These parameters can be found in Table 2. The sensing area is defined by the existing sensor utilized in our laboratory (see methodology section). This is comparable with studies that have defined the minimal measuring to be about 5 x 5 mm [51]. Pressure ranges were derived from accepted ranges for many pressure measuring mats and devices and to keep the sensors comparable to the competition, 1 MPa (1kN of force) was defined as the maximum normal stress to be measured.

The specifications represent an evolving estimate. For normal force, and empirically speaking, we estimate the load needed by assuming a weight of 75 kg, and convert it to newtons, which gives us 735.8 N. Now the area that is contacting the ground is different depending on what stage of the cycle we are in, but the smallest area that the foot will contact the ground with is when the heel strikes at the beginning of the cycle. This area can be calculated by taking the foot length, which is generally defined being 0.152 of an average height of 180 cm, measured to be about 27.4 cm, and then multiplying by 0.15 to get the heel radius of 4.1 cm [52]. Convert this into the area and you have 0.0053 m^2, which divided by the force on one foot, gives a max pressure of 139 kPa. Even if you were to take the last stage of the gait cycle, which is toe liftoff, and you concentrated all the force on the big toe, assuming an average toe is 50 mm by 30 mm, you would have a max pressure of 491 kPa [53]. Of course, this analysis doesn't consider momentum or the angle the heel or toe are contacting but in the general sense, it gives an idea of the forces experienced.

In terms of shear stresses, there is very little literature, but of the little that is described, there seems to be a range of around 150 to 200 kPa of max pressures experienced by patients [16]. To investigate this more deeply, a look at the definition of shear modulus can help us define the maximum amount of displacement that we need to use to achieve these kinds of shear pressures. First, we can take a simplistic look at having all the force from our total weight (75 kg) be experienced while shearing in a walk cycle. If we assume that the averaged acceleration of walking from stance-to-stance phase is 2.0 m/s^2, then using $F= ma$ we can get the force experienced in the direction of walking to be 150 N. Converting this into shear strain using the previous area calculated for the heel (0.0053 m^2), we get shear stress of 28.3 kPa. The relationship of shear modulus to shear strain can be calculated by multiplying the shear strain ($G\varepsilon_{shear} = \sigma_{shear}$, where G is shear modulus, ε_{shear} is shear strain and σ_{shear} is shear stress). Here we need to know the shear modulus of the material we ultimately used if we assume the shear modulus of Dragon Skin 10 to be 71 kPa [54]. Using this we can calculate the shear strain, which is around 28%. Shear strain is defined by the displacement in the direction of shear divided by the thickness of the dielectric area ($\Delta x/t$). Using this definition and a thickness of dielectric of 1.5 mm (See sensor overview in the Methods section) we get a displacement of 4.2 mm. Given that our sensor will be using a different mixture of materials with varying shear moduli and the thicknesses will also vary, this number will change when the experiments are performed. This example gives us an idea of the displacements needed and of the calculations used. This thesis will also work to try to define this number better when testing the system experimentally and add to the literature on shear sense.

The frequency of measurement that is needed is a consequence of what is necessary to measure in the environment of the shoe. Since this sensor is being targeted as an active monitoring system, it needs to refresh fast enough to capture meaningful events during activity. Initially, these sensors are targeted for a more sedentary lifestyle that includes standing, sitting, and walking. The refresh rate is needed is estimated based on the gait cycle of walking at an average speed of a healthy 40 to 49-year-old, which is 1.4 m/s [55]. When the gait cycle is broken up into its components there are two main sections, the stance phase, and the swing phase. We are primarily interested in the stance phase because this is the phase where the foot starts and stops to contact the ground [56]. The stance phase can then be subdivided into 5 different stages: heel strike, loading response, mid-stance, terminal stance, and pre-swing. The stance phase takes about 60% of the overall gait cycle and if we convert the normal speed of walking to steps per second, consider that one step is the cycle of one foot, we need to scan each foot every second. To capture the individual stages, we divided the total time (600 ms for the stance phase) by 5 to get the time for each section, which is 150 ms. Converting this to a frequency we get about 70 Hz, this is the speed that we need the sensor to operate at if we want to measure the gait cycles once. Multiply this by ten then we have ten points of data per stage, and we get our final number.

Table 2: Desired Device Specifications

Parameter	Value
Sensing Area (mm)	11 x 11
Normal Pressure Range (kPa)	0-1000
Normal Pressure Resolution (kPa)	5
Shear Pressure Range (kPa)	0-200
Shear Pressure Resolution (kPa)	2
Refresh Rate per Taxel (Hz)	70

1.6 Thesis Overview & Research Question

This thesis works to adapt previously accomplished work in our lab which has focused on creating sensitive artificial skin for the use of humanoid robots. The adaptation is to make these normal and shear stress sensors into capable measurement tools to measure forces in the foot of a diabetic. The main goal is to have a very similar sensor characterization that has been done repeatedly with our sensors in terms of normal as well as shear stress. To begin with, the thesis looks at implementing newer, stiffer materials that can withstand the forces described in the sensor specification. This includes a thorough mechanical characterization of three different materials (Ecoflex 00-30, Dragon Skin 10, Sylgard 184.) Similarly, concerning stiffer materials, they need to be able to shear without applying too much force - so there is a limit to how stiff the materials can be. A way to get around this is by changing the dielectric of the sensor so that the overall structure buckles and shears. The thesis looks at the stiffer materials and a variety of pillars and pitches to find a stiff enough formulation that can shear as well. All this characterization is done in two thickness formats, one thinner (3.5 mm) that closely resembles the previous sensors and represents a very thin insole, while another is a thicker (6.5 mm) insole that is closer to the cushioning insoles used as offloading devices. The information from this mechanical study will inform subsequent work including the construction of sensors that will be electronically characterized both for normal force and shear forces. These sensors will also be tested using a less standardized method by stepping on the sensor like it would be in real-life situations using a simulated walking task. Lastly, in terms of sensor design, the thesis looks at what an insole that would include these sensors might look like, with the guidance of a professional orthopedic surgeon and how this insole might be constructed, and its specifications.

This thesis operates to introduce an innovative pressure sensor design that includes the elusive shear capability that is missing from many in-shoe monitoring devices, all while using inexpensive materials that are skin-friendly. The document also helps to expand knowledge around the sensors that our laboratory has developed to higher forces in both modalities and encourage the use of this sensor to many different applications that go beyond artificial robot skin or diabetic pressure ulcer detection including gait analysis, bedsheet, and wheelchair cushion monitoring, smarter pressure sheets and much more.

Chapter 2: Methodology & Experimental Design

In this chapter, we will be covering the methodology used in this thesis including the basics of the sensing technology, manufacturing the sensors, experimental setup, and administration. The sensor basics go over the governing principles of well-established sensor technology from our lab. We then delve into how the sensors are manufactured and what materials are used in each step. The last sections of the chapter will go over each experimental section (normal stress, shear stress, and real-life characterization). Detail about experimental setups and a run-through of the steps taking for each experiment will be covered. Lastly, in the last section, we will cover the investigation of a full device that this technology could be used in. The discussion of this device will inform future work that will be covered later on what steps need to be taken for this to be fulfilled and more.

2.1 Sensor Overview

The development of a smart insole follows a trend in our laboratory to apply novel sensing technology to medical applications. In this case, we are taking previously described artificial skin sensors developed by a postdoc in our lab, Dr. Mirza us Sarwar. These sensors have evolved from being a gel-based, ionic liquid architecture, to now an elastomer-based pressure and shear sensor [55], [56], [57]. As described before, these sensors were designed for the grasping and sensing of objects by the hands of robots. The sensor is capacitive and uses readily available elastomeric materials to create soft and stretchable sensing that mimics skin. One project in the laboratory is looking to expand this idea into sensing pressure in medical applications by investigating an array format of the sensor to measure pressure ulcer formation in SCI patients after prolonged sitting or lying on a bed. In this instance, prolonged pressure is the measurable variable that is used, and a detection system is being developed to warn caregivers of the potential location of pressure ulcers. The future of this project looks to implement an all-in-one device that can relieve the increased pressure detected by using a pneumatic system. The thesis at hand works to contribute to this trend and use the existing design with the help of stronger materials to develop a sensor capable of measuring normal and shear stresses found in the shoes of diabetics.

This chapter highlights the principles behind the technology being used, primarily a capacitive based normal and shear stress sensor, the materials being investigated to achieve a linear deformation under higher loads, and the electronics being used to read out and display the information. The following chapter will then take this information and explain the various experiments used to characterize the sensors mechanically and electrically.

2.2 Working Principles

2.2.1 The Capacitive Sensor

Through the formulation of the original flexible normal/shear stress sensor, there have been many iterations of the sensor, which in turn have worked to decrease the coupling capacitances between traces and include more features than that of a single taxel (measuring point) basic sensor. As can be seen in Figures 6 & 7, the "base" sensor consists of one main excitation electrode on one side and four sensing electrodes on the other with a dielectric layer of patterned pillars that act as a separation barrier between electrodes as well as a buckling mechanism for shear. The sensor is mainly made of Ecoflex 00-30 (*Smooth-On US*) which is a silicone-based elastomer readily available for a variety of applications ranging from prop making to caulking. The conductive electrode is made of a mixture between conductive carbon black and the Ecoflex 00-30. Traces are guided away from the electrodes so that they can be crimped to a metallic piece and soldered onto a PCB board where the capacitance data can be measured. The second iteration of the sensor worked to decouple the “trace-effect” that happens when interfering crossing traces on one side of the sensor interact with the other side and also to themselves, this sensor is lovingly called the “Sandwich” sensor. As seen in Figures 6 & 7, the sandwich ground electrode decouples the crossing traces between the two sides with a grounding layer in the middle while also allowing the trace fields to reach the other side of the sensor in the middle where the excitation sensor and the sensing electrodes align. It is this sensor that is carried forward into this thesis for further analysis, but before looking at the materials being investigated, the underlying working principles of the sensing need to be described.

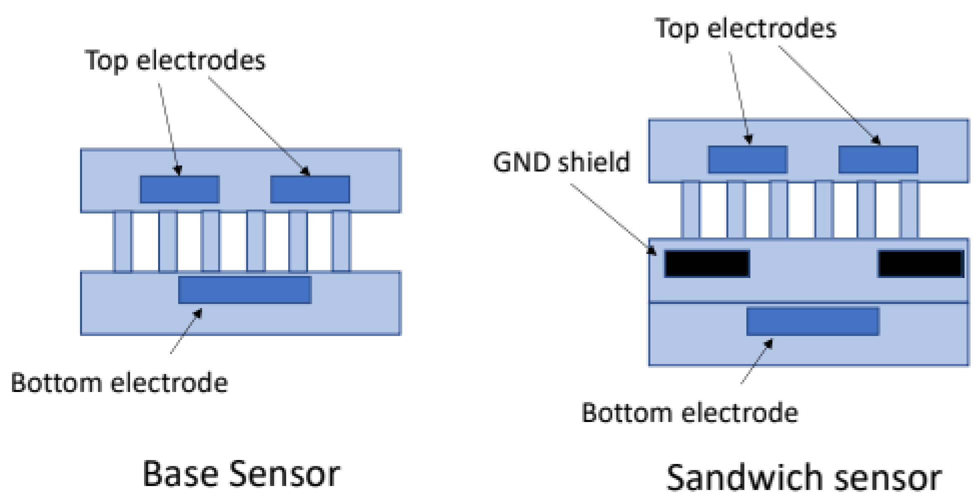

Figure 6: Cross-section of the base and sandwich sensors showing top and bottom electrodes and pillared dielectric layer.

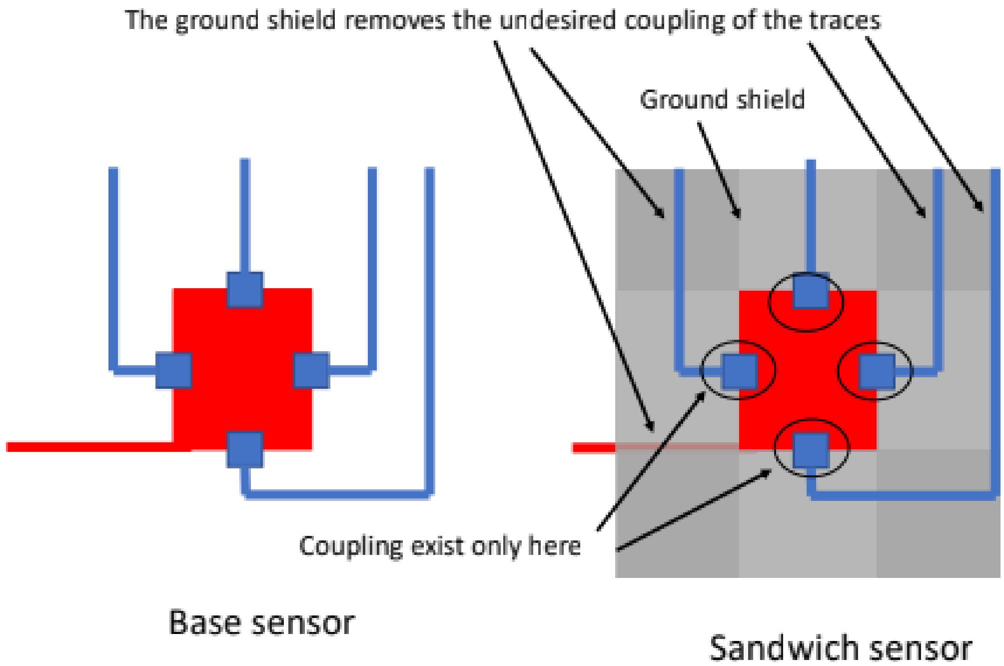

Figure 7: Overhead view of the two sensor iterations showing underlying grounding plane

2.2.2 Normal Stress Measurements

The sensor measures normal pressure using the generic formula for a parallel-plate capacitor. As pressure is applied from the top, the electrodes get closer together which causes a decrease in capacitance according to Equation 1. The change in capacitance is governed by the dielectric material properties, the size of the electrodes, and the distance between the electrodes. With our sensor we have four sensing electrodes, so essentially, we have four pressure taxels that couple with only one bottom excitation electrode. In the simplest terms, the bottom electrode is exposed to incoming voltage from the capacitive sensing chip, which excites the electrode and projects electric fields into the dielectric. The fields then couple with the sensing electrodes and that is read on the capacitance chip as a voltage.

$$C = \epsilon_r \epsilon_O \frac{A}{d}$$

Equation 1: Parallel-plate capacitance equation where ϵ_r and ϵ_o are the dielectric constants of the material and air respectively, A is the area of the overlapping electrodes and d is the distance between them.

The dielectric structure has become interesting to look at concerning capacitive sensors because the geometry of the dielectric can essentially change the material properties and in turn the change in capacitance. One study has looked at the difference between microstructures and the difference in capacitance concerning pressure [58]. While dielectrics affect the overall sensitivity of the sensors, their effect is also important in the shear aspect of the sensor, which will be covered in the next section. As can be seen in the results section of this thesis, a pillar architecture, similarly used in the sandwich sensor characterization, is not strong enough to hold the pressures needed in this environment, and a solid dielectric architecture was used for the final sensor formulation.

2.2.3 Normal Stress Plus Shear Stress Measurements

The way that the sensor is designed allows for the measurement of shear on the horizontal axis parallel to the ground. In this section, the method of interpreting the changes in capacitance of the four top electrodes concerning the bottom electrode is outlined. In Figure 7, two opposite electrodes from top to bottom are used to estimate shear in one direction, while the other two from left to right measure the other direction. The main principle regarding the capture of shear in the sensor follows again the same idea of parallel-plate capacitors, but now shearing past one another. The capacitance measured is based on the overlapping areas between the top and the bottom electrodes and can be seen clearly in Figure 8. To mathematically solve this, Equation 1 can be expanded to include two capacitances for each electrode in one direction and each has a third parasitic capacitance. The area is then expanded and the difference in shear displacement is added to result in Equation 2. When you combine two of these equations, C_1 and C_2, in one direction and assuming that the width and length of the two sensing electrodes are the same, then a combined capacitance-dependent shear equation can be formed (Equation 3). The equations are derived on the assumption that parasitic capacitance is affected very little by the displacement. The change in capacitance assumes a parallel plate interaction between the top and bottom electrodes, which changes linearly with the overlap, and that the additional parasitic and fringe capacitance components effects can be neglected. This approach has been shown to work by Sarwar *et al.* [ref his unpublished paper], including the ability to separate shear and normal force, following the method now discussed.

The picture changes when normal stress is applied at the same time as shear, and now two relative electrode displacements are changing simultaneously, one parallel to the sensor surface and the other in the thickness direction (Figure 9). Rearranging Equation 2 to include a change in displacement (η) and partially solving for shear again, we get Equation 4. For normal strain, we can add all the changes in capacitances together, and rearranging we get Equation 5.

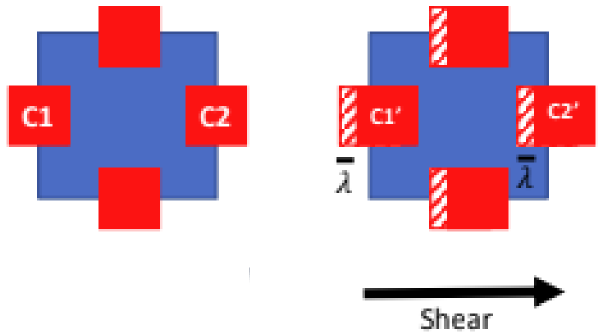

Figure 8: Overlapping area between bottom and top electrode changing based on applied shear. Red are the sensing electrodes and blue is the excitatory electrode. The dashed white sections denoted by λ indicate the change in displacement after applied shear.

$$C_1' = \epsilon_r \epsilon_O \frac{L_1\, x\, (W_1 + \lambda)}{d} + C_{p1}$$

Equation 2: Parallel-plate capacitance equation with width (W) and length (L) defined and parasitic capacitance added. λ is the difference in displacement after shear is applied.

$$\lambda = \frac{\Delta C_1 - \Delta C_2}{\frac{2\epsilon_r \epsilon_O}{d}}$$

Equation 3: Shear-only equation for displacement along one axis and dependent on change in capacitance between two electrodes (C_1 and C_2.)

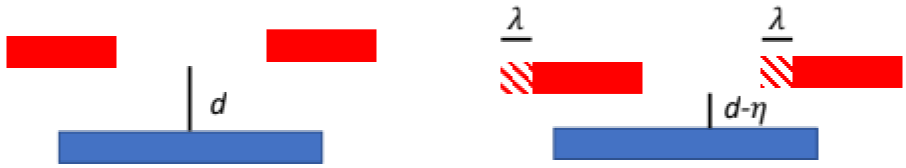

Figure 9: Change in displacement based on applying shear and pressure at the same time on the sensor.

$$\frac{\epsilon_r \epsilon_O W\lambda}{d} = \frac{C_2 C_1' - C_1 C_2'}{C_2' + C_1'}$$

Equation 4: Shear displacement equation when simultaneous normal pressure and shear are applied

$$\frac{\eta}{d} = \frac{\Delta C_1 + \Delta C_2 + \Delta C_3 + \Delta C_4}{C_1' + C_2' + C_3' + C_4'}$$

Equation 5: Normal strain equation when simultaneous normal pressure and shear are applied

2.3 Materials

In this section, we will cover the materials used and investigated as part of this thesis. Here we introduce the materials that make up the sensor, the elastomeric base, conductive material, and tools used to mold and shape these. Then we look at how the sensors are manufactured and what methods and materials we used to do so.

2.3.1 Bulk/Dielectric Material

The base of the sensor is made of an elastomeric component. In this thesis we will be using three main materials as the elastomeric component: Ecoflex 00-30, Dragon Skin 10 (*Smooth-On US*), and Sylgard 184 (Dow). We chose these materials specifically because they are similar to each other in composition and material properties. The one big difference being the stiffness, which increases respectively. All of these are liquid silicone elastomers that are cured by introducing a curing agent. In the case of Ecoflex and Dragon Skin, the curing mechanism is platinum-based. These materials are skin safe for short and long exposures. Ecoflex 00-30 and Dragon Skin 10 are mixed in an equal part A to part B mixtures while Sylgard-184 is made with a 10-1 mix ratio, with one part being the curing agent. All materials were cured at 60°C. Sylgard-184 and other materials have been shown to have different material properties based on the temperature at which they were cured [59].

The difference between the three materials is the resulting hardness once cured, increasing from the Ecoflex version used, which has a shore hardness of 00-30, Dragon Skin of 10A, and Sylgard 184 of 50A, respectively as can be seen in Table 3. The tensile strength, Young’s, and shear modulus also increase from Ecoflex 00-30 to Dragon Skin 10 then to Sylgard 184, as does the curing time for the materials. (Additionally, there is an antifungal version of Dragon Skin 10 which would be important in the application of developing smart insoles.

Antifungal and anti-bacterial materials would be needed for the application of in-shoe insoles and are found in various insoles already used for diabetic foot ulcer management). Ultimately a mixture of 10% Sylgard-184 and Dragon Skin 10 was used as the final formulation of the sensor as this enabled a more linear deformation up to the peak loads expected in the shoe of ~ 1 MPa of normal stress (See more in the results section.).

Table 3: Material Properties for Elastomers used

Material	Ecoflex 00-30	Dragon Skin 10	Sylgard-184
Shore Hardness	00-30	A-10	A-43
Young's Modulus	0.100 MPa [60]	0.560 MPa [61]	1.32 MPa [59]
Shear Modulus	26.2 kPa [62]	71 kPa [62]	600 kPa [62]
Tensile Strength	1.4 MPa [60]	3.3 MPa [61]	6.7 MPa [59]
Curing Time @ 60°C	10 minutes	20 minutes	1 hour

2.3.2 Conductive Material

For the electrodes, carbon black (H30253 Carbon Black Super P® Conductive, 99+%, Alfa Aesar by Thermo Fisher Scientific) and carbon nanofibers (719781 Carbon nanofibers, Sigma Aldrich) were used to create a carbon/elastomer hybrid that could be incorporated into the elastomeric materials. Previously in our lab, experiments have shown that a 10% by weight mixture of carbon black and elastomer (Ecoflex 00-30) gives us stable conductivity when introduced to compression (Figure 10). We see changes in conductivity due to compression in lower concentrations of the carbon black. Mainly we see these changes are thought to occur because, under compression, a hybrid system like this tends to change its path of conductivity at low concentrations, while at higher concentrations the path is more defined and suffers fewer changes [63]. Additionally, the conductivity of the hybrid mixture changes over time, but previous data generated in the lab shows that resistance in the conductive material is more stable in a mixture that contains 5% of the carbon nanofiber mixture (Figure 11). Testing resistance over time gives us an idea of how stable a system is over time. Carbon nanofibers add more conductivity to the system and our laboratory has introduced them into the carbon black/elastomer mixture to reduce resistivity in the system and increase response time. In Figure 11, the introduction of carbon nanofiber reduced the resistance by 10-fold in all the materials and is very stable over time compared to carbon black by itself.

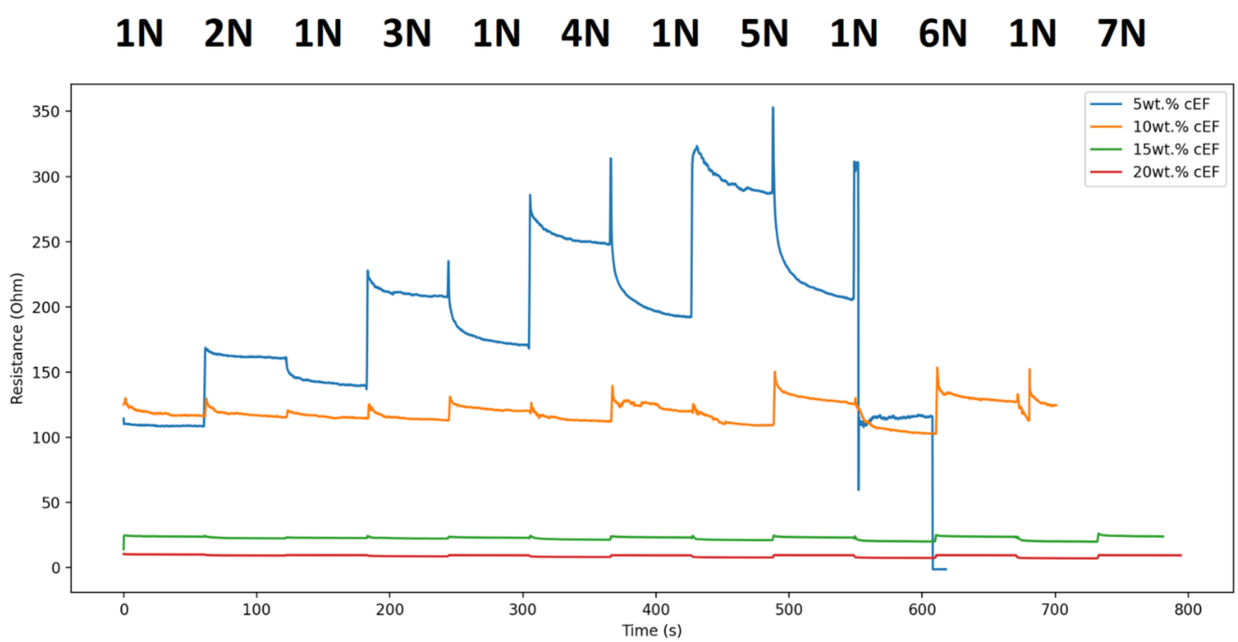

Figure 10: Resistance under compression of varying carbon black weight % and increasing force. cEF stands for carbon black mixed with Ecoflex 00-30. The numbers on the top represent the force applied at that instance. After 5N the experiment was stopped.

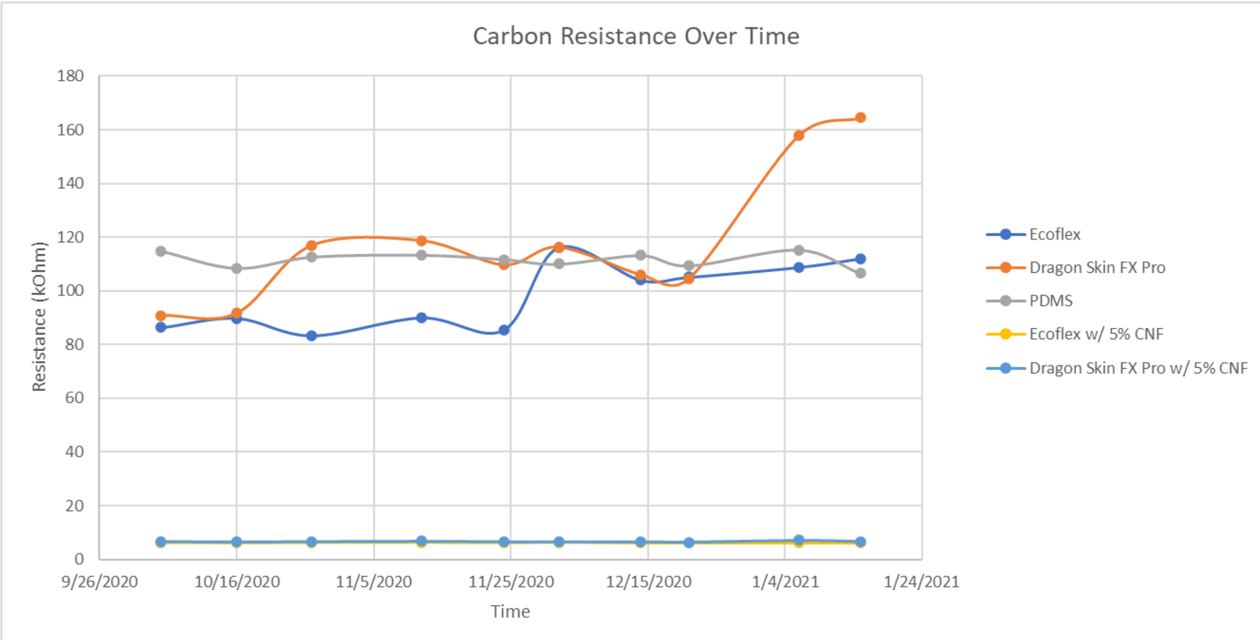

Figure 11: Resistance over time in carbon black/carbon nanofiber composite samples.

2.3.3 Masks and Molds

Laser-cut masks were used to stencil the electrode layers as a part of sensor fabrication. They were created by the laser-cutting transparent film (Staples, Inkjet Transparency Film). There were three mask types used: one for the four taxel electrodes on the top, one for the grounding middle layer, and one for the bottom single electrode (Figure 12). Electrodes in this thesis differ from previously used electrodes in the sandwich architecture because the application demanded higher displacements in shear and the previously used architecture only allows for 1.5 mm total of displacement, based on the overlapping area of the sensing electrodes and excitation electrode. The new design allows up to 2.5 mm of displacement in shear and requires the other masks to be scaled equally. Molds were prepared using fused deposition modeling (FDM) 3D printed material with a FlashForge Dreamer (Zhejiang Flashforge 3D Technology Co, China) and the printing material was acrylonitrile butadiene styrene (ABS) which doesn't bend at the curing temperature (60°C). The molds can be seen in Figures 13 & 14, the details for these will be described in the next section. The indenter for applying force to the samples was printed using Polylactic acid (PLA) with the same 3D printer. It measured 50 x 50 mm^2 so the samples being compressed are always smaller (31 x 31 mm^2).

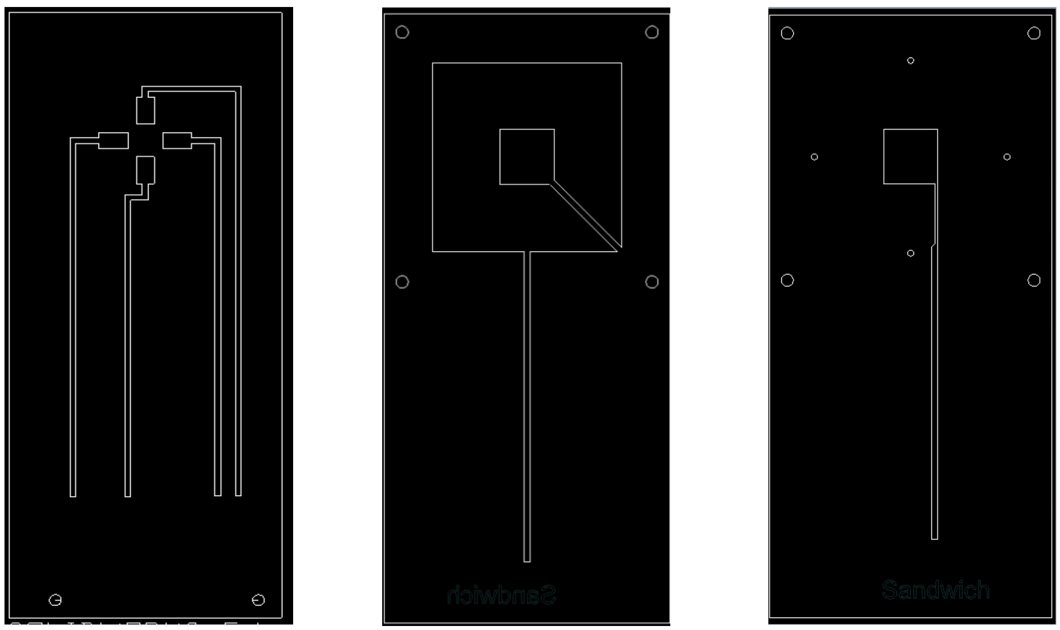

Figure 12. Laser cut masks. Left most mask is used for the sensing electrodes, middle mask is used for the grounding layer in between and right most mask is used for the excitation electrode.

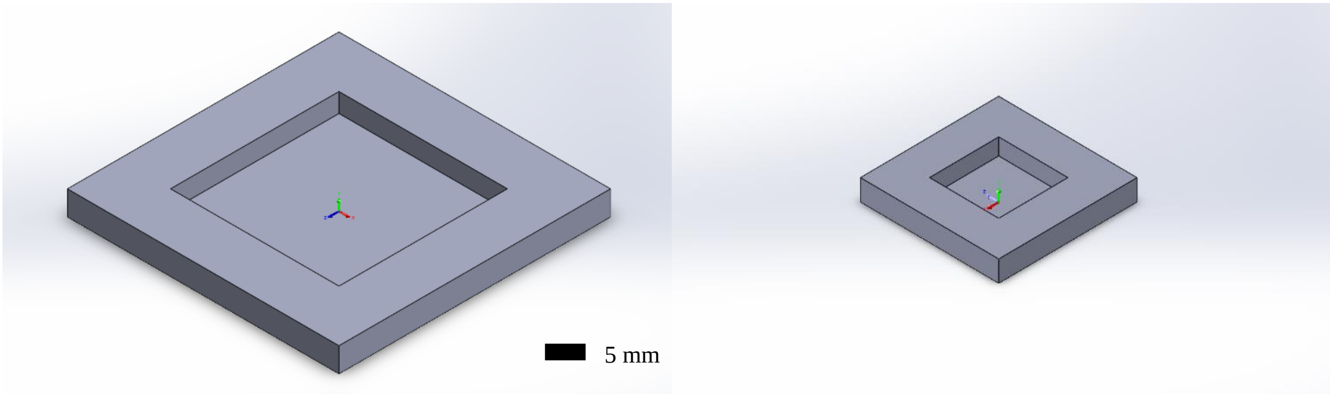

Figure 13. Molds for material testing, left mold for 31x31 mm samples and right one for 15 x 15 mm samples.

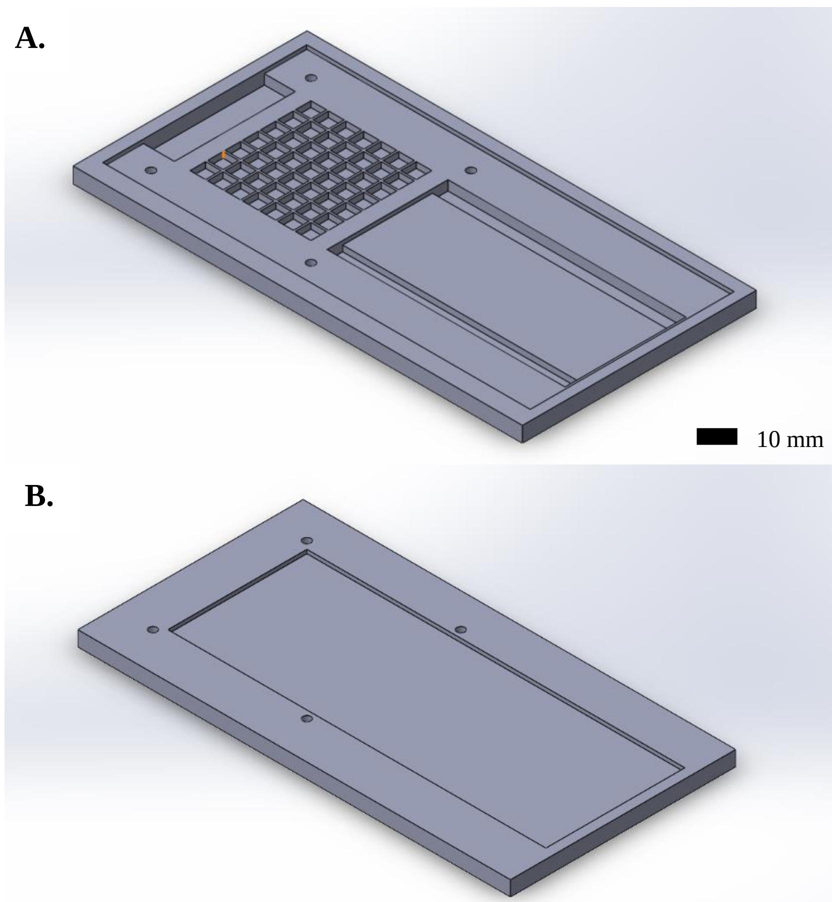

Figure 14. Molds used in material testing and pillar sample fabrication: A. 7x7 pillar dielectric mold, B. 1 mm base mold,

2.4 Fabrication Methods

In this section, the fabrication methods will be discussed. The first part will look at the fabrication method for the samples that were used in material testing. The second part looks at the fabrication of a complete sensor. Finally, the last part looks at fabrication methods of a potential

2.4.1 Sample fabrication for material testing

The material testing of the three selected elastomers consisted of compression testing using an Instron 5969 (Instron USA) with a 2kN load cell (Instron USA) to determine the material response due to increasing strain. Samples of each material were prepared at the size of the sensor plus some clearance for a total size of 31 x 31 mm^2. Several thicknesses were studied to compare the difference between already studied dielectric thickness of 1.5 mm in previous iterations of the sandwich sensor (1.5 mm plus 1 mm for each electrode layer to a total of 3.5 mm thickness) and a thicker, more common thickness for insoles of 6.5 mm with a 4.5 mm thickness of the dielectric. We do not expect thickness to change the measurement range since silicone rubbers and other rubbers are incompressible, meaning that they do not change in geometry when compressed [64]. What this means is that the material will squeeze out of the sides in a bulging manner when compressed. If the thickness is bigger, then there is more room for that to happen before it starts contacting the compressing area. Nevertheless, we will compare the two thicknesses at the same strain applied. Set up for material characterization can be seen in figure 20.

To create the test samples, ABS molds were made to the desired heights (Figure 13), the different mixtures were measured by weight using a scale, vacuum degassed, and then carefully poured into the molds. A glass slide was used to doctor blade the top of the surface to ensure flatness. Samples were then placed in an oven at 60°C to cure for the designated time, listed in Table 3. Once cured, samples were taken out of the oven and carefully removed from molds, any excess substrate was removed, samples were tested on the same day they were made. Similarly, the pillar experiment sample was fabricated by using two different molds (Figure 14). Mold C which is a simple 1 mm thick indentation and mold A, which is the same 1 mm indentation plus a dielectric region measuring 31 x 31 mm. This region was divided up into different pillar dielectric structures by affecting the pitch between them in the same area. Samples were made using 7x7, 6x6, and 5x5 dielectric layers, each pillar measured 4x4 mm and the pitch for each formulation from center to center of pillars were 2.5, 5.4, and 6.75 mm respectively. Once cured, the two sides were glued together using uncured Ecoflex in between and weight was applied for a flat and even adhesion (see last part of Figure 15). Once joined, the samples were cut into 31 x 31 squares and tested using the same parameters as the solid dielectric samples.

For shear material characterization, the method of measuring shear stress and displacing the sample had to be changed from previous methods. The setup that was used to originally characterize the sandwich sensors only allows to measure forces lower than 10 N in all axes. Since we are looking to go up to 150 N of force in the x and y-axis for the plantar foot, this setup would not work. A different setup was devised to measure shear stresses using the Instron machine. Using silicone poxy (Sil-Poxy, *Smooth-On US*) silicone rubbers like Dragon Skin 10 can adhere to plastics and other materials. With some initial testing, it was found that the substrate could adhere much better to glass versus 3D printed plastics that are commonly used in the lab. A setup was made to use two parallel glass pieces that would adhere the sample in a corner so that the setup could be rotated 90 degrees to measure each axis without having to unbind the sample. Each glass piece was clamped on each end and one end moved the distance needed (See Material Testing Methods for more details).

2.4.2 Sensor fabrication

The sensor fabrication method is adapted from previous fabrication methods of single-point sensors that have been developed in our lab. Similar mold types to the ones used for the pillar experiments were used here (Figure 14). The steps for fabricating the sensor are described in Figure 15. There are two streams to fabrication 1 & 2, as seen in Figure 15. Stream 1 is used to fabricate the 4 taxel sensing electrodes. Stream 2 is used to fabricate the grounding electrode that will go in the middle of the sensor and the excitation electrode on top. Both streams follow the same general fabrication method of solid base elastomer shaped into a mold, cure, mask electrode onto cured elastomer, cure, then add a thin layer of elastomer to protect electrodes. The only difference between the two streams is that stream 2 incorporates two electrodes and will have two thin layers of elastomer between the grounding electrode and the excitation electrode to prevent shorting between them.

Now following the steps in order on each stream on Figure 15, the sensor fabrication will be explained in detail A mixture of Dragon Skin 10 and 10% by weight of Sylgard PDMS was used as the substrate for sensor making, was mixed by weight, vacuum degassed then poured into two molds of B from Figure 14. Each mold would follow a different stream, either 1 or 2. A solid dielectric layer was used for sensor fabrication because like described before a pillar dielectric architecture collapses under lower loads than necessary (see Material Testing Results section). The molds were then doctor bladed using a glass slide to ensure flatness in-between steps. Both molds were then placed in the oven at 60°C to cure for about 30 minutes.

For stream 1, on top of the cured elastomer still in the mold, the conductive material is masked using the sensing electrode mask in Figure 12 (Step 1a on Figure 15). The mask was placed on the mold using guiding pillars that would sit on the four corners of the mold to allow for proper location placement of the electrodes on the elastomer. The conductive material for the electrodes was prepared using the more conductive mixture of carbon nanofibers/ carbon black and Ecoflex 00-30. The conductive material was measured by weight to achieve a 10% concentration of carbon black and 3% carbon nanofiber. Conductive material was weighed in a vial which would be placed in a tabletop centrifugal mixer with equivalent Ecoflex 00-30 to achieve a consistent mixture. Once masked, the molds with conductive material were cured at 60°C for 10 minutes. In the last step for stream 1, 1b, tape was placed at the bottom of the trace on the cured conductive material so any further steps would not cover the end of the trace to be used for electrical connection later.

Now for stream 2, once the initial mold was cured of the very initial step, similarly a mask was used to lay down the conductive layer for the grounding electrode using the second mask in Figure 12 (step 2a on Figure 15). The tape was laid down at the end of the trace once the conductive layer had cured for 10 minutes to protect it from the next steps (step 2b). Thin layers were placed using a spin coater at 300 rpm to achieve a layer of 200 microns thick. Two layers were laid down to ensure no shorting between the grounding electrode and the next step (step 2c). Once the spun layers were cured, another conductive layer was masked using the excitation electrode mask in Figure 12 (step 2d). This would cure, and a final spun layer was added to the top of the excitation electrode to finish stream 2 of fabrication to protect the excitation electrode and ensure flatness to the sensor (step 2e).

To put it all together, the two streams were glued together in the final step. The crafted material from stream 2 was carefully removed from the mold and aligned on top of the four taxel electrodes using cylindrical pillars on the corners of the mold in stream 1. The top of the sensor was gently squeezed to remove any air in between, a weight was placed on top to ensure proper adhesion, and the assembly was placed in the oven to cure for 30 minutes

The last step of sensor fabrication is connecting the exposed traces (currently covered in tape) to copper crimp connectors. Firstly, the sensor was dissected to expose all traces from the tape covering them and the layers that were added on top. The traces were trimmed to be able to fit into the crimp easily. Conductive material was prepared in the same manner as previously and a small amount was applied to the open side of the crimp, traces were carefully placed into the opening, pushed into the conductive material, and then crimped. The sensor was then placed in the oven so the conductive material would cure around the trace and in contact with the crimp. The sensor was then tested with a multimeter to check for continuity along all traces. Figure 16 shows a picture of the sensor at this stage. The sensor is then soldered onto the PCB and is ready to be characterized.

An enclosure was made to allow easy-to-use characterization of sandwich sensors, as seen in Figure 17. Inside the enclosure, the PCB is housed, and the sensor rests on top of the flat portion of the enclosure to be available for characterization. Lead traces fold into the middle of the enclosure and to the PCB. Connection to the PCB is made without having to disturb the leads of the sensor, or the sensor itself.

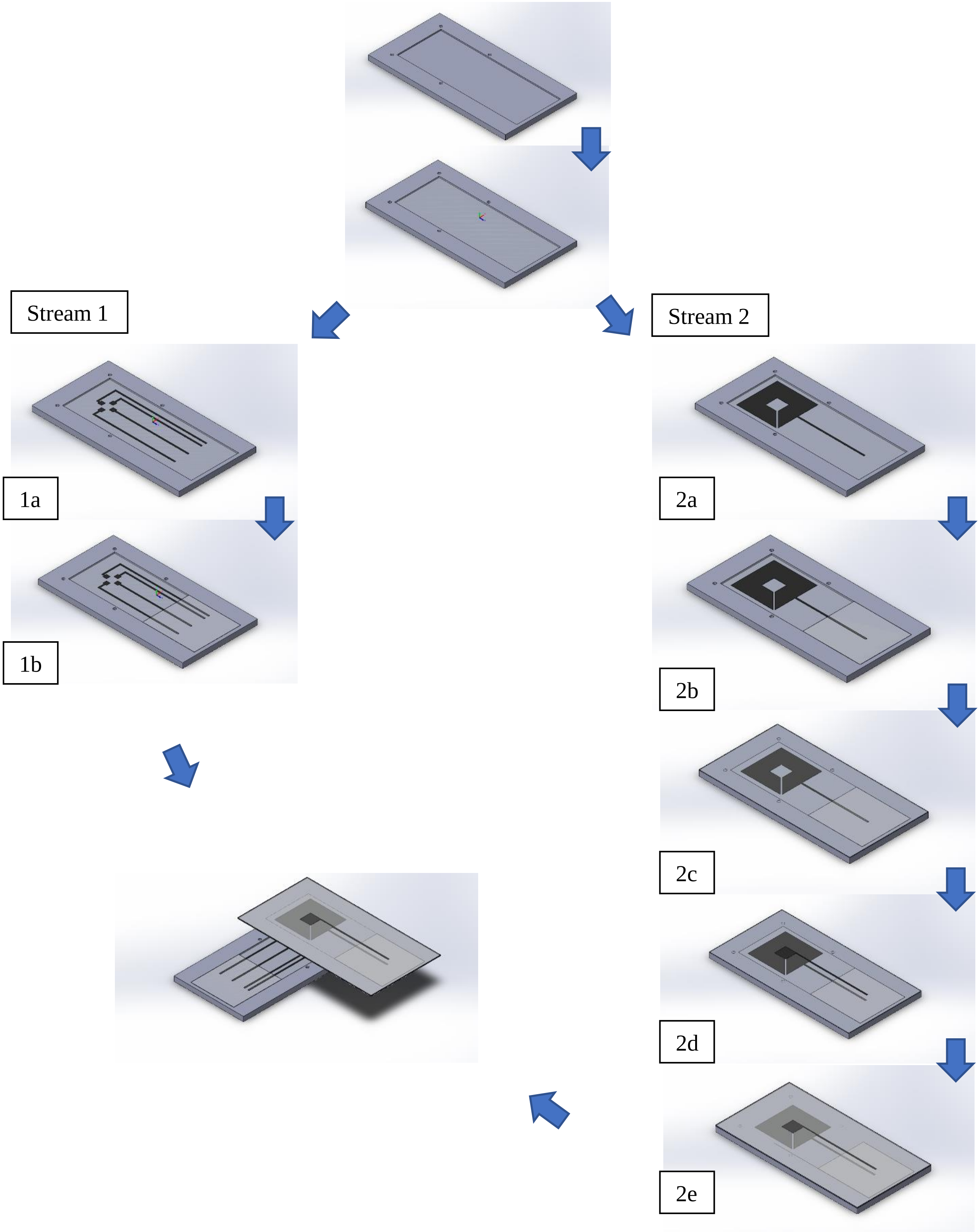

Figure 16: Sensor Fabrication Outline, see text for more details. Two streams that use the same base mold. Stream 1 houses the sensing taxel electrodes, stream 2 houses the grounding electrode and the excitation electrode. Each stream has steps respectively.

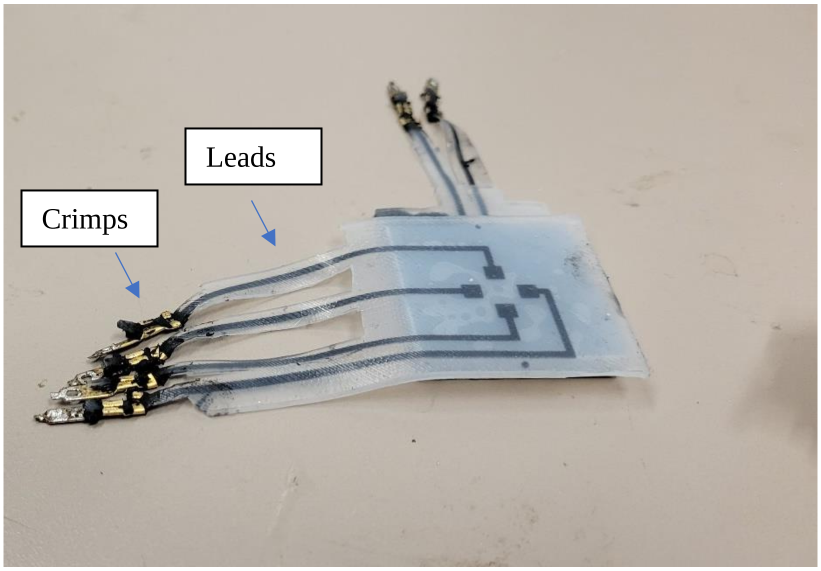

Figure 17: Finished fabricated sensor with crimped leads.

Figure 18: 3D printed enclosure holding PCB inside and Sensor on top.

2.4.3 Future Insole Design & Fabrication

The groundwork for a device, in this case, an in-sole, was done to imagine and design a general prototype. The areas that experience the most stress and consequently the most pressure ulcers on the plantar foot include the hallux (big toe), first metatarsal head (generally the medial forefoot), heel, and the 5th metatarsal head (lateral forefoot) (Figure 18) [65]. The intention is to have individual sensors in these relevant locations to monitor the shear and normal stresses (Figure 19). For simplicity, the first step is to have a single square pad to test for proper mechanical and electronic sensitivity. The results of the study are then used to guide further design and development as follow-on work to this thesis.

Centroids of each location were taken manually as the center of the hallux, center of the first metatarsal head, center of the fifth metatarsal head, and the heel, as can be seen in Figure 18. These centroids were used then to build molds and masks that correspond to the locations of interest to align with the center of sensors that would be placed in the same location. The distances used are based on the model can be seen in Figure 19.

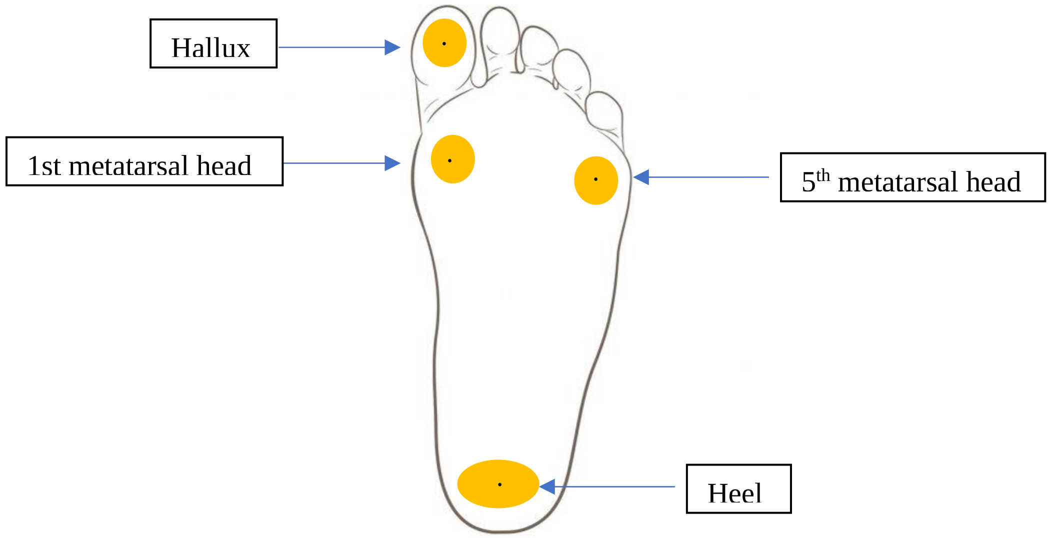

Figure 19: Anatomically relevant locations of sensors targeting the most sensitive locations for pressure ulcer formation and centroids for each.

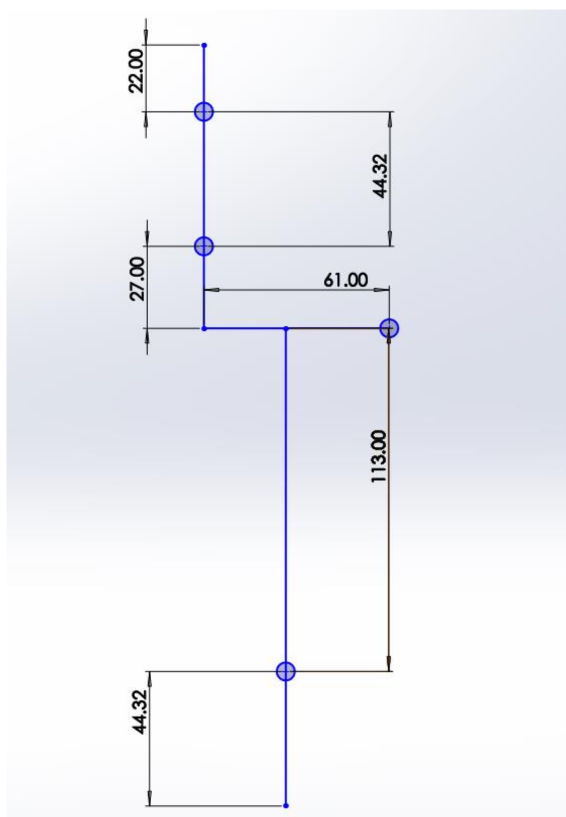

Figure 20: Measurements of location of centroids for sensor placement in insole mat device (measurements in mm).

The insole pad will be fabricated in the same way as the single sensors, except with bigger molds and masking multiple sensors at the same time. Since the molds are too big to be placed on a spin coater, intermediate layers between the ground electrode and the bottom electrode, supporting bottom layers, and the gluing layers were all laid down using a squeegee to spread the layers over the cured molds. This would be done several times, just like the multiple spins in sensor fabrication to ensure flatness and no shorting between layers. The ends of the traces on all sensors would be taped to ensure exposed carbon black for later crimping. The gluing step is like sensor fabrication but instead of aligning it perpendicular to each other, the dielectric molded side would be peeled off, using thick guides on the side of the top mold, and was placed directly on top. Traces on the 4 taxel mold were modified from the sensor fabrication to ensure no trace was overlapping another from top to bottom and ground electrodes eliminate parasitic capacitance between top and bottom too. A grounding layer that covers the whole middle layer of the sensor would be necessary to decouple all traces leading away from the sensors.

An alternative to the insole design would be to incorporate the elastomeric component of the sensor into a modified shoe. In this way, we would be eliminating some of the issues we have from testing shear (requires the sensor to be glued down since it is so stiff.) and housing at least part of the electronics in the sole of a shoe. This idea would adhere the bottom part or the sensor, sensing electrode, to a PCB that on it would be deposited 4 taxels of the same geometry as the elastomeric ones. This would not eliminate all traces since the excitation electrode would all need to be connected to the PCB but does eliminate the four traces for each sensing unit. While an innovative idea, this approach also has many setbacks which are covered in detail in our limitation and future work section of this thesis. The general design can be seen in Figure 20.

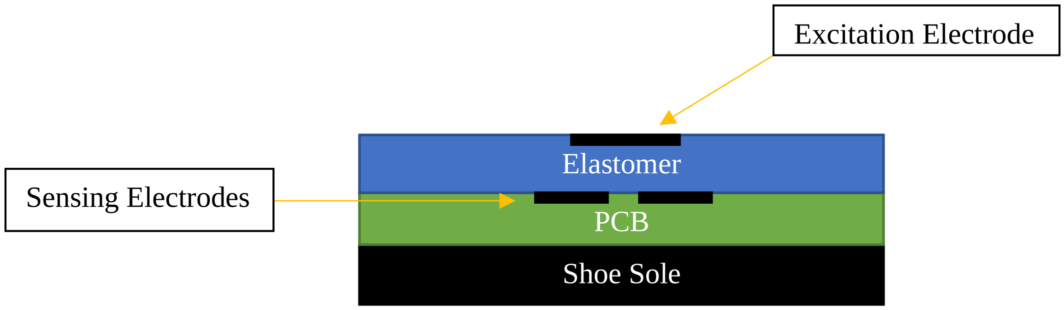

Figure 21: Sensor system imbedded into shoe sole. Sensing electrodes are deposited into PCB and elastomer is bonded to PCB

2.5 Testing & Experimentation Methods

In this section, we will go over the different experimental setups and the experiments that were used to characterize the materials and the sensors used in this thesis.

2.5.1 Material Testing Methods

2.5.1.1 Stress vs Strain Curves

Compression-based stress and strain curves are used to define the loading and offloading behavior of material concerning the stress being applied. These graphs indicate creep, hysteresis, and linearity. We are interested to know the behavior of the sensor due to stress so that we can translate that stress based on the capacitance we are measuring. By accounting for linearity, hysteresis, and creep we can accurately predict the pressures being applied, which will inform the user about the condition of their feet. For the material testing, we are only concerned with the maximum stress experienced at 50% strain, so we only look at the loading curves, or the ramping up of load, for that. 50% strain was chosen because we wanted to ensure that we did not reach the elastic limit (higher than 70% of strain) of the material that would result in a dent or altering the material as for it not to relax back to its original form. Offloading curves, or the ramping down of load, will be covered in the sensor characterization section of the thesis.

One sample for each material being tested at two thicknesses (3.5 vs 6.5 mm thickness) and tested the same day. Sample thicknesses were measured before each test and were used for pressure analysis later and were used to compute strain later. The stress versus strain test was a standard cycling analysis that was displacement controlled and went up to 50% strain to study at what strain did we experience 1 MPa of stress. (1.75 mm displacement for thin samples and 3.25 mm displacement for thicker samples). Sandpaper was placed down underneath the sample so there would be no slipping in between compression cycles. Before the test was started, a "touch" point was established by approaching the sample until a small amount of force was measured then proceeding to press up to 60 N of force (This was found to be the point needed to have a linear increase after the experiment was started). The test would start with a dwell of 5 seconds then proceed to increase pressure linearly at a rate of 20 mm/min up to the described displacement, then decrease pressure at the same rate to zero displacements. The cycle is repeated 5 times. The setup for normal force stress material characterization can be seen in Figure 21. Data was collected from the load cell at a rate of 20Hz.

The shear testing setup can be seen in Figure 22. Essentially, one glass piece is pulled upwards, while the other is held in place. The elastomer that bonds the two pieces together undergoes shear. In a similar sense to normal stress, shear stress was tested by applying 5 sinusoidal compression cycles using a 2 mm/second rate. The test involves applying 2 mm of displacement as – more than this level of displacement could lead to loss of bonding of the sample to the glass. A preload was applied to the system so the linear increase can happen at the beginning of the test.

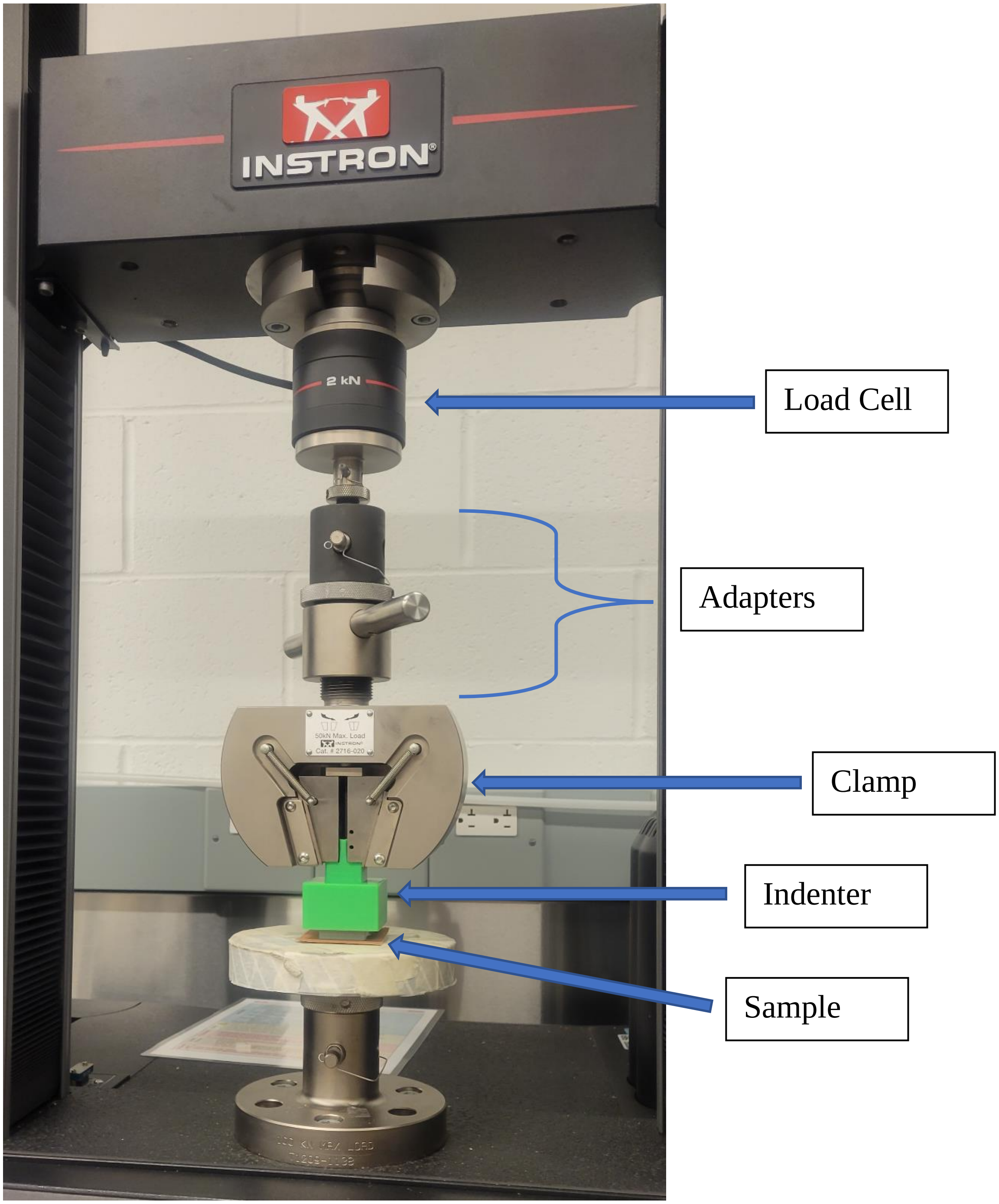

Figure 22: Sample & sensor characterization setup for normal force.

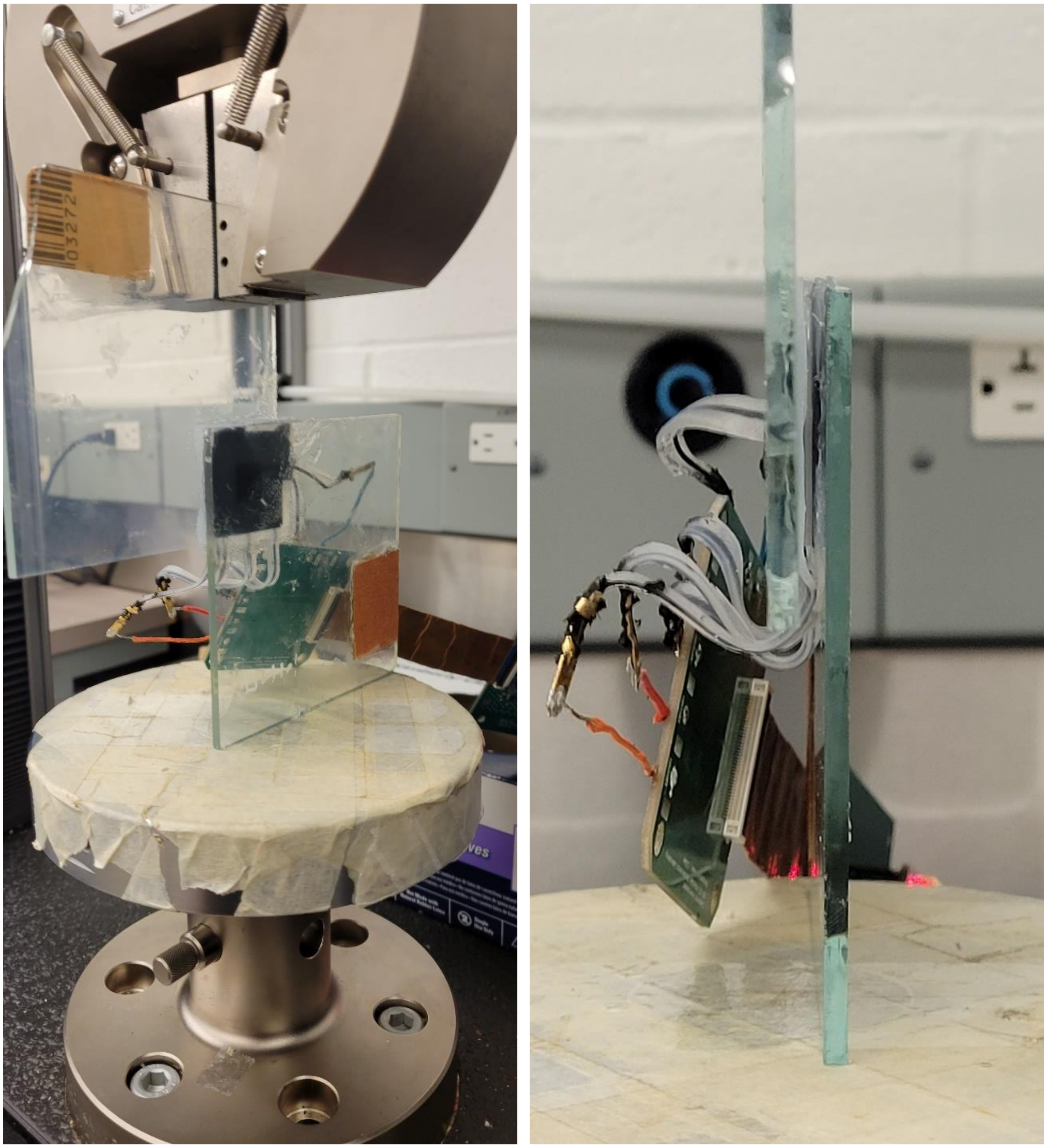

Figure 23: Shear Characterization Set up. Picture on right shows more clearly the bonded sample in between the two pieces of glass

2.5.2 Sensor characterization methods

The testing of sensors follows a very similar approach to the material testing methods, employing the Instron mechanical analyzer in the geometries shown in Figures 21 and 22 above, but now patterned electrode layers (described in sensor fabrication section) and with electronics connected to record capacitance (as depicted in Figure 17). Tests are done for both normal force response and shear. Experiments are used to gather information about linearity and hysteresis using stress vs strain curves, stress relaxation, and repeatability by testing the sensors in the separate time regimes experienced in standing and walking simulated experiments. With sensors, during these mechanical tests, we are measuring capacitance from the sensor to evaluate the capacitance change with force and displacement.

The capture of the capacitance data follows methods developed in our lab by Sarwar *et al.* [57]. An Arduino Uno and custom PCB were used to capture capacitance data in real-time. The sensor electronics were housed in a 3D printed box to protect the leads and PCB from forces being applied (Figure 17). Electronics specifics will be covered in a later section. Refer back to the geometry of the sensor. Sandpaper was glued to the top of the box to prevent the sensor from shifting during the experiments (Figure 17). The basic sensor normal stress characterization looked at sensitivity as well as how the sensor reacts in the two distinct time regimes of standing and walking. The same Instron was used from the material testing in displacement control mode. Captured pressure data were collected from the Instron computer and compared with capacitance data to analyze sensor performance.

In the past, at low pressures, testing of these sensors resulted in a linear relationship with stress. Often, we use these curves to calibrate our measurements with the stress being applied. This information can give us the sensitivity of our sensor as well as the linearity error. In addition to this stress versus strain calibration, we also conducted a calibration-specific experiment where we applied 5 different displacements to the sensor (.1, .25, .50, .75, 1 mm). The Instron ramped up at a rate of 1 mm/s each time, was held for one second at the desired displacement, then returned to zero after resting for one second between tests.

Shear testing was done using a custom shear characterization setup seen in Figure 22. After performing normal stress measurements, samples adhered to two pieces of glass with leads poking out of the side of the apparatus. Almost identical to the material testing for shear, stress/strain curves were performed using the same rate as the normal stress experiments of 2 mm/second. Displacement was capped at 2 mm (corresponding to about 50 N of force) to avoid loss of adhesion with the glass as previous experiments failed due to excessive displacements for repeated cycles. This is lower than the 5 mm (about 150 N of force) displacement that would be the max shear load we would expect for the application, we go up to this force in calibration experiments mentioned later. Additionally, the sensor was only tested using the walking regime protocol since we do not expect to see any shear in a static standing trial. As will be described in the next section, this testing is followed by a simulated walking protocol that went for 5 cycles to look at shear relaxation and repeatability in that regime. Lastly, shear displacements were applied between1 mm and 5 mm, going up to the desired displacement and back down to 0.25 mm (to ensure the sample was not being pulled in the opposite direction) at a ramp rate of 1 mm/second and resting for one second after each ramp. These experiments were done to gather information about the shear response to the sensor in all given directions.

2.5.2.1 Time Dependence of Sensor Response

Two primary loading regimes are envisaged for the sensor. One mode is in standing, where a constant force is experienced by the sensor over time. The other is during movement, and particularly in walking. Walking gait involves periodic loading and unloading. These regimes give us an idea of both extremes we want our sensor to operate under - one in long exposure to force, while the other involves short, periodic loading. For the standing regime, we define a typical standing bout to be about 10 minutes long. This is pure standing and no movement to give an idea of response to a constant load. Often, we stand for long periods, but we do so while fidgeting or moving around to relieve constant pressures on our feet. For the walking regime, using the same mechanism of gait used previously to describe refresh rate, we know that on average a human takes a stride a second while walking. Separating this into the different phases of gait, we know that 60% gait is spent in a stance phase and 40% in the swing phase. Like done before, breaking up the time in each phase we get 600 ms in stance and 400 ms in swing [66]. With these values, we can set a simulated walk protocol with ramping up to the maximum strain and holding for 600 ms then relaxing for 400 ms. One important aspect about both regimes is to have high enough rates of ramping that it seems almost instantaneous. This is because we want to study the natural stress relaxation of the material as it reaches its highest strain before having time to start relaxing. For this, we employed rates that would take the ramp-up to desired displacement change in half a second. Based on our previous results, 30% is the strain necessary to produce or exceed 1 MPa of stress which is the upper limit of stress for our sensor specifications. Using only 3.5 mm samples we then ramp up to 1 mm of displacement in less than 500 ms or 2 mm/s. This fast-ramping speed is used to mimic the almost instantaneous ramping rate that is necessary to measure the immediate response of the material as the load is placed.

2.5.3 Stepping & Walking Experiment

Several "real-life" mimicking experiments were developed to gather more realistic force response information. Simply, the experiments examine two specific criteria to study the behavior of the sensor: up and down steps (normal force), and an analysis of gait using a pseudo walking experiment. The up and down step experiment was used to study real-life forces of the weight on one heel with both feet flat on the ground. The right foot was used for measurement and the left foot was positioned comfortably next to the sensor, so balance was good. Using myself as the test subject, the experimental procedure followed was that my heel was pressed down into the sensor as naturally as possible, as in standing upright, and I continued to press down for different times (1, 5, and 30 seconds). Then I lifted the heel and held it for the same time. This was repeated 5 times for the different sets. Pictures of the down and up movement can be seen in Figure 22.

The pseudo walking experiment involved a short step gait test to observe the response to both pressure and shear. Using guides around the sensor to follow natural gait, the sensor was stepped on as part of a natural walking movement, without fully lifting the measuring foot (to ensure alignment is maintained). Figure 23 shows pictures of the experiments describing the different steps of gait. A weight scale was used to monitor the force being applied during the experiments. The time progression of weight was recorded by video. This information was used to give a general idea of what force was being applied at what time during the experiment.

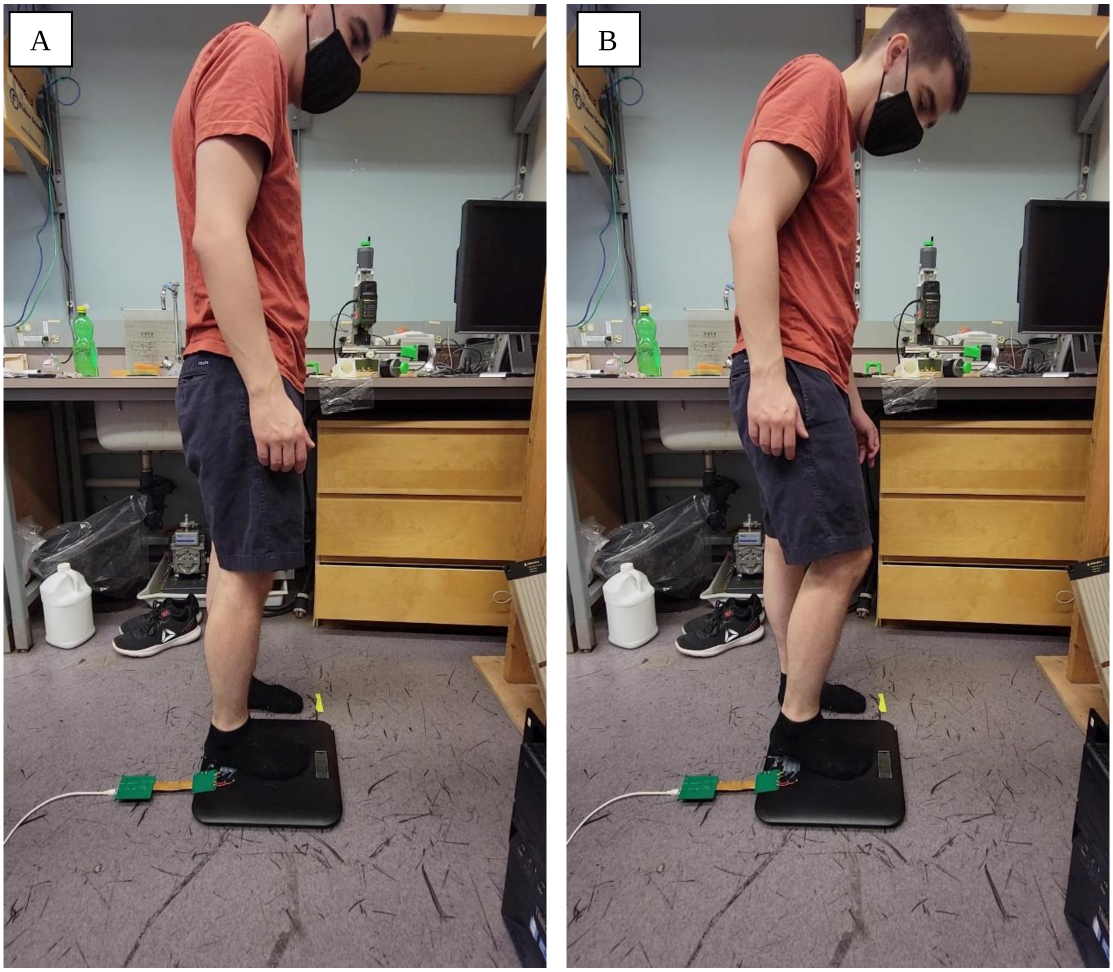

Figure 24: Stepping experiment, A with the foot down and straight and B with the heel lifted.

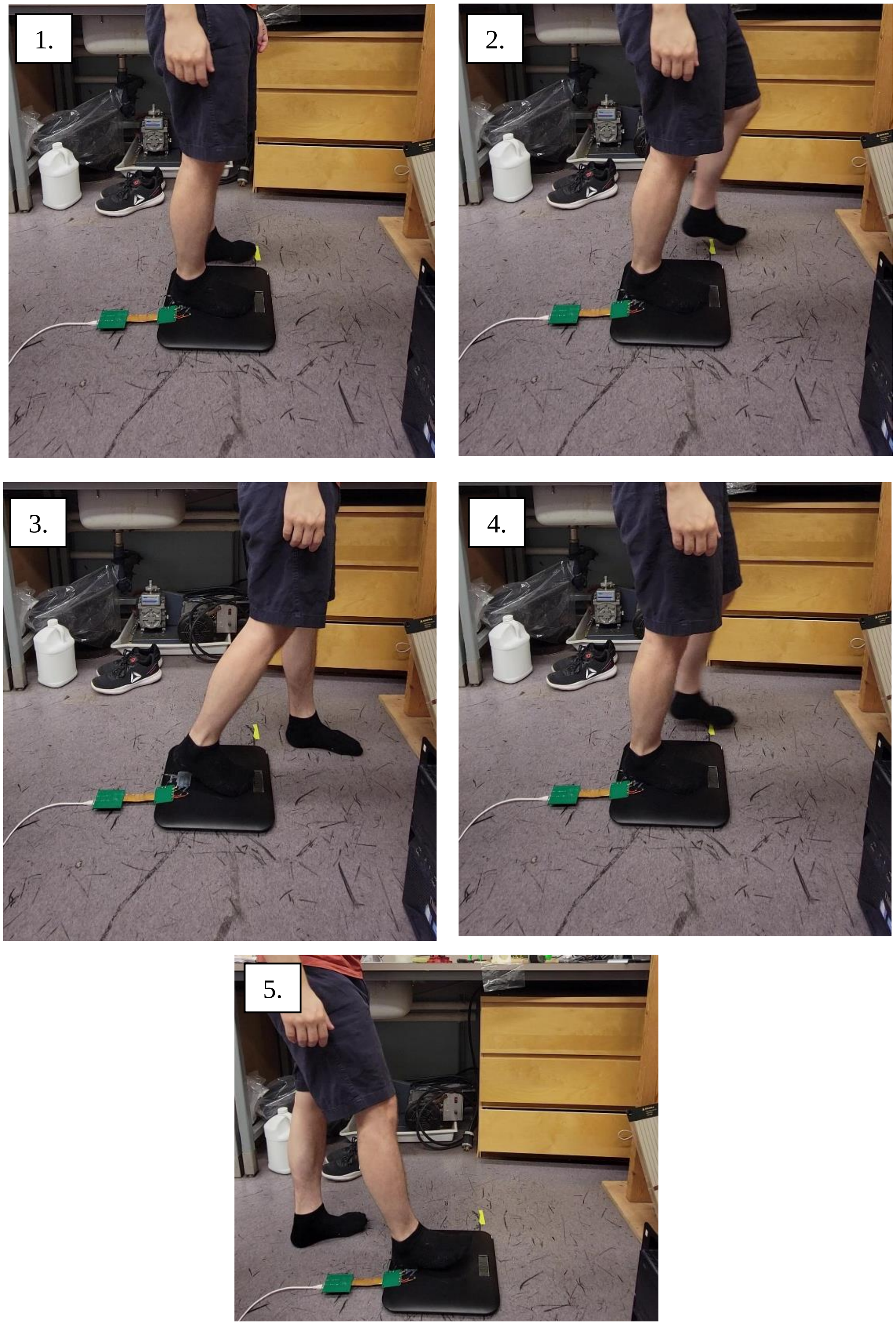

Figure 25: Walking experiment with different stages of gait. 1. Flat and straight standing, 2. Full force on foot swing on left foot, 3. Heel off sensor, 4. Swing backwards, 5. Half force on heel.

2.6 Electronics & Software

2.6.1 Single Sensor Electronics

The electronics components used for capturing the capacitance of our sensors include the combination of a personalized PCB board used specifically for sandwich sensors, and an Arduino Uno as a microcontroller to initiate and relay information to and from the sensor. The PCB implemented in this thesis can be seen in Figure 26, it holds the capacitance to digital converter (AD 7754, 24-Bit, Analog Devices) used in our lab as the main capturing circuit for capacitance. The readout circuit of the PCB excites the larger electrode on the bottom of the sensor and reads capacitance from the 4 taxels at the top of the sensor, the ground in the middle is grounded on the PBC and Arduino. A customized Arduino (C++) script reads the voltage information and converts it into a capacitance.

In the future, as will be discussed in the future work section, the use of a more portable PCB and microcontroller design can be used to reduce the footprint and incorporate the electronics onto the outside of a shoe or imbed it into the shoe itself. The smaller Piksey Pico (Bits N Blobs Electronics), which is the smallest Arduino prototype, could be used instead of the Arduino Uno, and a battery could be used to power the system, without the need to plug it directly into a computer. It is also a Cypress-based all-in-one chip that is being developed in the lab which would bring the sampling rate up to around 200 Hz per taxel. It has a microcontroller, multiplexer, and cap measurement all housed in a small footprint. This piece will be discussed in more detail in the future work section of the thesis.

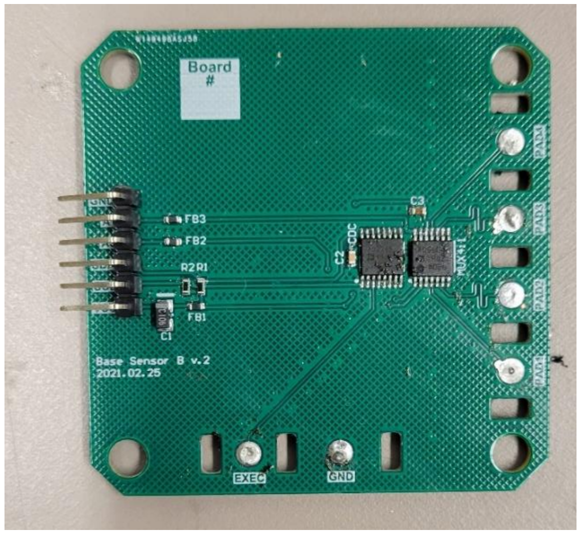

Figure 27: PCB used for capturing capacitance. Shown in the picture is the CDC used, multiplexer and the pads where crimped leads from sensor

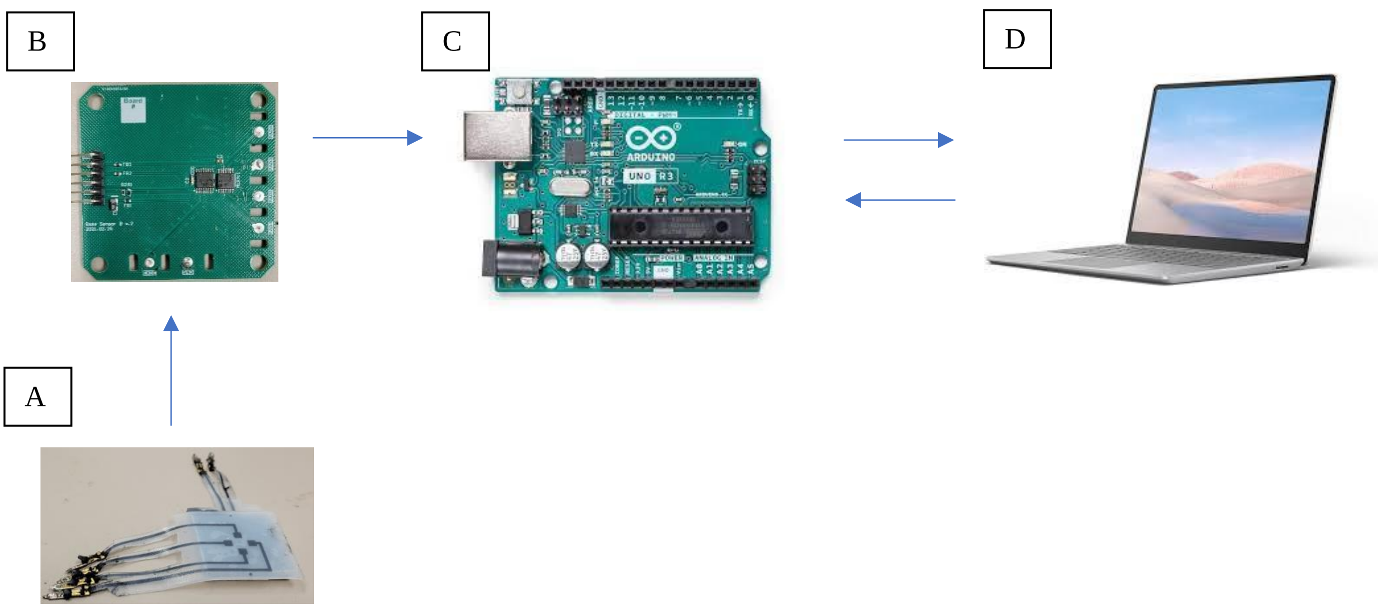

Figure 28: Signal pathway from sensor to computer. A is the sensor, B is the PCB, C is the Arduino housing the microcontroller, and D is the where the data saved on the laptop while also powering both the Arduino and the circuit.

Chapter 3: Results & Discussion

In this chapter, we look at the results of the experiments outlined in the previous chapter. This includes results from material testing, normal and shear stress sensor experiments, and real-life experiments. Overall, the sensor responds as expected to the different experiments and characterization is possible with the described set ups. With that said, some challenges were faced including hysteresis, creep, and gluing issues which are described here but will be discussed further in the next chapter.

3.1 Material Testing Results

3.1.1 Solid Samples

With the previous formulations of the sandwich sensor, the use of Ecoflex 00-30 was problematic for the application in an insole due to the nonlinear behavior of the material at high forces, as discussed in the background section. Additionally, the material could reach its elastic limit where it would not be able to return to its original shape after deformation permanently. It was clear that stiffer materials were needed to be used to reach higher forces based on previous early experiments of stress versus strain. Here the stress-strain responses of several materials are compared to find a good compromise between sensitivity and range. While it is expected that the more compliant the elastomer, the more sensitive it will be to changes in stress, increasing compliance will generally be associated with lower stress limits.

The characterization of the different elastomeric materials was carried out to ensure that the sensor could deform linearly under the necessary pressures. As described in the material testing section, the experiment for characterizing the material properties of the three materials was described, but it will be briefly explained here. Each material was compressed using an

Instron testing machine and a 50 mm x 50 mm indenter. The experiment was cyclic, displacement controlled, and reached 50% strain as the maximum deformation then returned to zero. Figure 26 shows the stress versus strain deformation of each material on the way up (loading pressure) for samples that are 3.5 mm thick. The materials tested, in order of ascending elastic modulus, are Ecoflex --30, Dragon Skin, Dragon Skin 10 mixed with 10% Sylgard 184 PDMS, and Sylgard 184. Ecoflex 00-30 behaves as expected, becoming nonlinear only after 50-100 kPa of pressure. Sylgard 184 is the stiffest (with the steepest slope) and it is linear throughout the measuring region from 0 to 1 MPa, while Dragon Skin 10 has some nonlinear behavior starting at about 800 kPa. With the addition of 10% PDMS, the Dragon Skin substrate can withstand upwards of 1000 kPa while still providing a relatively straight-line response.

As expected, the same behavior is replicated with the 6.5 mm samples and can be seen in Figure 28. The curves are "stretched" out a bit, meaning they can go up to slightly higher pressures. This might be the case since the estimations of equal and opposite forces on the thicker samples are overcompensating, spreading out the forces throughout the material. This is an attractive feature of a thicker sensor because if they can distribute the same pressure over a wider displacement range, the foot will experience less force at similar displacements. Of course, there is a limit to this, and we can see the extent of that in Figure 29. Additionally, we are seeing similar nonlinearity at high stresses.

The goal of the material testing was to find an elastomeric formulation that could go up to 1 MPa of pressure, while ideally giving a straight-line response. While Sylgard 184 can also do this, it is stiff, which reduces sensitivity. As will be shown below, the pillared architecture does not work for these pressures, so the dielectric for the sensors will be solid. Materials like Dragon Skin which has a hardness that is about halfway between that of Ecoflex 00-30 and Sylgard 184 are attractive materials for this application. Similarly, Dragon Skin is from the same family of elastomers as Ecoflex 00-30 and has some of the same elongation and stretchability characteristics. For this reason, with added strength from PDMS, the mixture of Dragon Skin 10 with 10% PDMS was used as the substrate material for all sensor fabrication. It is important to state though, that the hysteresis of these materials - which will be covered later - is problematic and is a challenging feature to compensate for with these sensors. But this behavior is found in all of the materials tested, including Sylgard 184.

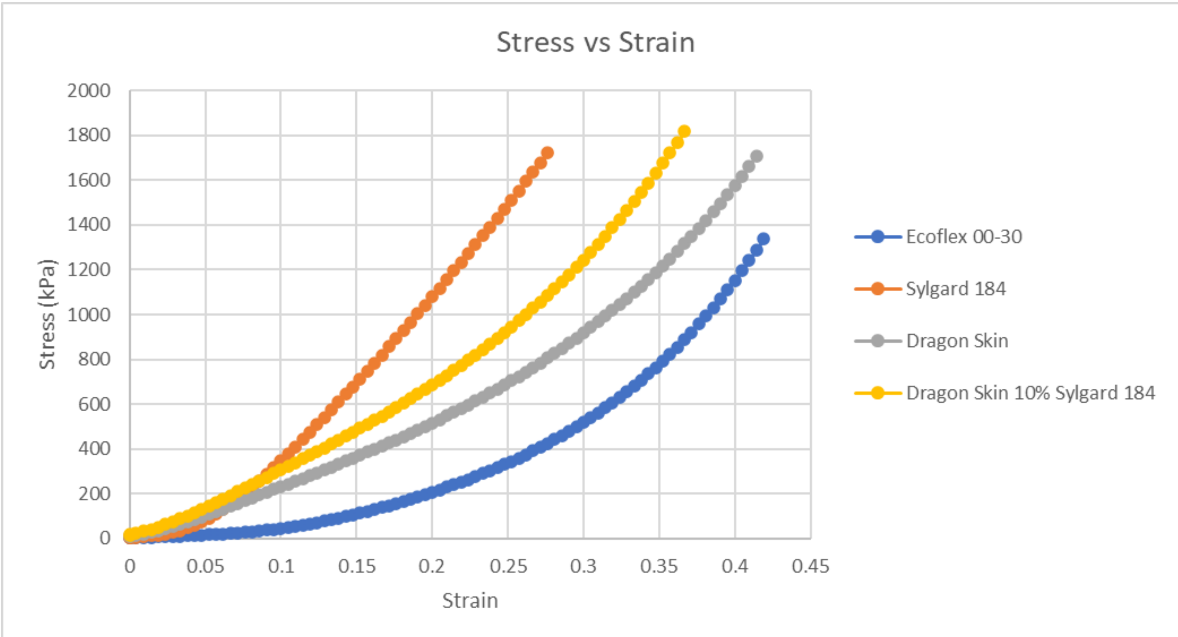

Figure 29. Stress Strain curves of onloading 3.5 mm thick samples up to 50% strain. Curves end prematurely because of reaching the limits of the 2 kN loadcell.

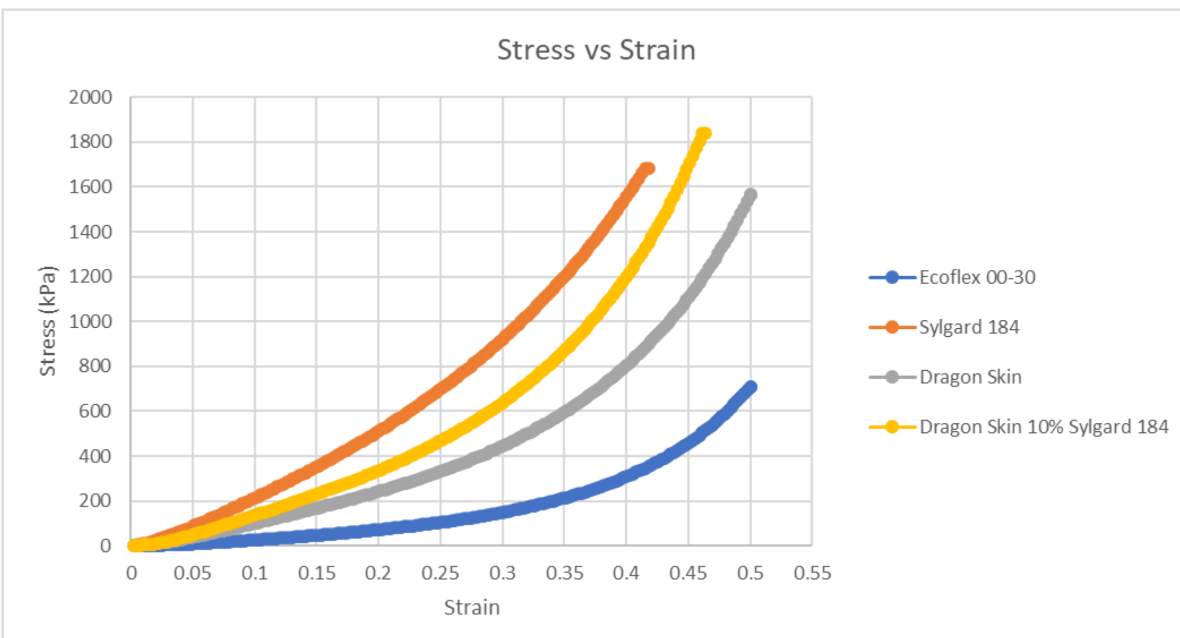

Figure 30. Stress Strain curves of onloading 6.5 mm thick samples up to 50% strain.

3.1.2 Pillar Dielectric Samples

The pillar experiment was used to investigate the possibility of using a patterned dielectric like the sensors previously used in the lab. The pillars allow for the shearing element of the sensor to be quite sensitive compared to a solid dielectric. To study this, as described previously, patterned dielectric samples were made using different numbers of pillars in the same space of 31 mm x 31 mm by affecting the pitch between the pillars but keeping the pillar size constant. The samples were tested in a similar cyclic fashion to the solid samples, at up to 50% strain. Figure 30 shows the stress and strain curves for the different pillar formulations using the Sylgard 184 PDMS substrate. The first immediate observation is the elbowing effect that happens when the pillars are collapsing onto each other. Firstly, we see that the elbow stiffening of the 7-pillar sample happens almost immediately, causing it to perfectly mimic the solid sample. Very little force causes the pillars to contact each other, and it acts like a solid piece rather than a unique curve on the graph. The elbow is then seen clearly in the 6-pillar and 5-pillar samples, happening at a higher pressure on the 6-pillar sample, which is expected. The points at which the elbow happens are worth interest, in the 6-pillar sample, the collapse happens at around 600 kPa while the 5-pillar sample collapses at around 250 kPa.

These results do not indicate the use of a pillared patterned sensor will be effective in providing enough support. Sylgard 184 was used to test the pillar design because it is the stiffest material being used and worked as a model for investigating possible pillar structures strong enough to take the load before collapsing. The relationship between the number of pillars and the force they can take can be simplified to the proportion of surface area available versus the indenting surface area. When altering the number of pillars, we are altering the surface area overall, and it decreases with fewer pillars. The higher the surface area covered the more force the sensor can take. With these conclusions, and the fact that at 7-pillars or 2.5 mm pitch (basically only 0.5 mm separating the pillars) contacts other pillars almost immediately because of contacting neighboring pillars, the stiffest material being studied is not stiff enough to support the loads need without collapsing.

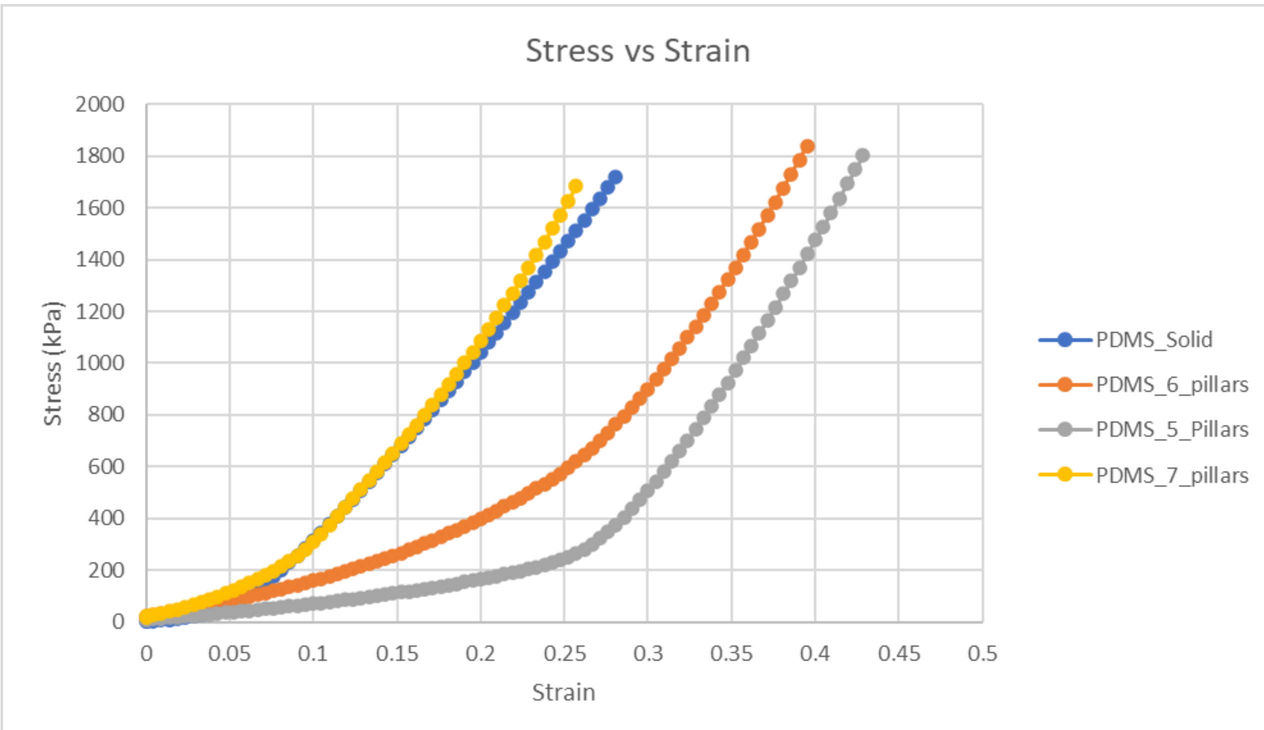

Figure 31: Pillar experiment shear versus strain characterization just for onloading

In summary, the material properties of the different materials are as we would expect in terms of stiffness. Leveraging a balance between sensitivity and stiffness we decided that the formulation of a solid Dragon Skin 10 with 10% Sylgard 184 would be the best for the sensor. While having a stiffness that can withstand the necessary pressures (1MPa), it is not so stiff that it would be uncomfortable to wear (although this was not directly tested).

3.2 Sensor Testing Results

In this section, results specific to sensor characterization will be covered. These include both normal and shear stress results as well as real-life experiments done with fabricated sensors. Overall, the sensor seems to respond well in the standing and walking time courses and can capture different stages of gait in real-life experiments. The sensor's response follows displacement more so than the force which is expected since it is inversely proportional to capacitance (see equation #1). This section will delve deeply into the considerations of each experiment and what might be expected for future work in the next chapter.

3.2.1 Normal Stress Sensor Testing

3.2.1.1 Stress vs Strain Curves

The Dragon Skin with 10% Sylgard is selected as a promising candidate thanks to its relative linearity of response to 1 MPa, and its greater compliance, relative to the Sylgard, which should enable higher sensitivity. Testing of sensors followed a similar procedure to sample mechanical testing, but the normal force experiments only went up to 30% strain since that is sufficient to exceed the 1MPa limit in the stiffer samples. Capacitance was measured at the same time to investigate the behavior of the sensor as strain is increased. Dragon Skin 10 with 10% Sylgard 184 was used as the substrate for all sensors, each sensor was tested using the Instron system seen in Figure 20. The results from these experiments describe the overall performance of the sensor under compressive normal stress. This includes the strain-stress behavior of the sensor overall, hysteresis found in loading and unloading sensors, how capacitance reacts to normal stress, and its linearity, sensitivity, and performance over various cycles.

The overall loading and unloading behavior of the sensor can be seen in the full stress-strain curve in Figure 31. Generally, the loading and unloading curves follow different paths, suggesting a viscoelastic response. This is primarily due to the viscoelastic nature of the material, which might require relaxation to deform similarly as in loading. This is inherited in many elastic materials and cannot be avoided. This brings into question the potential of using extremely stiff materials or non-elastic materials that are still soft, like foams. As expected, the maximum pressures reached are in line with the solid sample characterization. As stated before, the apparent hysteresis loop is problematic when developing simple linear models of capacitance measurements. Relating force to displacement becomes a challenge because it is now history and step dependent. We need models and mathematical tools to better represent it than simple fitted curves. In our case though, we will be fitting a 2nd -order polynomial fit line that bisects between the loading and offloading curves. What is seen is a variation in stress between the loading and unloading cases is up to 300 kPa – giving a 30% uncertainty of full-scale load (1 MPa).

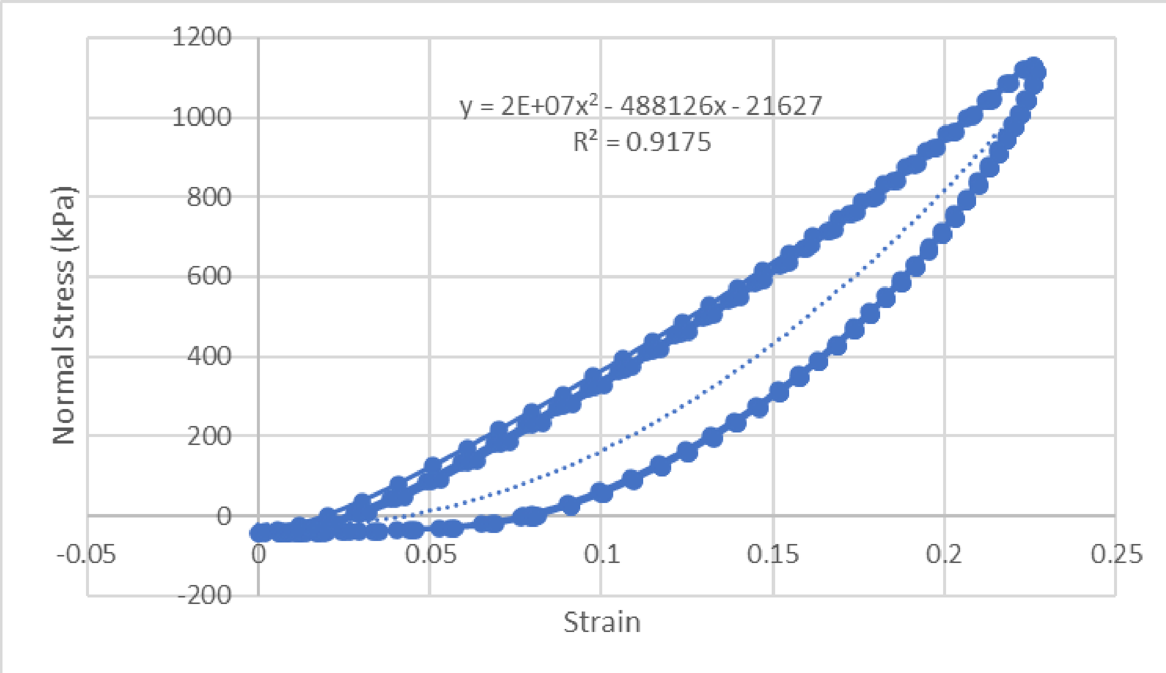

Figure 32: Stress vs Strain curve for normal stress of fabricated sensor with Dragon Skni 10 and 10% of Sylgard 184. Fitted line is a second order polynomial to bisect off loading and onloadling curves.

Since this is a capacitive measurement, defined by Equation 1, we expect the capacitance to follow the displacement of the sensor closely. For this reason, we plotted in Figure 32A the percent change in capacitance (defined as the change in capacitance from baseline (unloaded) divided by the baseline) versus the displacement. As can be seen, the capacitance follows the displacement more linearly than the force. As expected, we see a similar apparent hysteresis being repeated on part B in figure 32.

A

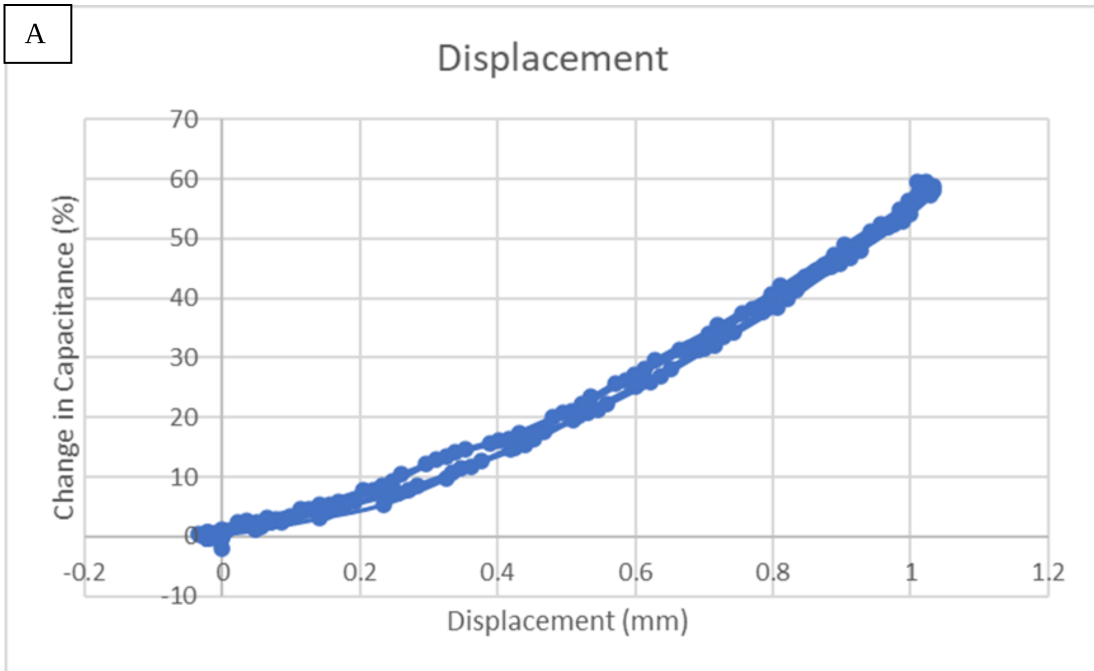

B

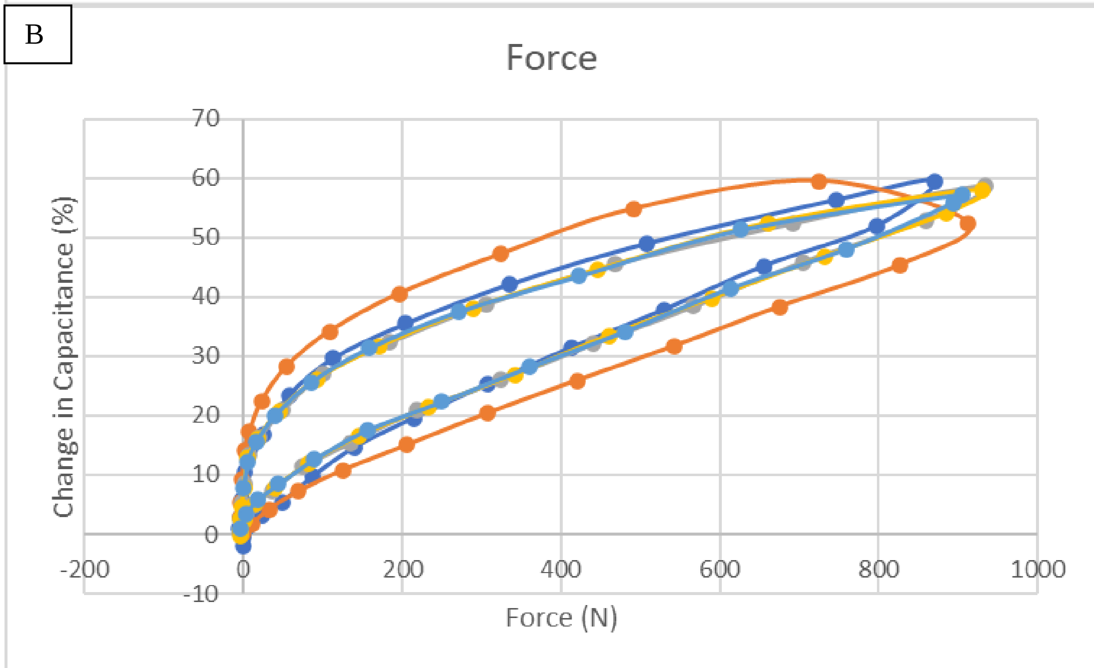

Figure 33: A, percent change in capacitance versus displacement. B, percent change in capacitance versus force.

Using these curves, we can begin to look at the sensitivity of the sensor for displacement and force. While a line fit could be used to calculate the slope on Figure 32 A, a 2nd order polynomial fits the graph much more closely with a R^2 value of .9974 or a fit error of only 0.26%. Doing a similar 2nd order polynomial curve fit to Figure 32 B, we see that the non-linearity error of 9.1% is much greater because of the inherent hysteresis. In the limitation and future sections, much discussion included how options to handle the fitting of viscoelastic curves, and whether it is useful to use the displacement measured by the sensor as a clinical indicator rather than force.

Hysteresis can also be calculated from the curves in Figure 30 by taking the biggest difference between the loading and offloading curves and averaging that location between trials. Part A results in a hysteresis measurement of 2% of the full scale and part B of 25% of the full scale. This is not ideal, especially in the case of making a calibration between capacitance and force because a 25% difference could mean mistaking a 200 N force to a 400 N force. To enable more accurate force measurement, one option is to build models that can either predict the viscoelastic response based on the history of deformation. That means keeping track of the history of displacement (given by the capacitance measurement). Another option is to change materials altogether to something linear throughout, but likely at the expense of sensitivity. This discussion will be covered in detail in the limitation section of the thesis in the conclusion chapter.

3.2.1.2 Standing Sensor Experiment

For the different time regimes of walking versus standing, experiments were developed to mimic the conditions using the displacement controlled Instron testing machine. As described previously, the standing simulation experiment is like a creep or in this instance a stress relaxation experiment, where a fast ramp was applied, and the material was left to relax for 10 minutes before returning to zero displacements. Figure 33 shows the results of the stress relaxation experiment. As expected, the capacitance closely follows the displacement on part B of Figure 33. We still see a small overshoot in displacement when ramping due to the speed of loading and the Intron machine limitation, but this overshoot is quite short and has very little effect on the response. The force follows a stress relaxation curve on part A of Figure 33.

Overall, we see a 33% change in force over the ten minutes, for the full scale. This pattern is not replicated with capacitance because displacement is kept constant. Even with the overshoot we only see a 0.18 % change in capacitance between the beginning and the end of the 10 minutes. Additionally, from this graph, we can calculate the peak-to-peak noise found in our capacitance signal. This was calculated by talking about the difference of the maximum and minimum residuals of the datapoints at the top force versus a fitted curve. This results in a peak-to-peak noise of 3.1% of the full scale which corresponds to about 0.0194 pF or 19.4 fF. This can be characterized as the resolution of the sensor at max force since anything higher than this peak-to-peak noise is the lowest accurate measurement of force for the sensor.

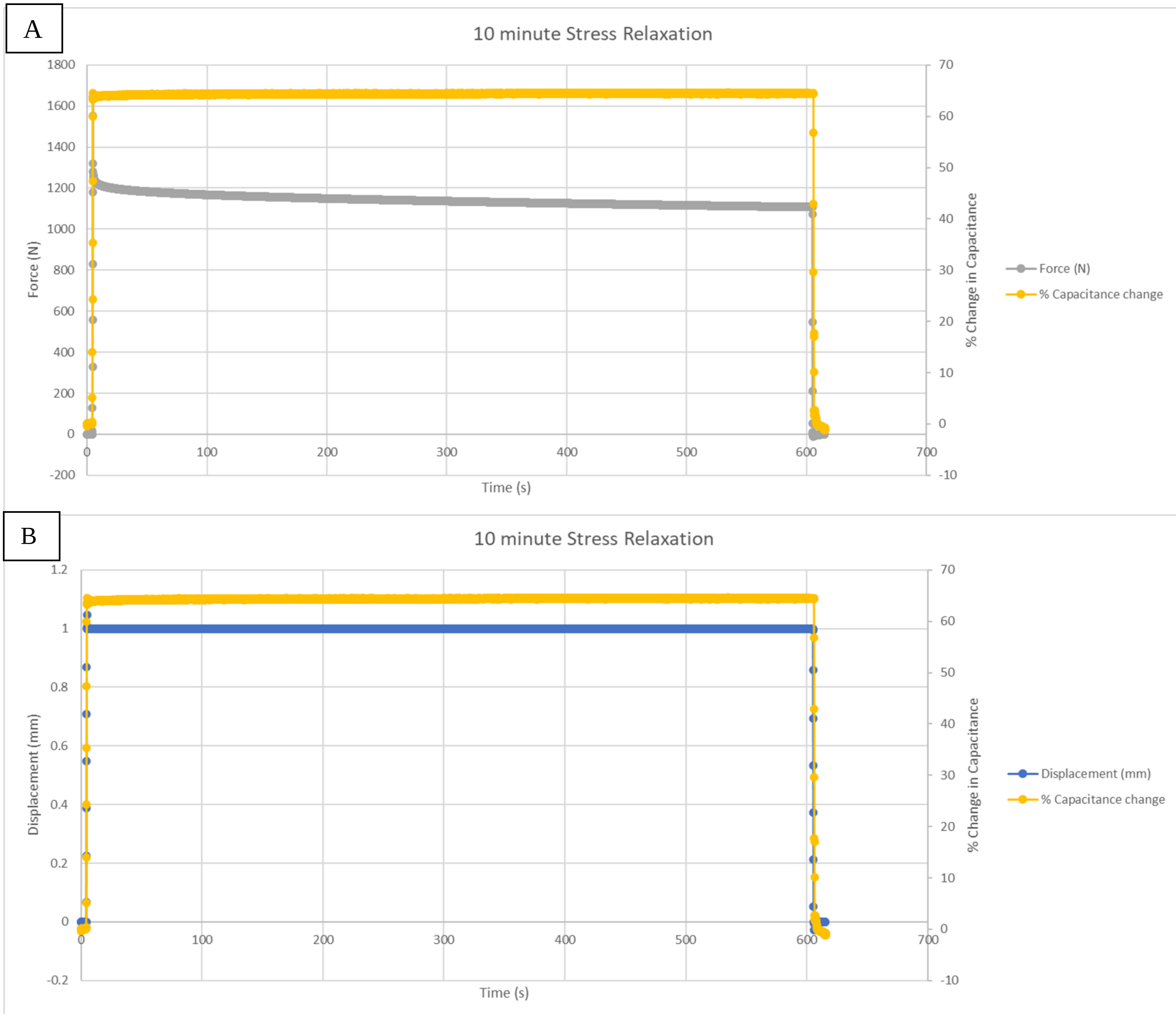

Figure 34: Stress relaxation experiment. A shows the force relaxation curve vs capacitance. B shows the capacitance relaxation curve versus displacement.

3.2.1.3 Walking Sensor Experiment

The walking simulated experiments capture the faster time regime these sensors would experience. The results of the experiment can be seen in Figure 34. Like the standing experiments, we can see that the capacitance response mimics the displacement on Part A. The force also tries to decay in the time that it has at the top of the ramp, but the capacitance does not follow as can be seen in Part B of Figure 34. From this experiment, we can calculate the repeatability of the sensor by looking at the standard error of the mean between the 5 different trials. Since we don't see a detectable change, the repeatability is 3.1% of the full scale concerning applying the same displacement for the five trials. The sensor does well to respond to movement at the fast time scale range. Applying constant force would be closer to real-world application and would probably result in a slight creep from the capacitance as has been seen in previous work in the lab. Nevertheless, this data gives us information of the capability the sensor has in these faster regimes and given a much faster sampling rate, could potentially be used in running time-scale regimes.

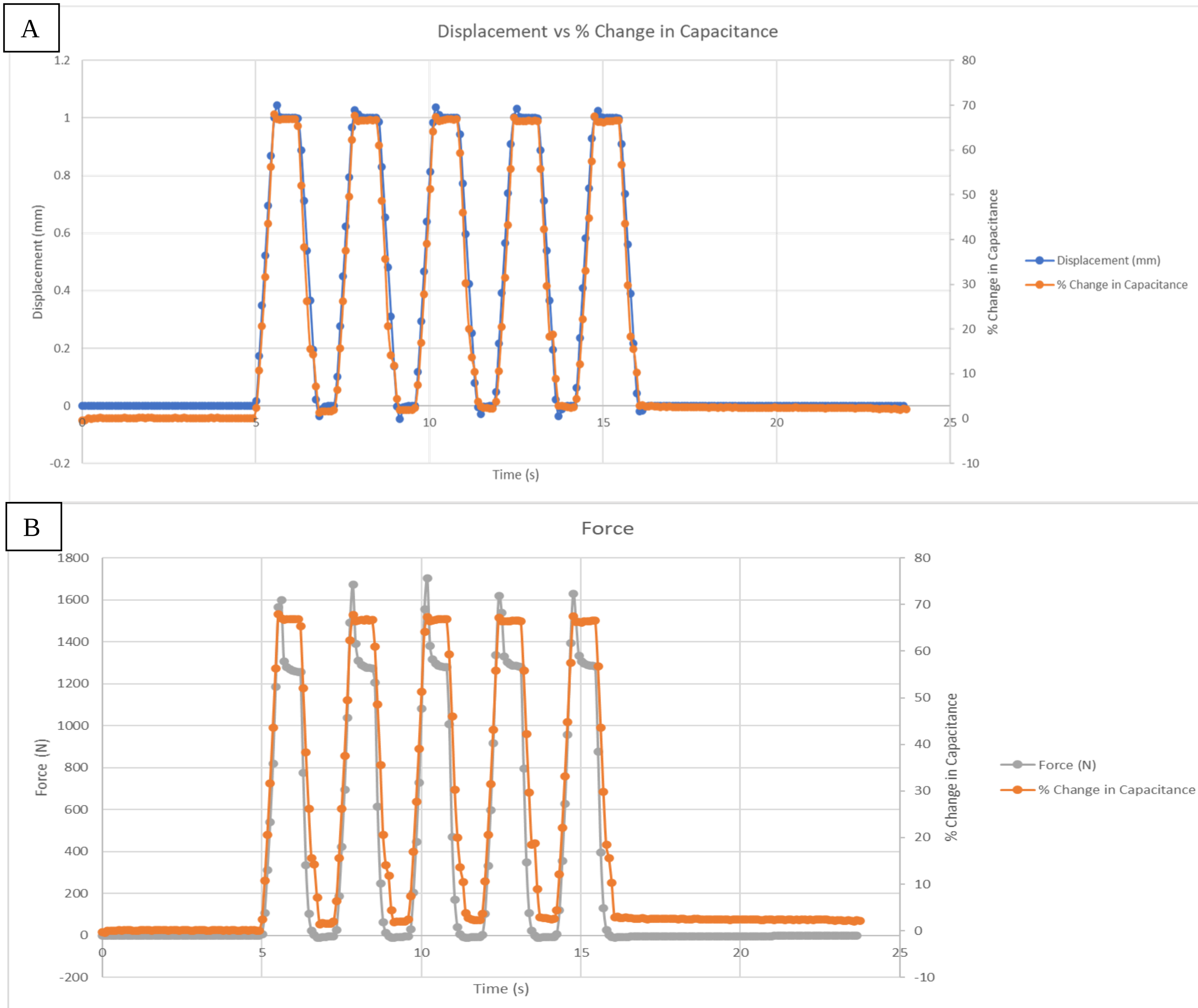

Figure 35: Walking simualted experiments. A shows the capacitance response versus displacement. B shows capacitance response versus force.

3.2.1.3 Normal Stress Calibration Experiments

A calibration experiment was devised to look at the response of the sensor when different pressures were applied. Results for this experiment can be seen in Figure 35 As expected, in 36A we see the capacitance response follows the displacement very closely, while in 36B the force relaxes when the displacement is held steady, with the capacitance remaining steady. From this data, we can calibrate the sensor based on estimated normal strain versus actual normal strain. To do this we use Equation 5 on page XX and calculate the averaged normal strain on the 4 taxels. The results can be seen in Figure 36, with an R^2 value of 0.97 so the linearity is within 3% error. From this, we can see that the curve is mostly linear. This curve is useful to predict what strain we are expecting from the sensor giving the capacitance value but does not give us stress directly. For this, we would need the value calculated here to be input into the formula generated from the fit curve in Figure 31.

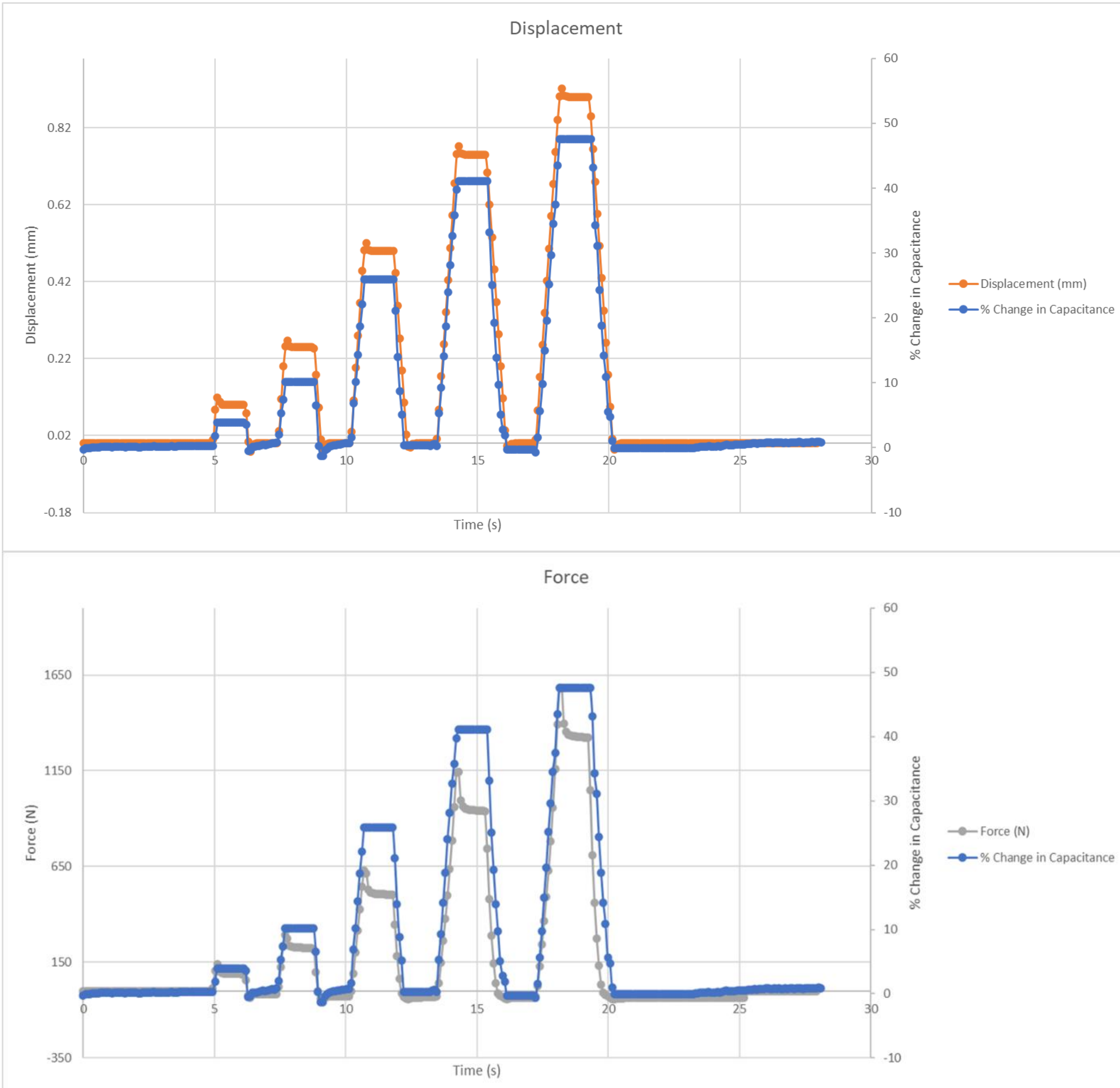

Figure 36: Normal stress calibration experiment. Displacement steps of 0.1, 0.25, 0.5, 0.75, 1 mm.

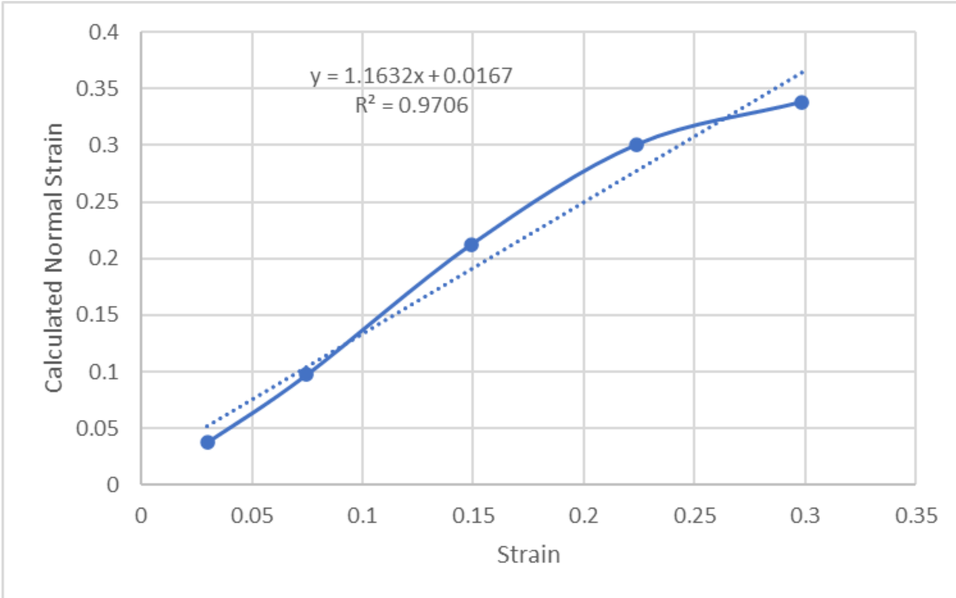

Figure 37: Normal strains calibration curve. Linear fit line is plotted and resulting equation and R^2 value are displayed.

3.2.2 Shear Stress Sensor Testing

3.2.2.1 Shear Stress vs Shear Strain Curves

Shear stress experiments, as described in the methods section, used a modified method of applying shear by adhering the sample between two pieces of glass. While the adhesion is strong, it is not perfect. For this reason, high repetition experiments like the stress vs strain were done only up to 2 mm of displacement. The higher limit of shear is tested in a calibration-based experiment described later. Figure 37 shows the shear stress versus shear strain curve, and as can be seen, there is slight hysteresis present in the graph. This would be expected to be much higher at 150 N which is the force expected at the max displacement of 5 mm. The calculated apparent hysteresis (similar calculation to that of normal stress) is 9% of the full scale.

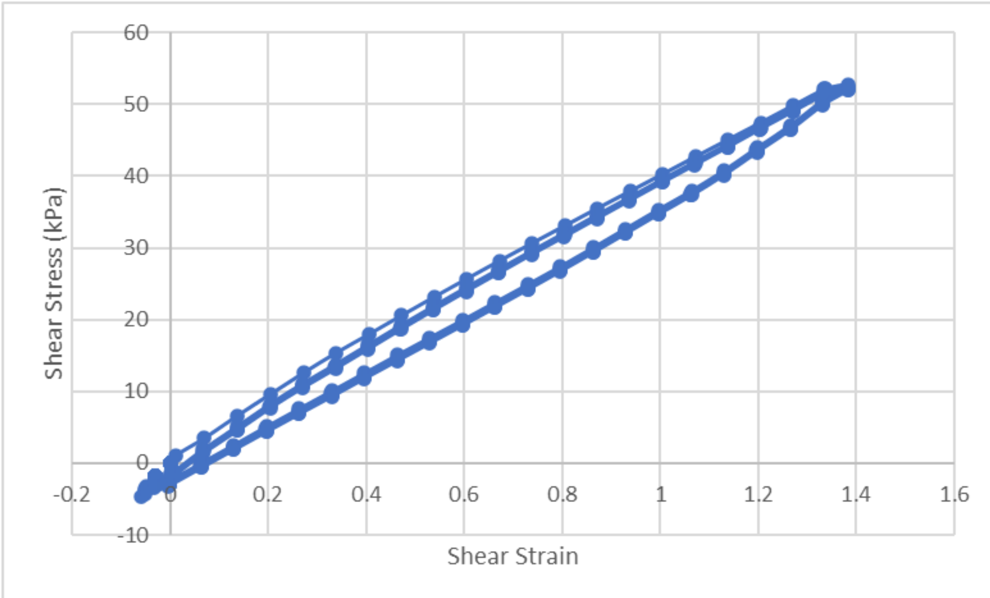

Figure 38. Shear stress versus shear strain curve

3.2.2.1 Shear Calibration Experiments

The calibration experiments for shear involve applying discreet shear displacements on each axis of the sensor (both positive and negative). This was done to garner information on each taxel and to determine how accurately the sensor is performing shear measurements, for actual displacement being applied. In this test, shear displacement is ramped up and down with an amplitude starting at 1mm and increasing to 5mm, in 1 mm increments. Ramping is done at a rate of 1mm/s. After each ramp up and each down ramp, the displacement is held constant for one second. The initial displacement and the position between ramps is 0.25mm rather than 0 mm because we would not want to lift the glass of the base so to ensure that we only go down to 0.25 mm. Figures 38-41 show the results of the experiments, with Figures 38 & 39 showing positive and negative X-axis shear displacement responses, respectively, and Figures 40 & 41 showing positive and negative Y-axis responses. Each figure has a key on the top right-hand corner to guide the viewer on what direction is being sheared. The blue and the gray taxels are most sensitive to Y-axis displacements, while the yellow and the orange taxels are used to measure the X-axis shear. Each figure also has a curve showing either the displacement or force being applied at each step for each direction sheared. As before, the displacement and capacitance track each other well, while the force shows a significant relaxation that is not seen in capacitance or displacement.

Looking at the positive X-axis (Figure 38) we can see that the response between taxels is very close to what we would expect. Taxel 4 is increasing in capacitance as it shears, while taxel 2 is decreasing in capacitance. This is expected as the top layer of the sensor shears across the bottom since the overlapping capacitive area for taxel 4 is increasing while it is decreasing for taxel 2 (description in shear background section for more details). Since taxel 1 and 3 move along the X-axis, they should not be changing capacitance., This is not the case as we see a slight increase in taxel 1 and a decrease in taxel 2. Given our experience with shearing characterization, this is often the case when the setup is not perfectly aligned and there is a slight tilt, here it seems there is a tilt that is guided towards a positive y and negative x directions.

The negative X-axis results for shear calibration show the same amount tilt as the previous positive X-axis, as can be seen in Figure 39. As expected, we see an increase in capacitance on taxel #2 and a corresponding decrease in taxel #4. We see a smaller increase in capacitance on taxel #3 and a smaller decrease in taxel #1, suggesting a small tilt in the positive y and positive x-direction.

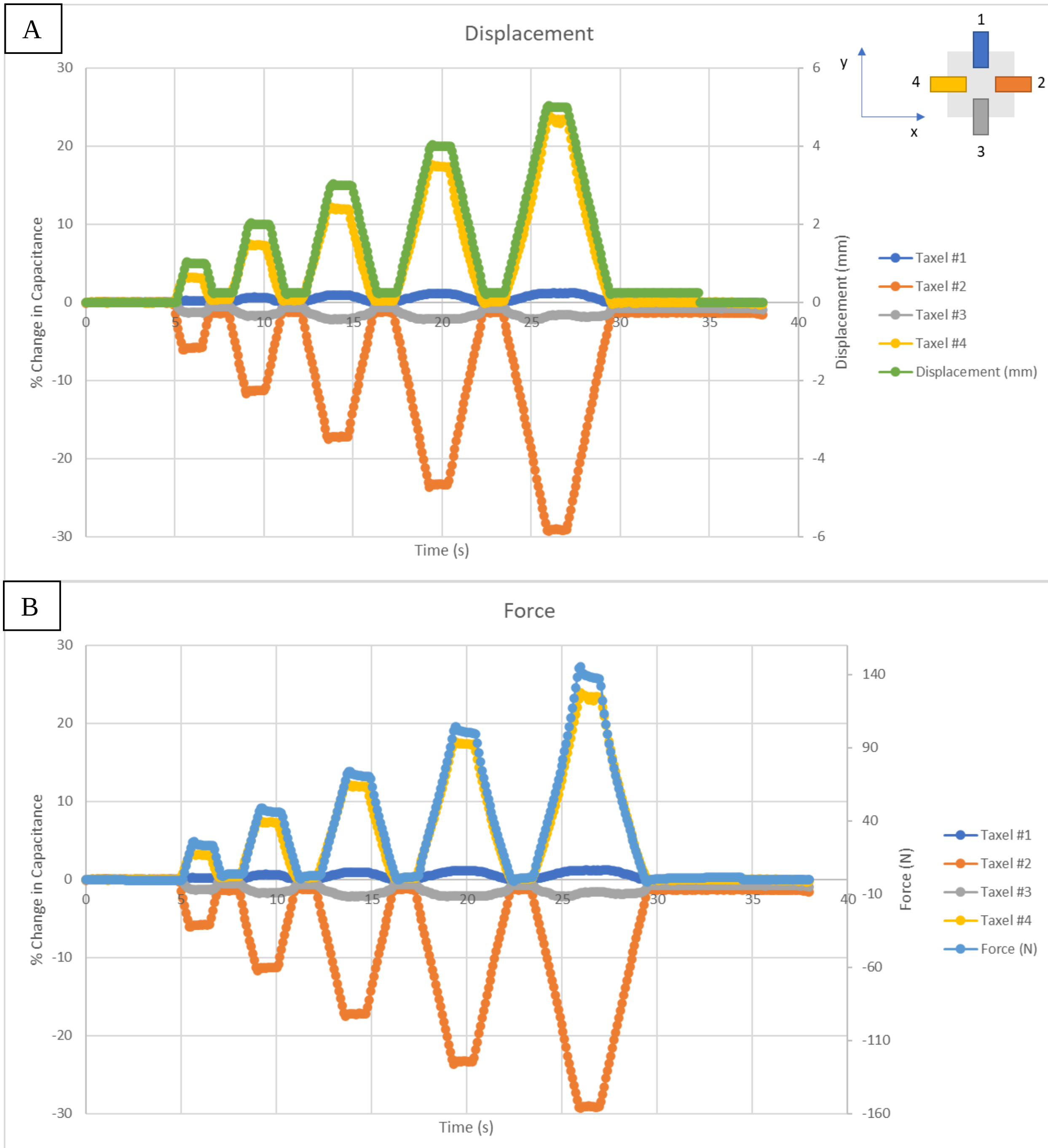

Figure 39: Shear calibration on the positive X-axis. A showing displacement curve and B showing force.

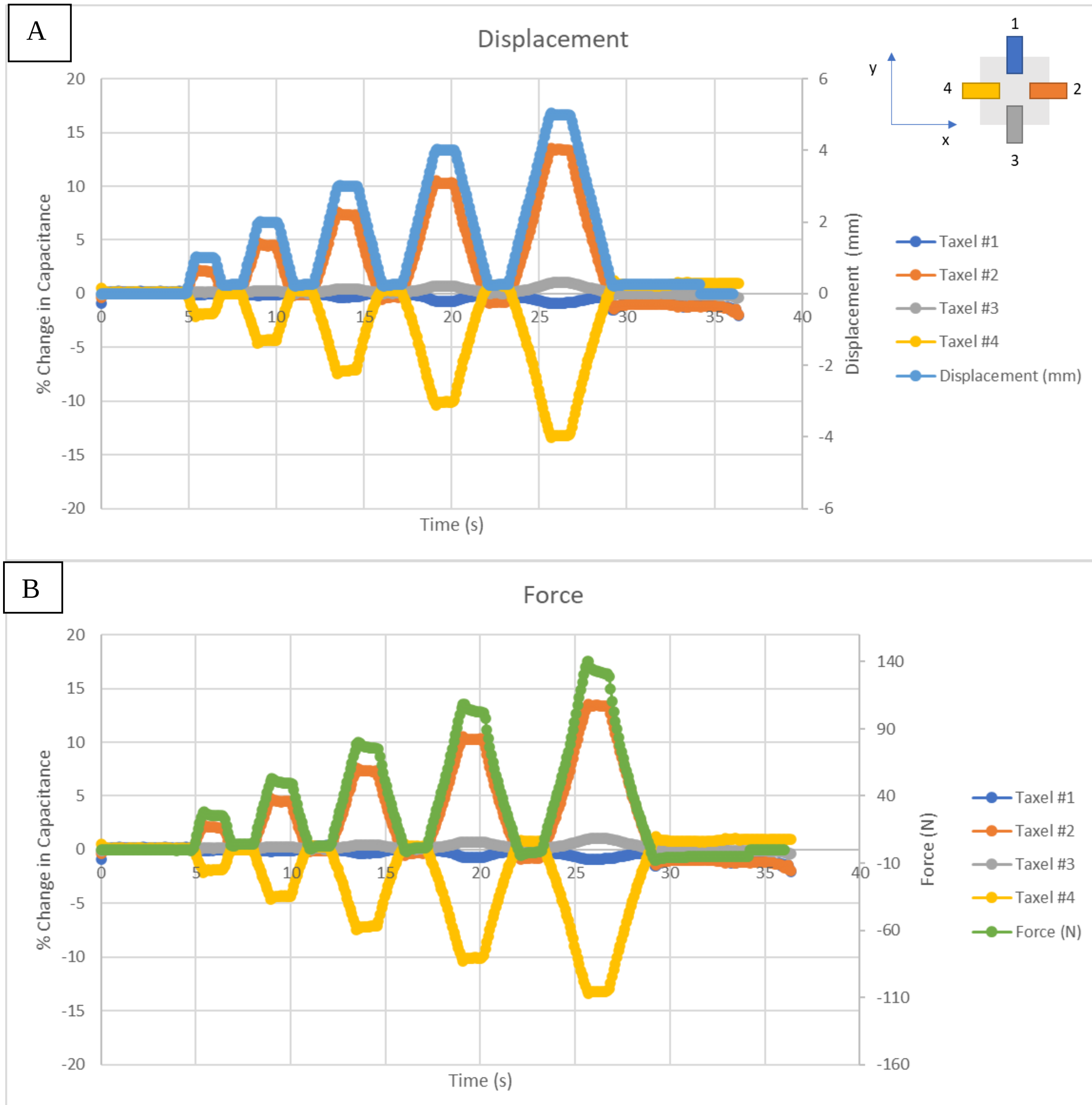

Figure 40: Shear calibration on the negative X-axis. A showing displacement curve and B showing force.

The positive Y-axis experiment of Figure 40 shows the shearing mechanism expected. Taxel 1 is decreasing capacitance while taxel 3 is increasing as it shears “upwards.” The two other taxels remain close to each other and close to zero, but both increase in capacitance. This might be because if there is a bit of tilt on the axis that is applying force into the material itself which might be causing the normal force to be applied on the sensor. Both the normal force and the shear force are being applied at the same time and are adding up. We can use our mathematical models to differentiate the two with Equations 4 and 5 in Chapter two.

The negative Y-axis response, which can be seen in Figure 41, shows large and positive capacitance changes for all taxels. As expected, there is a large difference between the responses from taxels 1 and 3, indicating shear is being detected. The x-axis sensors show a much smaller difference in response, also as expected. The large and positive change in capacitance in all sensor elements suggests that there is a substantial increase in normal force during testing. We will see in the calibration curves, next, that this normal force does not limit our ability to measure the shear being applied and results in an accurate calibration curve.

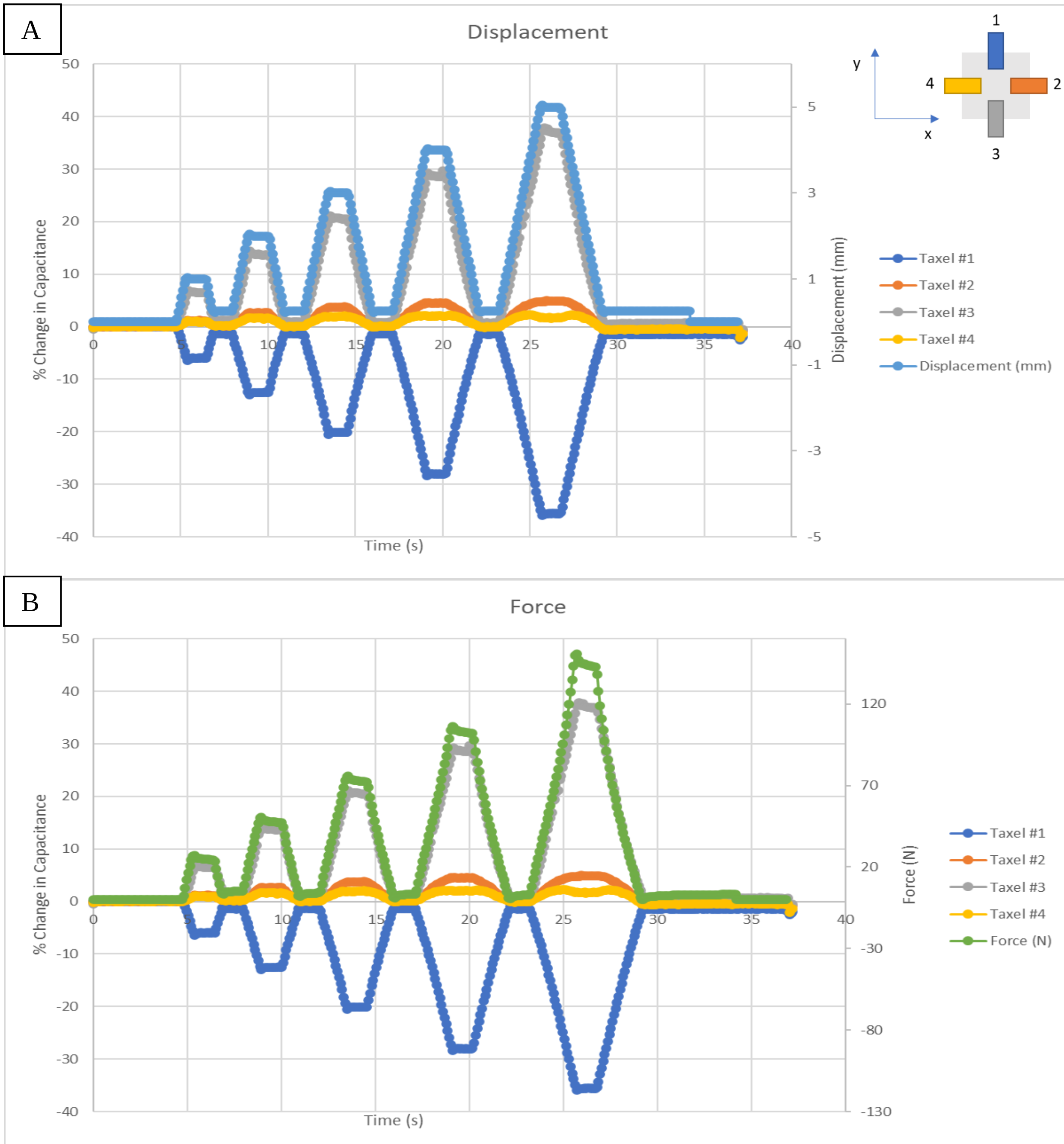

Figure 41: Shear calibration on the positive Y-axis. A showing displacement curve and B showing force.

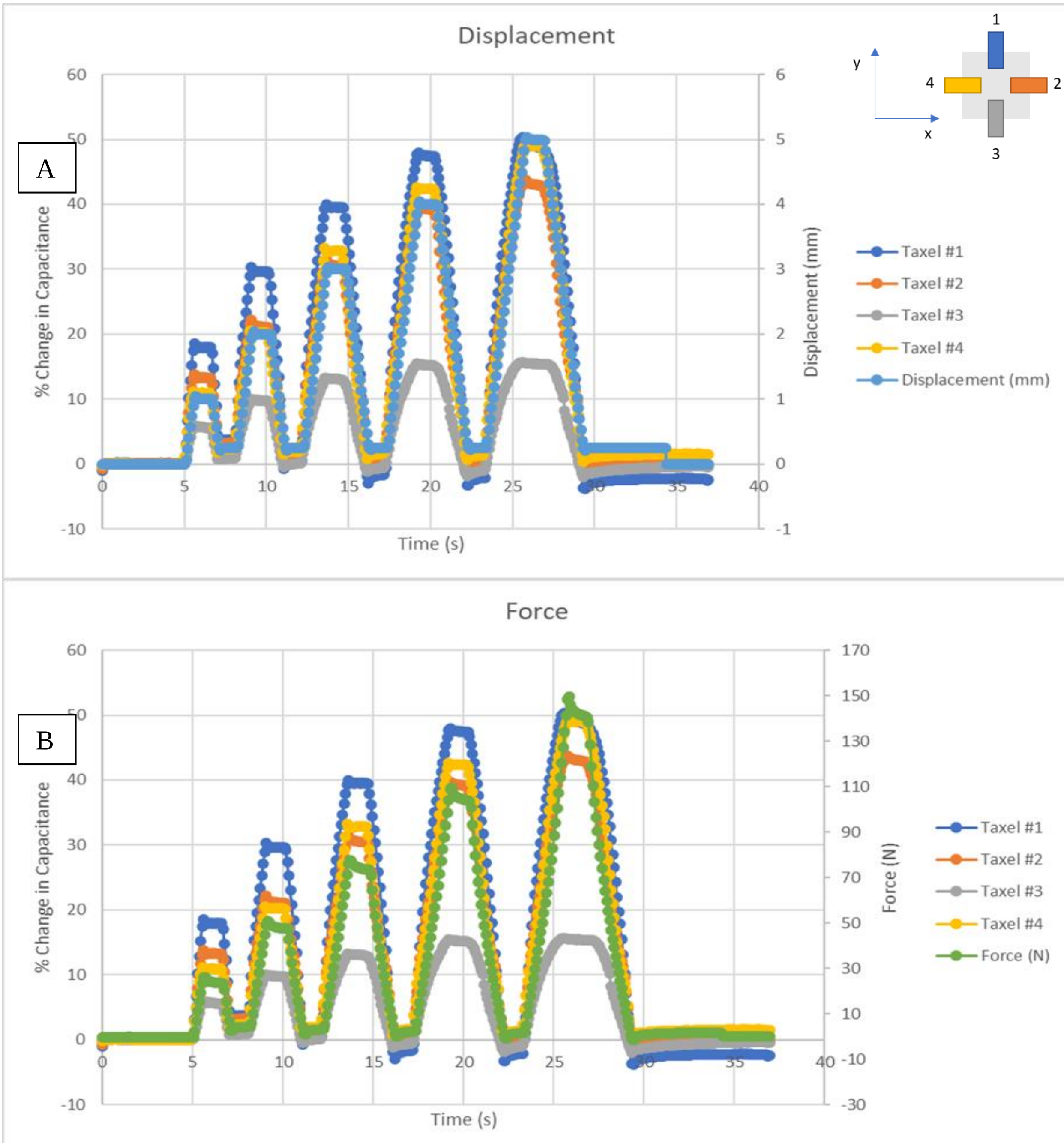

Figure 42: Shear calibration on the negative Y-axis. A showing displacement curve and B showing force.

To approximate how well the sensor is behaving, we compare the calculated displacement measurement estimated by Equation 4 with the actual displacement. This calculation is not expected to be perfect due to the difference in assumptions of parallel plate capacitor expectations and material properties. An alternative is using a fitted calibration curve to estimate the actual displacement based on the measured capacitance. The challenge with that approach is that it does not account for simultaneous shear and normal displacements. As can be seen in Figure 42, there is a nearly straight-line relationship between calculated and actual displacements for both axes. In shear displacement, the inactive axes show relatively little change. The X-axis shows a more significant response to Y-axis shear, likely due to tilt. Fitting linear curves to these axes can give us the respective sensitivity of the sensor on each axis at least for calculated displacement. Respectively we see a sensitivity of 0.4 calculated mm/mm on the X-axis and 0.5 calculated mm/mm on the Y-axis. The deviation from a straight line for both axes is small, with values of 0.8% and 0.64% for the X and the Y-axis respectively. Sensitivity calculation can then be translated to a force by using a modified version of the graph in Figure 37, where a line is fit to a graph of force versus displacement.

Lastly, at least in terms of shear measurements, we looked at the behavior of the sensor when exposed to the application of simulated walking loads. The results can be seen in Figure 43 and we used the positive y-axis as our axis of measurement, as it is set parallel to the direction of walking. For these measurements, we only went up to 2.5 mm of displacement because of the fear that the sensor could lose adhesion from the glass with fast repeated shear cycles. The sensor behaves identically to what is shown in Figure 40, as expected, and similarly to the normal force experiments, in that its capacitance follows displacement and does not decay with force relaxation. Overall, the sensor is just as robust in capturing this movement in the shear domain as it is in the normal force domain.

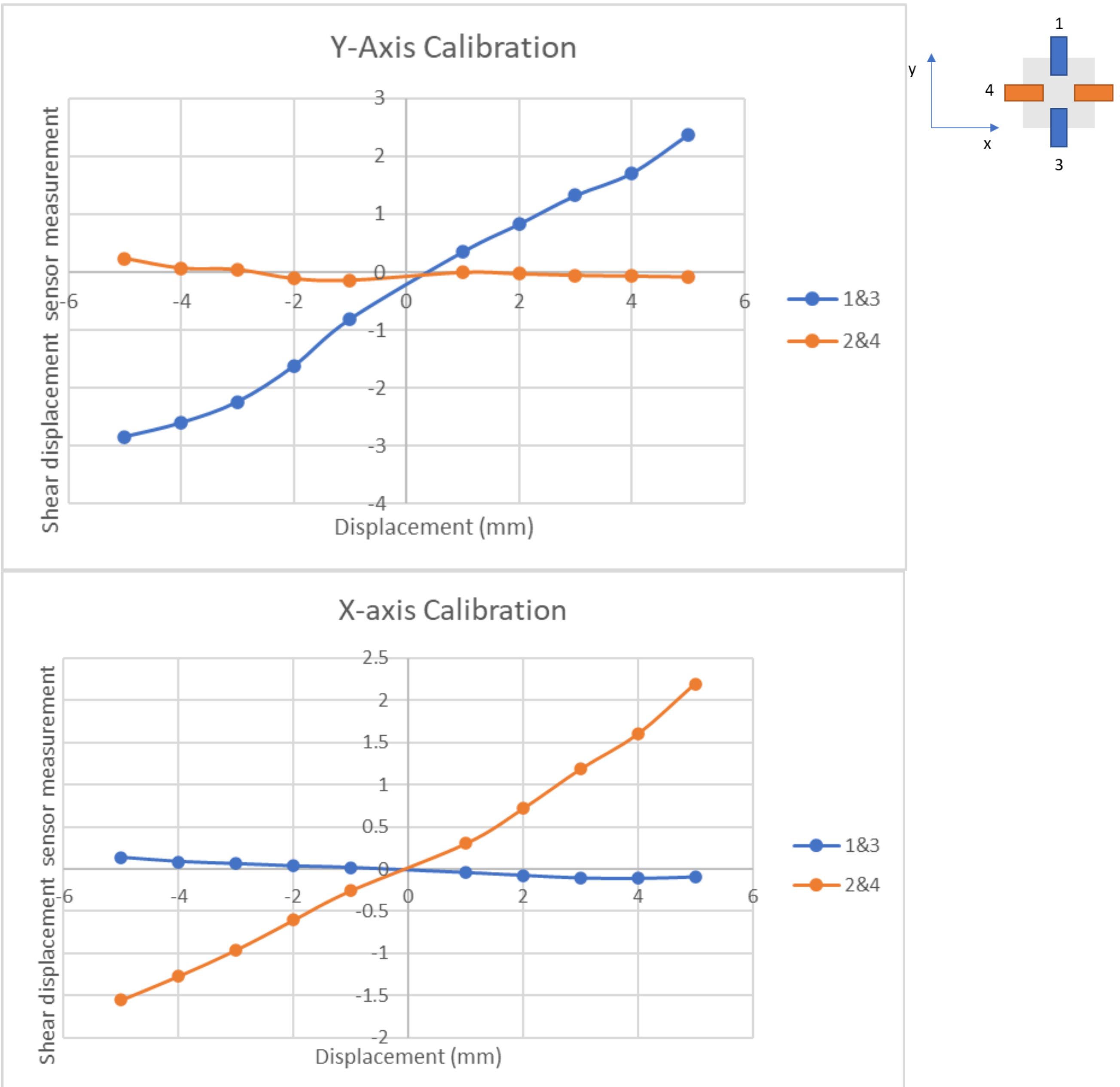

Figure 43: Shear calibration curves for each axis respectively

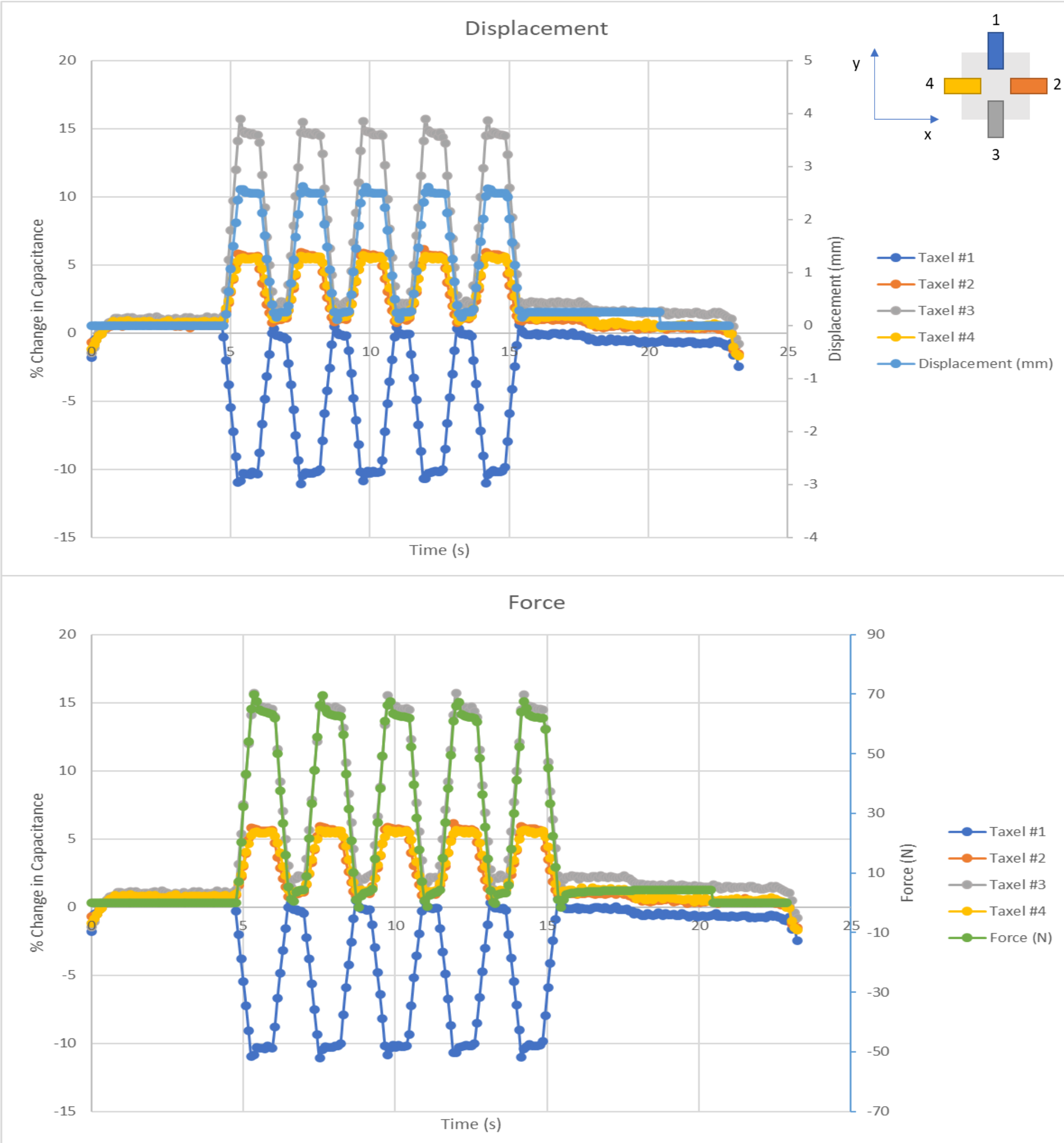

Figure 44: Simulated walking experiment for shear. A includes the displacement curve and B includes the force curve.

3.3 Stepping & Walking Testing Results

3.3.1 Step Experiments

Experiments to test real-life forces on the sensor have been described in detail in the methods section but to touch up on it briefly here; there were two experiments done to test the sensor with real-life forces, a stepping test, and a walking test. The stepping test was simply applying weight on the sensor with the heel of the foot, cycling between loading and unloading for 5 cycles with different amounts of time between cycles. One set was a single step that lasted for 30 seconds and can be seen in Figure 44. Here we can see that the taxels react to the force immediately, but don't all go to the same level. Force is estimated by using a scale to average forces being applied at the different steps. Although I am using my heel, which is relatively flat, there could be underlying anatomy causing the change even in the small area. One thing to notice is that since this is the first time we are properly applying "force" controlled deformation, we see the creep in our capacitance measurement from beginning to end. This creep, when calculated, amounts to about a 3% change in capacitance, with the total change being about 10% – 25%. We see a similar reaction when the load is taken off, as the material relaxes, but there may be some creep, as suggested by the capacitance coming to a new baseline value. This is consistent with our previous experiments using applied force and previous work in the lab.

The second stepping experiment looked at 5 steps with load applied for 5 seconds and no load for 5 seconds, the results can be seen in Figure 45. Like the first stepping experiment, the sensor follows the forces being applied, we see creep in the loaded and unloaded states, with the new baseline that the sensor returns to after each cycle again suggesting deformation following the steps. From this data, we can estimate the repeatability of the sensor, as was done previously, but now we have a force-controlled method rather than a displacement-controlled one. This estimate gives us repeatability of 5% to full scale.

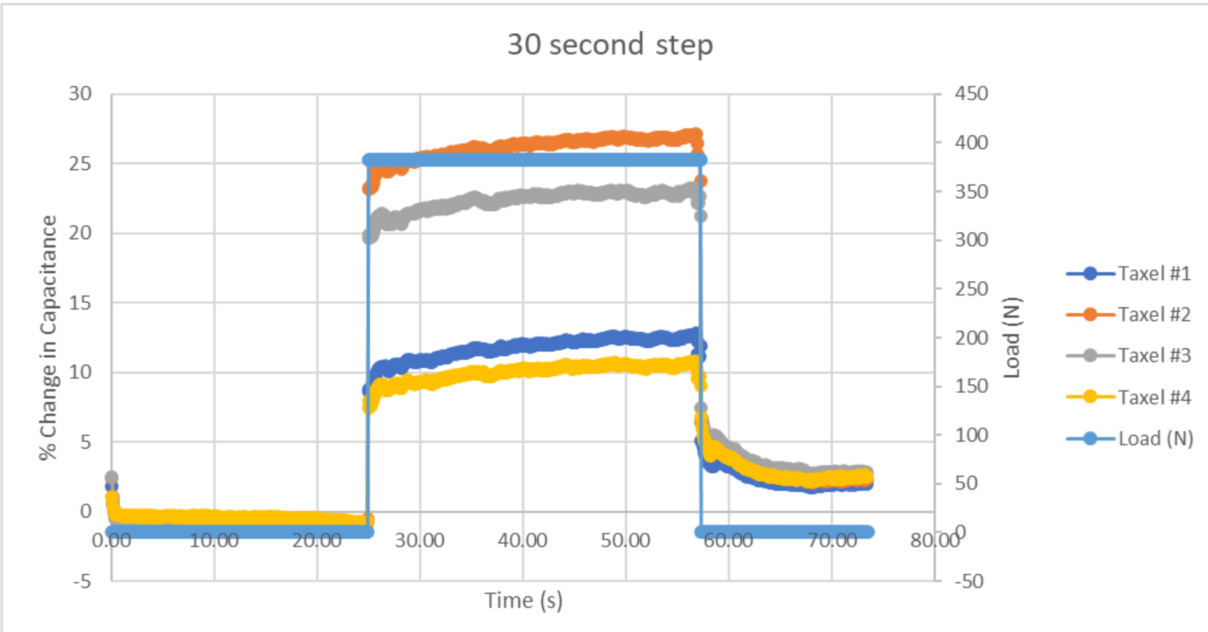

Figure 45: 30 second step experiment

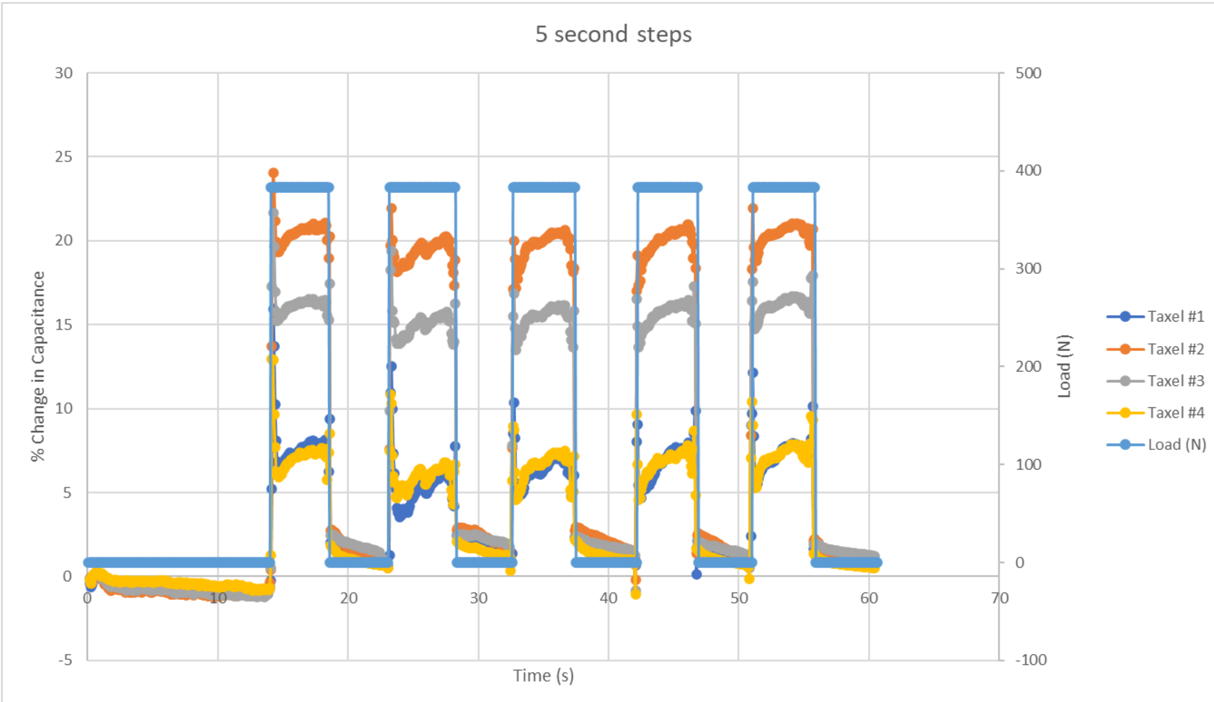

Figure 47: 5 second per step experiment

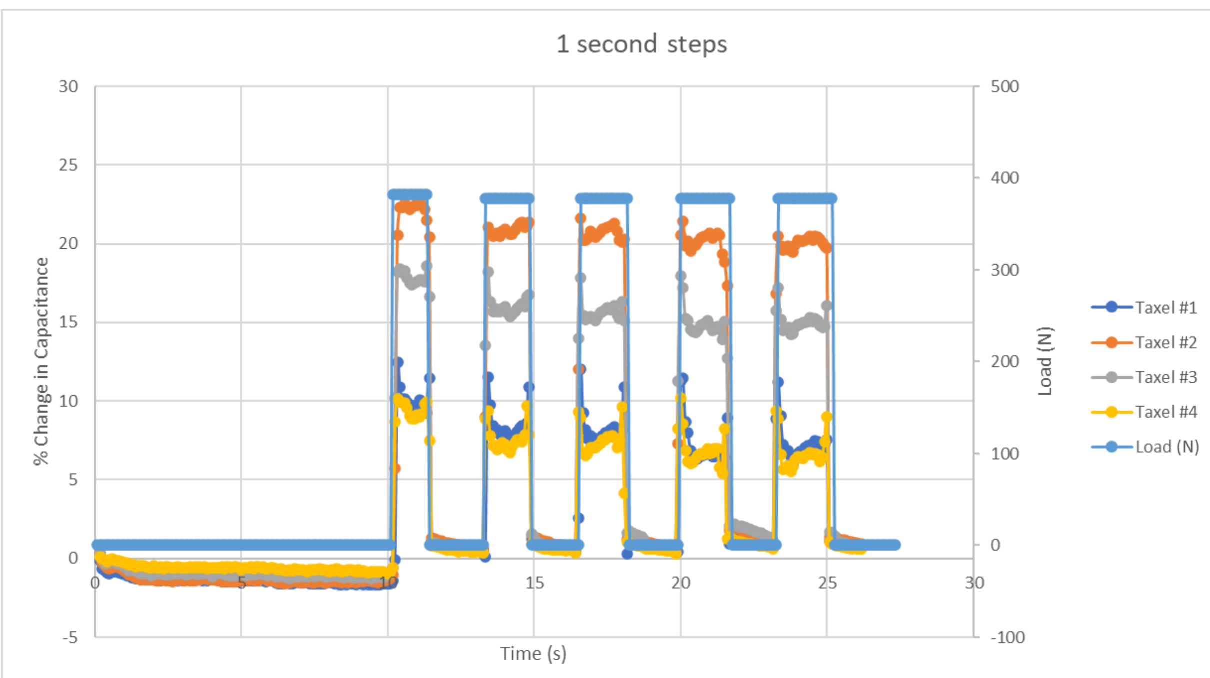

Figure 46: 1 second per step experiment

Lastly, the last step experiment with alternating 1 second applied load and 1 second no load can be seen in Figure 42. Repeating the same trend as the previous experiments we can see that the sensor can handle faster loading rates in real-time as well as the slower ones.

3.3.2 Walking Experiment

The walking experiment was described in detail in the methods section but to describe briefly, without fully lifting the foot being measured, a back-and-forth gait cycle was captured while stepping on the sensor with the heel. The cycle was repeated seven times and the results can be seen in Figure 47. First, the right foot was placed flat on the sensor, with the left foot comfortably to the side, and in line for 10 seconds, before beginning the gait cycles (see Part 1 on Figure 24). By following the curve of the force being applied, an explanation of what is happening at each step can be done by following the steps in Figure 24 in the methods section. The first swing phase by the right foot can be seen around the 20 s mark as more weight is applied to the foot (Part 1 on Figure 24). Then the measurement goes to baseline as the heel is lifted to mimic what would be the start of the lift-off (Part 3 of Figure 24). Immediately after, the full force of the body is once again placed on the sensor as the right leg swings back (Part 4 of Figure 24). Lastly, the right foot is planted flat on the floor and the sensor reading moved back to a baseline reading for half of the force (Part 5 of Figure 24). This cycle is repeated 6 more times, as can be seen clearly. There are moments like on cycles 3 and 6 where there could have been some imbalance and the reading was higher. This graph overall displays the ability of the sensor to be able to capture gait events. Also, what is interesting to notice is that there is very little shear being applied on any axis. This is artificial though because I never lift my leg and the momentum from the swing, whether forward or backward, isn't introduced.

3.4 Testing Real Life Shear

As a necessary aspect to study real-life shear, there were attempts to study shear stress on the sensor using simple shearing tasks on the sensor using the heel of a foot. This proved to be more challenging than expected. The plan was to shear along the different axes using the heel as the contact point, like normal stress measurements. The first hurdle with this method was to anchor the sensor down so as not to have the sensor lift when force is applied. Given that this had to be done for both the controlled characterization method and the real-life testing method, shows that the sensor will have to be anchored in some way to be used in this application. This leans towards having the sensor be embedded as a part of a shoe in the process of developing the device. Once the sensor was anchored in place, characterization was attempted on the sensor but resulted in frustrating conclusions. To begin with, it can be quite awkward to produce shear on the sensor while standing. While wearing socks, the foot simply slides along the sock to not produce any response. Without socks, it was observed that to produce any sort of shear change required a great amount of force. What this resulted in was building perspiration in the attempts to produce enough force and the foot sliding off the sensor.

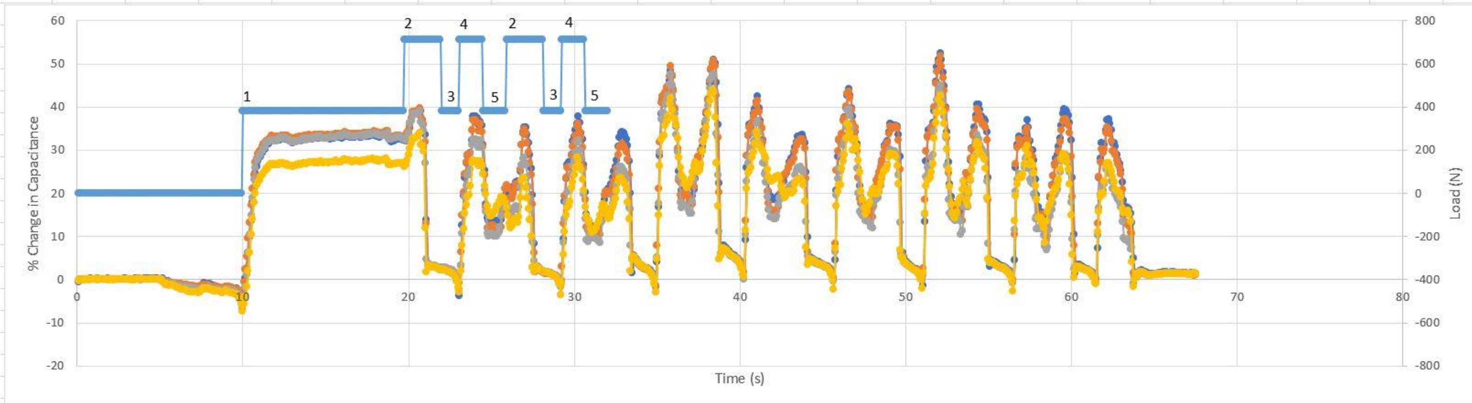

Figure 48: Pseudo-Walking Experiment. Load on the right axis. Only Two cycles of the load are shown as an example. Refer to Figure 24 for the numbers used to describe the gait moment on the load curve.

These attempts highlight two very important limitations of the current sensor technology: use with socks is problematic and when barefoot, the sensor still requires a large amount of force to produce a response. The main point from these observations is the need to redesign the shearing stiffness of the sensor so that is more sensitive. The pressure that was being applied by my foot was probably no more than 5 N. Before the lowest force we had measured was > 25 N in the first step of the shear calibration experiments. The solid dielectric may be too stiff to measure what seem to be very minute shear changes. Running the data through equations 4 and 5 gives almost no response in terms of shear in any direction.

Having already studied pillared structures, we observed that where the closest pillared architectures collapsed almost immediately when compressed (See Figure 30). There is going to have to be a sacrifice of overall stiffness for shearing sensitivity if this same elastomer system is to be used. Alternatively, the use of stiffer materials might be recommended but the lack of comfort could be problematic to patients and could cause discomfort in already insensitive feet of diabetics. Different dielectric structures other than pillars might also be more suited for holding the necessary loads, like a cross beam structure used in architecture. These more complex structures would be difficult to manufacture using the current molding techniques and might require 3D printing with elastomers, and they might not shear as easily as pillars. Potentially the sensor could be embedded into a sock and in contact with the skin, but issues with bending and curving could be problematic in measuring proper capacitance.

3.5 Sensor Parameter Table

To wrap up the result section, a parameter table was made to highlight some of the important characteristics of the sensor. It is difficult to compare these results to sensors available on the market since most only report sensing range, resolution, and refresh rate. Regardless this table gives us an idea of how the sensor behaves and what some of its weaknesses are. For example, we can see clearly that the apparent hysteresis is our biggest challenge in measuring force with precision. This could potentially be overcome by having smarter predictive models that use a history of deformation to estimate the force and stress. Similarly, the related stress relaxation of force is high (33% for standing and 24% for walking). Although our capacitance signal is stable, it needs to be able to report force in the end. We get a glimpse of our expected creep when controlled force is applied in Figure 44 and here, we see a creep of 3% of the full scale. We also calculated the signal-to-noise ratio (SNR) of the sensor by comparing the desired

Equation 6: SNR equation. ΔC is change in capacitance, MAV is the mean-absolute value of the noise

signal to the background noise. To do this we took the change in capacitance for a given signal (we used the signal at the peak force or 1 kN) and divided it by the mean absolute value at baseline as can be seen on Equation 6. We get a result of 62 dB, which is consistent with previous projects and is considered to be good by sensing standards [66].

$$SNR = 20 \log * (\frac{|\Delta C|}{|MAV_{noise}|})$$

Table 4: Sensor Parameter Table

Parameter	Value
Sensing Area (mm x mm)	11 x 11
Normal Pressure Sensing Range (kPa)	0-1000
Shear Pressure Sensing Range (kPa)	0-200
Stress Resolution	3.1 % FS
Refresh Rate (Hz)	11-13
Normal Stress Sensitivity	1.1632 calculated mm/mm
Shear Stress Sensitivity	X-axis : 0.4 calculated mm/mm Y-axis : 0.5 calculated mm/mm
Normal Stress Hysteresis	Displacement: 2% FS Force: 25% FS
Shear Stress Hysteresis	Displacement: 0.9% FS Force: 9% FS
Stress Relaxation (Standing)	Capacitance: 0.18% FS Force: 33% FS
Stress Relaxation (Walking)	Capacitance: 0.2% FS Force: 24% FS
Normal Stress Non- Linearity Error	Displacement: 0.26 % Force: 9.1 %
Shear Stress Non- Linearity Error	X-axis: 0.80 % Y-axis: 0.64 %
Repeatability	3.1 % FS
SNR (dB)	62

To compare our system with what could be considered the golden standard of in-shoe systems in the Tekscan F-scan system, we can see that there is a big difference in terms of thinness and spatial resolution. The F-scan system is resistive technology, which allows it easier to be much thinner. Our sensor could be just as thin, but the mechanics of sensing would change and require the dimensions to scale to the same degree as the thickness. In terms of spatial resolution, our system must cope with shearing displacements requiring more space so this might be a parameter we cannot change too much. Regardless we might be able to enhance and shrinking the overall size of the sensor would help in that regard. Additionally, an array format that has shearing capabilities is also an attractive solution to adding spatial resolution. On other specifications, the F-scan system is faster, at least when tethered, but has a similar pressure range in normal stress and lacks shear.

With the differences that have been described above, it becomes apparent that there can me modifications to the current sensor that could make it much closer to the golden standard. Additionally, there are some advantages to our system compared to F-scan, primarily being the stretchable capability of our sensor. Without this, the F-scan system suffers from some folding issues that may cause discomfort to the wearer. Being more compliant in this environment is better due to the changing forces and readjustments but this makes sensing that much challenging. As we saw in this thesis, we exposed the challenges of hysteresis and creep that elastic materials suffer from at higher forces and finding proper modeling techniques to deal with these will help in the development of this technology.

Table 5: Parameter comparison between our system and the Tekscan F-Scan

Variable	Our System	F-Scan
Thickness	3.5 mm	0.381 mm
Technology	Capacitive	Resistive
Spatial Resolution	.116 per cm^2 (For normal force)	3.9 per cm^2
Pressure Range	Up to 1MPa	Up to 862 kPa
Shear	Yes	No
Scan Rate	2,250 Hz (with new system)	250 Hz (Bluetooth)
Features	Stretchable & Bendable	Bendable only
Power	20 mW	10 W

Chapter 4: Discussion & Conclusion

4.1 Discussion

In this chapter, we will cover the progress made and the limitations of the current approach, helping set a path to a practical wearable sensor, setting a path for future work. Additionally, we will speculate on the improvements that could be useful and that will inform the discussion of future work in the next section

4.1.1 Material Properties

The sensor described in this thesis reacts well to the ramping rates that have been described for walking and standing. With that said, the first and most pressing setback of this thesis is the material properties of elastomeric materials concerning hysteresis. While we were able to identify material in Dragon Skin 10 plus Sylgard 184 that could deform with a nearly straight-line stress-strain curve under the necessary pressures, this material, and all the materials studied in this thesis, suffer from apparent hysteresis during unloading. The one that suffers the least out of Ecoflex 00-30, Dragon Skin 10, and Sylgard 184 is the latter. One issue with using Sylgard 184 as the material to fabricate the insoles is that is too stiff, having a Young's Modulus 10x times higher than Ecoflex 00-30. Insoles that go on shoes are usually rated similarly in hardness to Ecoflex, at 00-30 on the Shore hardness scale. It might be beneficial to start looking at different materials that could work for this application. Another material that is used in cushioning insoles for diabetes specifically is Plastazote which is a closed-cell, crosslinked polyethylene foam [67]. The use of semi-elastomeric foams might be more challenging to characterize than a full elastomer in our case, since their deformation profiles are unique, given their cell-based structures [68]. Foams do not have a linear relationship with stress over strain, additionally often the creep found in foam materials is much higher than elastomers and would not be ideal for the walking time frame discussed in this thesis. More rigid foams or ones that have higher concentrations of elastomers could be useful, but the main reason elastomers are useful in this application is that they are incompressible. Meaning that when they deform, they keep their volume, unlike compressible foams. This is important with a capacitive sensor that should keep the same dielectric distance from moment to moment without permanent deformation. Ultimately a very thin layered sensor of an extremely stiff elastomer that is cushioned by softer materials might be a solution, one that would sit above the sensor to cushion any force being applied. Although this would require a more complex characterization of multiple layers with different material characteristics to conspire. All in all, we have shown that the sensor is quite good at measuring displacement, and to measure force accurately, we need robust and innovative models that account for the shear and creep nature of these materials at high forces.

The conductivity and overall responsiveness of the sensor can be improved by using more conductive materials compared to carbon black. With the addition of carbon nanotubes, we increase the conductivity and potentially the stability of the sensor over time as we saw in the background section of the thesis and previous experiments in the lab. The effect of Dragon Skin 10 specifically has not been studied and could be added to the already studied effects of encapsulation of conductive material over time. Crimping of the leads is also an effective way to connect to PCB boards but could potentially be improved as we see an increase of resistance of about 5 times more between the lead and the crimp. Using a flexible and highly conductive fiber might be an attractive solution for insole-based measuring sensors. One group in the lab has looked to use this instead of crimps in the hopes of not inquiring about high resistance jumps at this junction. The method does add more fabrication steps that need to be further explored.

4.1.2 Fabrication Methods

The fabrication of the sensor is like the fabrication methods used when the development of this sensor was first conceived. Even though it is quite effective, there could be improvements in the development of helping scale up production. One of the biggest challenges in the fabrication of the sensors is ensuring that the top and bottom layers line up appropriately so that the location of the four sensing taxels is exactly above and in the correct location about the excitation electrode. This has been an ongoing problem with the fabrication of these sensors in our lab and there have been many ideas put forward to enable the exact placement of the layers of the sensor. One current methodology requires guides in the form of a rectangular fixture, where the different layers of the sensor can be “slotted” into position. In this way, during the curing process, the layers cannot move or shift and keeps the sensor in place.

The sensing group in our lab has also devised a sensor architecture that simplifies manufacturing by replacing one side of the sensor with a PCB. While this method still suffers from alignment issues, it makes one part of the sensor solid, and the PCB replaces a less conductive and more error-prone section of the sensor. While it is an attractive option for the insole design, it would have to be a flexible PCB that is used. There is an interesting point where the sensor could be embedded in special shoes, but this might detract potential users since they must buy new shoes to use the technology. Another potential pitfall with this technology is the adhesion between the PBC and the substrate. As we investigated in this thesis, showing that silicone epoxy is effective - but it is not perfect, so something like plasma bonding would need to be considered for this methodology. Longevity through cycling, especially with shear, would be important to look at in this formulation since the adhesion to the PBC has never been tested to the elevated shear stresses needed in this application.

4.1.3 Testing Methods

Testing methods and the improvement of them is a step forward to improve and reinforce the data shown in this thesis. The assumption is that with improved testing methods, we will be able to prove without a doubt that the experiments done in this thesis are agreeable with previous literature. The thesis was grounded on previously established testing methods for both normal and shear stresses, but these methods did not apply to the forces needed to investigate the applicability of the sensor inside a shoe. The normal and shear measurements had to be done in unique setups using an Instron mechanical analysis machine. The normal stress measurements were the most straightforward and were able to replicate the necessary forces to investigate normal stress in the plantar foot. The biggest obstacle from the Instron setup was the apparent delay from the load cell to the controlling mechanism. Because of this, all the normal stress experiments had to be done with displacement control. Normally, to study forces on the foot, a force control methodology is used to gather information about the creep of displacement as the same force is applied throughout. This is the case in terms of walking and standing since we do not change weight as we do the exercises. Because the system is unable to hold pressure in short spurts, it is incapable of being used at the necessary gait cycles (600ms on, 400 ms off). A more suitable system that is more “agile” would be needed to achieve this force-controlled study. Some of the smaller Instron models are attractive systems for this purpose

We devised a measuring setup where the sample/sensor sits between two pieces of glass and holds them together. A shearing action occurs as one glass plate slides parallel to the other when force is applied. The added variables to this setup that was not previously present in shearing characterization include the adhesive and the slipping of fixtures and grips. The initial issue with the characterization method, which is essentially a stage that moves the bottom of the sensor while the top helps in place, was that the sensor was slipping under higher forces. The same tension slipping can happen in the grips that hold the glass in the vertical setup. Care was taken to not exert the sample that was adhered to the glass to too many repetitive cycles at high forces and avoid loss of adhesion.

Lastly, the sampling rate of the electronics and in particular, the capacitance to digital converter being used is enough to gather data but not adequate for real-life use. The sampling rate ranged from 11-13 Hz between experiments. As was mentioned in the background section, the ideal sampling rate to capture multiple points in the different phases of gait would be around 70 Hz. The lack of sufficient sampling speed is evident, for example, in the missing of the overshoot in walking simulated experiments - overshoot that is captured by the Instron, whose sampling is performed at 50 Hz. Even so, we capture enough points to give confidence in the data we are reporting but it would be highly beneficial to improve the electronic system to have a higher sampling rate and this will be covered in the next section looking towards the future.

4.2 Future Work

In this section, we will cover what steps follow the work that this thesis has laid out, to develop a full working sensor. Importantly, what lessons need to be taken into future work with the results that have been produced here? Overall, the sensor works in the ranges that are needed to be used in the environment of the plantar foot, but as was discussed in the limitation section, there is a big lack of necessary equipment and electronic capability of the sensor to define the sensor in more robust terms. The main theme of the work that needs to be done to expand this technology and bring it to a point where it might be marketable revolves around dedicated funding to build custom characterization setups. Consequently, this section will cover how the design for a full sensor could be tested and implemented in real-life applications. Additionally, how a monitoring software for the technology might look and what it needs to keep in mind in terms of what is important for individuals and clinicians.

4.2.1 Further Sensor Testing

The extent of experimentation that was done in this thesis was enough to give an overall picture of the sensor's capabilities. While the normal characterization was sufficient to cover the ranges necessary in this application, the shear was not, and the need for a custom shearing characterization cannot be overstated. It was only mentioned in passing, but the shear characterization setup previously used for similar sensors in the lab could not handle the pressures needed for this application. To briefly describe the setup and as can be seen in Figure 48, the setup consists of a loadcell, indenter. and an automatic stage, where the sample/sensor is anchored. For this setup to be useful for the application of measuring shear stresses in the foot, one would need a load cell capable of going up to at least 200N in the horizontal axes and vertical axes. Additionally, the automatic platform would need to be able to withstand the same loads in all axes and be able to displace upward of at least 6 mm in each axis, this way we can rotate the sensor so we can shear in the other direction the same amount. Even with such setups, there are still some hurdles that need to be addressed. Another reason that the setup, which was being used previously was not sufficient for this application was the indenter slipping on the sensor due to the increased stresses. Like in the shear setup in this experiment, the indenter would need to be glued to the sensor and then be used in experiments. While this does not solve the shearing glue issue, one can use the shear modulus of the glue to better estimate calculations used in the future, or the indenter could be plasma bonded to the sensor to ensure there won't lose adhesion.

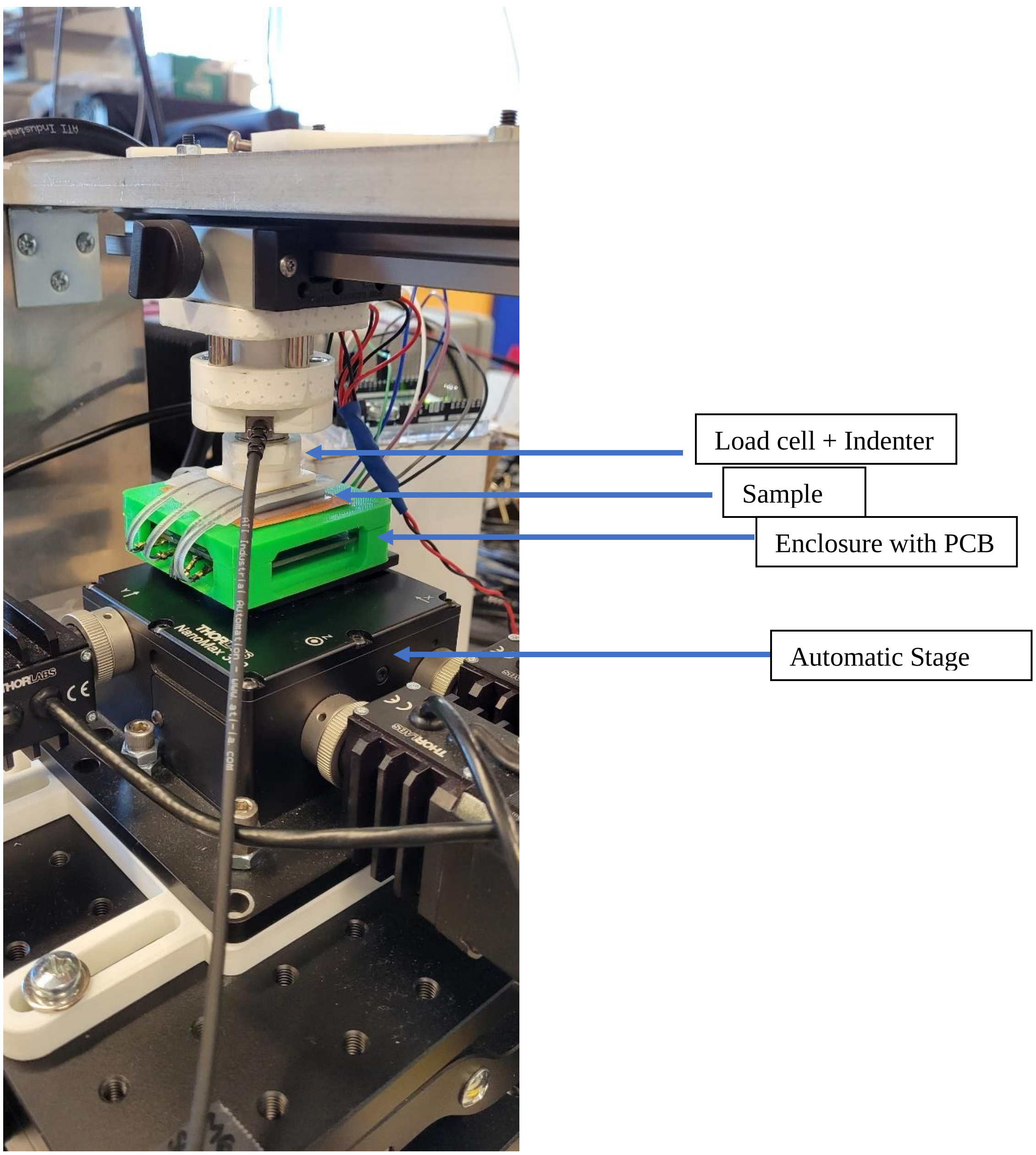

Figure 49: Previous shear characterization setup used for smaller force experiments.

To improve the normal stress measurements, these could be done with a smaller Instron machine that is capable of regulating load much faster than the current machine being used. There are a couple of smaller models that support similar load cells and are more “agile.” The 6800 series or the 3400 series that only go up to 50 kN of force max could be attractive options, they also have an accuracy of 0.5% of the force capacity compared to the 5969 series that has an accuracy of 5%. There are a couple of smaller models that support similar load cells and are more “agile.” This would allow for a closer examination of a load-controlled test at the different time regimes and faster load rates with fewer overshoots.

4.2.2 Modeling and dealing with apparent hysteresis

While finding other materials, or a combination of materials that might make the deformation more linear or easier to work with, another option is to use mathematical models to an algorithm to predict the loading curves. The sensor can be useful in gathering displacement information, which is accurate using a fitted curve. Once this is obtained a model could be fitted to our stress versus strain curves to create a better match with the force and stress data rather than a fitted polynomial. Some of the models that have been developed to mimic hysteresis include the Duhem and the Preisach models [69]. These models do a better job of following the loading curves but are rate-dependent. This is where the importance of history comes into play. The use of algorithms and predictive models could give us an advantage in reading current situations and predicting the rate at which we are deforming[70]. An investigation needs to be done as to whether these models and algorithms are accurate enough to compensate for the 25 % hysteresis measurement.

4.2.3 Insole device fabrication & considerations

In this thesis, we went into a brief design consideration for a full-sized device utilizing the sensors in 2.4.3, one that has a single sensing unit at relevant high-stress locations on the plantar foot. This sensor could be fabricated using similar methods as described in this thesis and could be a useful first edition of the insole sensor. One important discussion with the consideration of a sensor like this is where to place the electronics and how accessible that makes the technology. While an acquisition unit that sits outside of the shoe with leads traveling all from the location of the sensors in the insole and out of the shoe, might suffer from noise and be awkward to wear. On the other hand, an insole system that was entirely layered on a rigid or flexible PCB could reduce the noise and compartmentalize all the electronic components in what would now be more of a shoe system rather than an insole. A system like this could suffer more from the degradation of overuse due to the adhesion between substrate and PCB and might be less expensive if it is a whole shoe rather than a reusable insole. Probably the true answer for the insole system lies in between these two extremes. Where there could be a portion of the electronics compartmentalized in the insole or shoe, and there are leads out of the shoe for charging or getting out data.

One aspect that would be improved in an insole system or future iteration of the sensor is the sampling frequency of the CDC chip. Currently, a team in the lab is working on implementing an all-in-one processing unit with a built-in capacitance capability with the BLD54 Cypress microcontroller. Presently, in some preliminary setup and characterization, this chip can achieve sampling rates of over 200 Hz per taxel (compared to our current setup of 11-13 Hx per taxel). This is a great boon to the current chip that can only measure around 12 Hz per taxel. Although the current chip was still capable, the upgrade to this chip would allow the measurement of important information when walking trials are done with the sensors. As can be seen in the walking trials in our sensor, we do not capture any points on the way up in the ramping of the on and offloading of the steps. This chip would allow us to capture that data and all relevant information during quick adjustments during walking. Additionally, the PCB that is being designed is half the size of the PCB currently being used (40 x 40 mm) and houses the microcontroller which would replace the Arduino Uno being used.

4.2.4 Monitoring Software

Software that would be used in conjunction with the sensor would need to relay relevant information to the user or clinician in an easy-to-understand manner. Relevant information that can be captured with the sensor includes stress-based measures like current stress in relevant locations, stress history, and extended stress intervals. The sensor is also suitable for measurements of limb location and changes in anatomy. Alternatively, it could be useful for detecting deformations in bone structure and tissue which is also prevalent in the feet of diabetics. A profile of the individual’s foot would need to be established and a monitoring software could check for changes in anatomy that surpass a clinically relevant threshold. Finally, the monitoring software could be sophisticated enough to recognize patterns in cadence and gait that could entail clinically important milestones of the development of poor gait or loss in walking strength. Often these issues are ignored in individuals and can lead to further damage of the lower limbs if not corrected.

While the technology described in the thesis is mainly targeted toward measuring passive pressure ulcers in standing and walking situations, this technology could branch out to other vulnerable populations like those with heart disease, poor skin conditions, and even normal individuals who due to a lot of high-intensity exercises or are on their feet for a long extended amount of time, experience pressure ulcers. These might happen due to awkward pronation and not proper shoe wear. This technology could be beneficial to these individuals as a more accessible and less clinical-oriented product.

4.3 Conclusion

In this thesis, we set out to expand the existing architecture of a normal and shear stress sensor to the necessary forces found in the plantar foot. This was done to examine the capabilities of this capacitive elastomeric sensor in the environment needed to measure pressure ulcers in the foot environment. A suitable substrate was identified to be used in sensor fabrication, one that is safe to use with skin and has an anti-fungal option. It was shown that the sensor mimicked the deformation as expected using displacement-controlled experiments at the different time regimes the sensor would be used in. The sensor was then shown to respond to real-life experimentation with simple stepping trials. Overall, there is still a lot of work that needs to be done to bring this technology to a marketable stage and this was outlined respectively. The prospect of monitoring and avoiding some of the detrimental side effects of diabetes could be very beneficial to those individuals and health authorities. As well as the expansion to other sectors, this technology could help bring smart insoles and shoes into the limelight and allow individuals to lead healthy lives even with diabetes or other complications.

Bibliography

[1] A. G. LeBlanc, Y. J. Gao, L. McRae, and C. Pelletier, "Twenty years of diabetes surveillance using the Canadian chronic disease surveillance system," *Heal. Promot. Chronic Dis. Prev. Canada*, vol. 39, no. 11, pp. 306–309, 2019, doi: 10.24095/hpcdp.39.11.03.

[2] Public Health Agency of Canada and Pan-Canadian Public Health Network, *Key health inequalities in Canada: A national portrait*. 2018.

[3] G. B. J. Mancini, R. A. Hegele, and L. A. Leiter, "Dyslipidemia Diabetes Canada Clinical Practice Guidelines Expert Committee," *Can. J. Diabetes*, vol. 42, pp. 178–185, 2018.

[4] C. G. C. Joan Canavan, Peggy Dunbar, Jessica Dupuis, *Diabetes in Canada*. Public Health Agency of Canada, 2011.

[5] R. Goeree *et al.*, "Prevalence, total and excess costs of diabetes and Related complications in Ontario, canada," *Can. J. Diabetes*, vol. 33, no. 1, pp. 35–45, 2009, doi: 10.1016/S1499-2671(09)31007-2.

[6] A. Johannesson, G. U. Larsson, N. Ramstrand, A. Turkiewicz, A. B. Wiréhn, and I. Atroshi, "Incidence of lower-limb amputation in the diabetic and nondiabetic general population: A 10-year population-based cohort study of initial unilateral and contralateral amputations and reamputations," *Diabetes Care*, vol. 32, no. 2, pp. 275–280, 2009, doi: 10.2337/dc08-1639.

[7] "Wound Care," *Canadian Association of Wound Care*, 2013.

[8] R. B. Hopkins, N. Burke, J. Harlock, J. Jegathisawaran, and R. Goeree, "Economic burden

of illness associated with diabetic foot ulcers in Canada," *BMC Health Serv. Res.*, vol. 15, no. 1, pp. 1–9, 2015, doi: 10.1186/s12913-015-0687-5.

[9] H. Gilpin and K. Lagan, "Quality of life aspects associated with diabetic foot ulcers: A review," *Diabet. Foot J.*, vol. 11, no. 2, pp. 56–62, 2008.

[10] Canadian Diabetes Association, "The Economic Impact of Offloading Devices for the Prevention of Amputations in British Columbia," 2016, [Online]. Available: https://www.diabetes.ca/DiabetesCanadaWebsite/media/Advocacy-and-Policy/Advocacy Reports/Economic-Impact-of-Offloading-Devices-on-DFU-Costs-in-BC_FINAL.pdf.

[11] A. Raghav, Z. A. Khan, R. K. Labala, J. Ahmad, S. Noor, and B. K. Mishra, "Financial burden of diabetic foot ulcers to world: a progressive topic to discuss always," *Ther. Adv. Endocrinol. Metab.*, vol. 9, no. 1, pp. 29–31, Jan. 2018, doi: 10.1177/2042018817744513.

[12] C. LaCalle, "This smart scale can prevent thousands of foot amputations every years," *Dreamit Ventures*, 2017. https://www.dreamit.com/journal/bluedrop-medical-scale (accessed May 13, 2021).

[13] F. D. Alosaimi, R. Labani, N. Almasoud, N. Alhelali, L. Althawadi, and D. M. Aljahani, "Associations of foot ulceration with quality of life and psychosocial determinants among patients with diabetes; A case-control study," *J. Foot Ankle Res.*, vol. 12, no. 1, pp. 1–11, 2019, doi: 10.1186/s13047-019-0367-5.

[14] S. Watson-Miller, "Living with a diabetic foot ulcer: A phenomenological study," *J. Clin. Nurs.*, vol. 15, no. 10, pp. 1336–1337, 2006, doi: 10.1111/j.1365-2702.2006.01521.x.

[15] A. Gefen, "How much time does it take to get a pressure ulcer? Integrated evidence from

human, animal, and in vitro studies," *Ostomy Wound Manag.*, vol. 54, no. 10, 2008.

[16] M. Yavuz, H. Master, A. Garrett, L. A. Lavery, and L. S. Adams, "Peak plantar shear and pressure and foot ulcer locations: A call to revisit ulceration pathomechanics," *Diabetes Care*, vol. 38, no. 11, pp. e184–e185, 2015, doi: 10.2337/dc15-1596.

[17] M. Yavuz *et al.*, "Temperature as a predictive tool for plantar triaxial loading," *J. Biomech.*, vol. 47, no. 15, pp. 3767–3770, 2014, doi: 10.1016/j.jbiomech.2014.09.028.

[18] H. F. Foong, B. M. Kyaw, Z. Upton, and L. Tudor Car, "Facilitators and barriers of using digital technology for the management of diabetic foot ulcers: A qualitative systematic review," *Int. Wound J.*, vol. 17, no. 5, pp. 1266–1281, 2020, doi: 10.1111/iwj.13396.

[19] W. Clayton and T. A. Elasy, "A review of the pathophysiology, classification, and treatment of foot ulcers in diabetic patients," *Clin. Diabetes*, vol. 27, no. 2, pp. 52–58, 2009, doi: 10.2337/diaclin.27.2.52.

[20] M. P. Khanolkar, S. C. Bain, and J. W. Stephens, "The diabetic foot," *Qjm*, vol. 101, no. 9, pp. 685–695, 2008, doi: 10.1093/qjmed/hcn027.

[21] M. Zubair, A. Malik, and J. Ahmad, "Clinico-microbiological study and antimicrobial drug resistance profile of diabetic foot infections in North India," *Foot*, vol. 21, no. 1, pp. 6–14, 2011, doi: 10.1016/j.foot.2010.10.003.

[22] M. Brownlee, "The pathobiology of diabetic complications: A unifying mechanism," *Diabetes*, vol. 54, no. 6, pp. 1615–1625, 2005, doi: 10.2337/diabetes.54.6.1615.

[23] A. Y. W. LEE and S. S. M. CHUNG, "Contributions of polyol pathway to oxidative stress in diabetic cataract," *FASEB J.*, vol. 13, no. 1, pp. 23–30, 1999, doi:

10.1096/fasebj.13.1.23.

[24] I. Giardino, D. Edelstein, and M. Brownlee, “Nonenzymatic glycosylation in vitro and in bovine endothelial cells alters basic fibroblast growth factor activity. A model for intracellular glycosylation in diabetes,” *J. Clin. Invest.*, vol. 94, no. 1, pp. 110–117, 1994, doi: 10.1172/jci117296.

[25] A. S. Charonis *et al.*, “Laminin alterations after in vitro nonenzymatic glycosylation,” *Diabetes*, vol. 39, no. 7, pp. 807–814, 1990, doi: 10.2337/diab.39.7.807.

[26] L. R. Mañas, C. A. Bouzon, and M. C. Rodríguez, “Peripheral Arterial Disease in Old People with Diabetes,” *Diabetes Old Age Third Ed.*, vol. 26, no. 12, pp. 39–49, 2009, doi: 10.1002/9780470744093.ch4.

[27] R. Ross and L. Agius, “Diabetologia,” vol. 100, pp. 34–40, 1992.

[28] P. M. Ridker, M. Cushman, M. J. Stampfer, R. P. Tracy, and C. H. Hennekens, “Plasma concentration of C-reactive protein and risk of developing peripheral vascular disease,” *Circulation*, vol. 97, no. 5, pp. 425–428, 1998, doi: 10.1161/01.CIR.97.5.425.

[29] H. Steinberg and A. Baron, “Vascular function, insulin resistance and fatty acids,” *Diabetologia*, vol. 45, no. 5, pp. 623–634, 2002, doi: 10.1007/s00125-002-0800-2.

[30] C. A. Abbott *et al.*, “The North-West Diabetes Foot Care Study: Incidence of, and risk factors for, new diabetic foot ulceration in a community-based patient cohort,” *Diabet. Med.*, vol. 19, no. 5, pp. 377–384, 2002, doi: 10.1046/j.1464-5491.2002.00698.x.

[31] J. J. Mendes and J. Neves, “Diabetic Foot Infections: Current Diagnosis and Treatment,” *J. Diabet. Foot Complicat.*, vol. 4, no. 2, pp. 26–45, 2012.

[32] K. Agrawal and N. Chauhan, “Pressure ulcers: Back to the basics,” *Indian J. Plast. Surg.*, vol. 45, no. 2, pp. 244–254, 2012, doi: 10.4103/0970-0358.101287.

[33] D. G. Armstrong, A. J. M. Boulton, and S. A. Bus, “Diabetic Foot Ulcers and Their Recurrence,” *N. Engl. J. Med.*, vol. 376, no. 24, pp. 2367–2375, 2017, doi: 10.1056/nejmra1615439.

[34] M. Yavuz, A. Erdemir, G. Botek, G. B. Hirschman, L. Bardsley, and B. L. Davis, “Peak Plantar Pressure and Shear Locations,” *Diabetes Care*, vol. 30, no. 10, pp. 2643–2645, 2007, doi: 10.2337/dc07-0862.A.

[35] M. Yavuz *et al.*, “Temperature- and Pressure-Regulating Insoles for Prevention of Diabetic Foot Ulcers,” *J. Foot Ankle Surg.*, vol. 59, no. 4, pp. 685–688, 2020, doi: 10.1053/j.jfas.2019.05.009.

[36] K. Vowden, “Diabetic foot complications.,” *J. Wound Care*, vol. 6, no. 1, pp. 4–8, 1997, doi: 10.12968/jowc.1997.6.1.4.

[37] C. C. Cychosz, P. Phisitkul, D. A. Belatti, and D. K. Wukich, “Preventive and therapeutic strategies for diabetic foot ulcers,” *Foot Ankle Int.*, vol. 37, no. 3, pp. 334–343, 2016, doi: 10.1177/1071100715611951.

[38] D. G. Armstrong, W. F. Todd, L. A. Lavery, L. B. Harkless, and T. R. Bushman, “The natural history of acute Charcot’s arthropathy in a diabetic foot specialty clinic,” *J. Am. Podiatr. Med. Assoc.*, vol. 87, no. 6, pp. 272–278, 1997, doi: 10.7547/87507315-87-6-272.

[39] S. R. McGee and E. J. Boyko, “Physical examination and chronic lower-extremity ischemia: A critical review,” *Arch. Intern. Med.*, vol. 158, no. 12, pp. 1357–1364, 1998,

doi: 10.1001/archinte.158.12.1357.

[40] N. A. Khan, S. A. Rahim, S. S. Anand, D. L. Simel, and A. Panju, "CLINICIAN ' S CORNER Does the Clinical Examination Predict Lower Extremity Peripheral Arterial Disease ? QUESTION TO ANSWER WITH," *Jama*, vol. 295, no. 5, pp. 6–8, 2006.

[41] Registered Nurses' Association of Ontario (RNAO), "Clinical best assessment and management of foot ulcers for people with diabetes," *RNAO Best Pract. Guidel.*, no. March, pp. 15–156, 2013, [Online]. Available: http://rnao.ca/sites/rnao-ca/files/Assessment_and_Management_of_Foot_Ulcers_for_People_with_Diabetes_Second_Edition1.pdf.

[42] "Debridement Procedures for Managing Diabetic Foot Ulcers: A Review of Clinical Effectiveness, Cost-effectiveness, and Guidelines [Internet]," *Ottawa (ON): Canadian Agency for Drugs and Technologies in Health*, 2014. https://www.ncbi.nlm.nih.gov/books/NBK253769/.

[43] M. Turns, "Prevention and management of diabetic foot ulcers," *Br. J. Community Nurs.*, vol. 20, no. C, pp. S30–S37, 2015, doi: 10.12968/bjcn.2015.20.Sup3.S30.

[44] S. Bhattacharya and R. Mishra, "Pressure ulcers: Current understanding and newer modalities of treatment," *Indian J. Plast. Surg.*, vol. 48, no. 1, pp. 4–16, 2015, doi: 10.4103/0970-0358.155260.

[45] "Plantar Pre s s u res Are Elevated in the N e u roischemic and the Neuro p a t h i c," vol. 22, no. 12, pp. 5–9, 1999.

[46] T. W. Kernozek, J. F. Greany, and C. Heizler, "Plantar loading asymmetry in american

indians with diabetes and peripheral neuropathy, with diabetes only, and without diabetes," *J. Am. Podiatr. Med. Assoc.*, vol. 103, no. 2, pp. 106–112, 2013, doi: 10.7547/1030106.

[47] O. A. Fawzy, A. I. Arafa, M. A. El Wakeel, and S. H. Abdul Kareem, "Plantar pressure as a risk assessment tool for diabetic foot ulceration in egyptian patients with diabetes," *Clin. Med. Insights Endocrinol. Diabetes*, vol. 7, pp. 31–39, 2014, doi: 10.4137/CMED.S17088.

[48] Y. Cong, J. Tak-Man Cheung, A. K. L. Leung, and M. Zhang, "Effect of heel height on in-shoe localized triaxial stresses," *J. Biomech.*, vol. 44, no. 12, pp. 2267–2272, 2011, doi: 10.1016/j.jbiomech.2011.05.036.

[49] M. Yavuz, A. Tajaddini, G. Botek, and B. L. Davis, "Temporal characteristics of plantar shear distribution: Relevance to diabetic patients," *J. Biomech.*, vol. 41, no. 3, pp. 556–559, 2008, doi: 10.1016/j.jbiomech.2007.10.008.

[50] C. Price, D. Parker, and C. Nester, "Validity and repeatability of three in-shoe pressure measurement systems," *Gait Posture*, vol. 46, no. 2016, pp. 69–74, 2016, doi: 10.1016/j.gaitpost.2016.01.026.

[51] A. H. Abdul Razak, A. Zayegh, R. K. Begg, and Y. Wahab, "Foot plantar pressure measurement system: A review," *Sensors (Switzerland)*, vol. 12, no. 7, pp. 9884–9912, 2012, doi: 10.3390/s120709884.

[52] D. B. Wibowo, A. Widodo, G. D. Haryadi, W. Caesarendra, and R. Harahap, "Effect of in-shoe foot orthosis contours on heel pain due to calcaneal spurs," *Appl. Sci.*, vol. 9, no. 3, 2019, doi: 10.3390/app9030495.

[53] P. V. Munuera, J. Polo, and J. Rebollo, “Length of the first metatarsal and hallux in hallux valgus in the initial stage,” *Int. Orthop.*, vol. 32, no. 4, pp. 489–495, 2008, doi: 10.1007/s00264-007-0350-9.

[54] J. L. Sparks *et al.*, “Use of silicone materials to simulate tissue biomechanics as related to deep tissue injury,” *Adv. Ski. Wound Care*, vol. 28, no. 2, pp. 59–68, 2015, doi: 10.1097/01.ASW.0000460127.47415.6e.

[55] R. W. Bohannon and A. Williams Andrews, “Normal walking speed: A descriptive meta-analysis,” *Physiotherapy*, vol. 97, no. 3, pp. 182–189, 2011, doi: 10.1016/j.physio.2010.12.004.

[56] C. Mummolo, L. Mangialardi, and J. H. Kim, “Quantifying dynamic characteristics of human walking for comprehensive gait cycle,” *J. Biomech. Eng.*, vol. 135, no. 9, pp. 1–10, 2013, doi: 10.1115/1.4024755.

[57] M. S. Sarwar *et al.*, “Bend, stretch, and touch: Locating a finger on an actively deformed transparent sensor array,” *Sci. Adv.*, vol. 3, no. 3, pp. 1–9, 2017, doi: 10.1126/sciadv.1602200.

[58] N. T. Nguyen *et al.*, “Transparent stretchable capacitive touch sensor grid using ionic liquid electrodes,” *Extrem. Mech. Lett.*, vol. 33, p. 100574, 2019, doi: 10.1016/j.eml.2019.100574.

[59] Mirza Saquib us Sarwar M.A.Sc., “SOFT CAPACITIVE SENSORS FOR PROXIMITY, TOUCH, PRESSURE AND SHEAR MEASUREMENTS,” University of British Columbie, 2019.

[60] W. Deng *et al.*, “Microstructure-Based Interfacial Tuning Mechanism of Capacitive Pressure Sensors for Electronic Skin,” *J. Sensors*, vol. 2016, 2016, doi: 10.1155/2016/2428305.

[61] I. D. Johnston, D. K. McCluskey, C. K. L. Tan, and M. C. Tracey, “Mechanical characterization of bulk Sylgard 184 for microfluidics and microengineering,” *J. Micromechanics Microengineering*, vol. 24, no. 3, 2014, doi: 10.1088/0960-1317/24/3/035017.

[62] J. Vaicekauskaite, P. Mazurek, S. Vudayagiri, and A. L. Skov, “Mapping the mechanical and electrical properties of commercial silicone elastomer formulations for stretchable transducers,” *J. Mater. Chem. C*, vol. 8, no. 4, pp. 1273–1279, 2020, doi: 10.1039/c9tc05072h.

[63] Y. Fouillet *et al.*, “Stretchable Material for Microfluidic Applications,” *Proceedings*, vol. 1, no. 10, p. 501, 2017, doi: 10.3390/proceedings1040501.

[64] P. Rothemund *et al.*, “A soft, bistable valve for autonomous control of soft actuators,” *Sci. Robot.*, vol. 3, no. 16, 2018, doi: 10.1126/SCIROBOTICS.AAR7986.

[65] S. Shang, Y. Yue, and X. Wang, “Piezoresistive strain sensing of carbon black /silicone composites above percolation threshold,” *Rev. Sci. Instrum.*, vol. 87, no. 12, pp. 1–6, 2016, doi: 10.1063/1.4973274.

[66] D. Steck, J. Qu, S. B. Kordmahale, D. Tscharnuter, A. Muliana, and J. Kameoka, “Mechanical responses of Ecoflex silicone rubber: Compressible and incompressible behaviors,” *J. Appl. Polym. Sci.*, vol. 136, no. 5, pp. 1–11, 2019, doi: 10.1002/app.47025.

[67] S. R. Sabapathy and P. Madhu, “Healing ulcers and preventing their recurrences in the diabetic foot,” *Indian J. Plast. Surg.*, vol. 49, no. 3, pp. 302–313, 2016, doi: 10.4103/0970-0358.197238.

[68] C. PCB, “What is Signal to Noise Ratio and How to calculate it?,” *Cadence.com*, 2020. https://resources.pcb.cadence.com/blog/2020-what-is-signal-to-noise-ratio-and-how-to-calculate-it (accessed Apr. 08, 2021).

[69] R. Coombes, “An Explanation of What Plastazote® Is,” *GWPGroup*, 2021. https://www.gwp.co.uk/guides/what-is-plastazote-foam/ (accessed Apr. 08, 2021).

[70] J. W. Brodsky, F. E. Pollo, D. Cheleuitte, and B. S. Baum, “Physical properties, durability, and energy-dissipation function of dual-density orthotic materials used in insoles for diabetic patients,” *Foot Ankle Int.*, vol. 28, no. 8, pp. 880–889, 2007, doi: 10.3113/FAI.2007.0880.

[71] I. D. Mayergoyz, “Mathematical models of hysteresis (Invited),” *IEEE Trans. Magn.*, vol. 22, no. 5, pp. 603–608, 1986, doi: 10.1109/TMAG.1986.1064347.

[72] K. Cao and R. Li, “Modeling of rate-independent and symmetric hysteresis based on madelung’s rules,” *Sensors (Switzerland)*, vol. 19, no. 2, 2019, doi: 10.3390/s19020352.